Helicopter Vibration Reduction Using Robust Control

Von der Fakultät Luft- und Raumfahrttechnik der Universität Stuttgart
zur Erlangung der Würde eines Doktor-Ingenieurs (Dr.-Ing.)
genehmigte Abhandlung

Vorgelegt von

Thomas Mannchen

aus München

Hauptberichter:	Prof. Klaus H. Well, Ph.D.
Mitberichter:	Prof. Ian Postlethwaite, Ph.D.
Tag der mündlichen Prüfung:	10.01.2003

Institut für Flugmechanik und Flugregelung
Universität Stuttgart

2003

Acknowledgements

I would like to take this opportunity to express my gratitude to the many people who have provided help and encouragement over the time leading up to and during the development of this work.

In particular, I would like to thank my supervisor, Professor Klaus Well, for his advice and encouragement. I am grateful as well to Professor Ian Postlethwaite, who has shown an ongoing interest in this work and provided valuable comments.

Support for this research provided by Eurocopter Deutschland is gratefully acknowledged. I am particularly indebted to Henning Strehlow and Oliver Dieterich.

My contemporaries in the Institute of Flight Mechanics and Control have made my experience at the University of Stuttgart very memorable.

On a personal note, I would like to thank my family for their encouragement and support. Finally, my heartfelt thanks to Sandra for her love and understanding.

Stuttgart, January 2003

Thomas Mannchen

Contents

Notation

Symbols

Listed below alphabetically are the principle symbols used in this text. Locally defined symbols that only appear in one section are not included.

a	Acceleration (with subscript) Blade section lift-curve slope
A	Rotor disk area State-space matrix
B	State-space matrix
c	Blade chord
c_d	Section drag coefficient
C	Damping coefficient State-space matrix
C_T	Thrust coefficient
C_ζ	Lag damper constant
d	Disturbance at plant output
d'	Disturbance at plant input
D	State-space matrix
e	Hinge offset
F	Control term Force (with subscript)
F_l	Lower linear fractional transformation
F_∞	State feedback matrix
g	Structural damping
G	System
H	Actuator dynamics
I	Generalized mass (with subscript) Identity matrix Moment of inertial (with subscript)
j	Imaginary unit

K	Controller Gain matrix Spring constant
K_β	Flap hinge spring constant
K_ζ	Lag hinge spring constant
m	Blade index Blade mass per unit length Generalized mass
M	Generalized mass Moment (with subscript)
N	Blade root moment (with subscript) Number of rotor blades
p	Integer variable
P	Plant
q	Generalized coordinate
r	Blade radial coordinate Reference signal
s	Laplace variable
S	Shear force (with subscript) State reduction matrix
S_u	Input sensitivity
S_y	Output sensitivity
t	Time
T	Period Thrust
T_u	Complementary input sensitivity
T_y	Complementary output sensitivity
u	Air velocity of blade section (with subscript) Input vector
u'	Input vector with disturbance
v	Control deviation
V	Helicopter or rotor velocity with respect to air
w	Exogenous input
W	Weighting function (with subscript)
x	In-plane deflection State vector
y	Output vector
z	Controlled output Out-of-plane deflection

α	Angle of attack
$\alpha_r r + \alpha_0$	Linear blade twist
β	Blade flap angle
β_p	Precone angle
β_0	Coning angle
γ	Angular mode shape Blade lock number ∞-norm of $F_l(P, K)$
δ	Degree of freedom
Δ_u	Multiplicative input uncertainty
Δ_y	Multiplicative output uncertainty
ζ	Blade lag angle Critical damping
η	Mode shape Noise signal
θ	Blade pitch angle
λ	Rotor inflow ratio
μ	Rotor advance ratio
ν_β	Rotating natural frequency of blade fundamental flap mode
ν_ζ	Rotating natural frequency of blade fundamental lag mode
ξ	Linear mode shape
ρ	Air density
σ	Singular value
ψ	Azimuth angle Dimensionless time
ω	Natural frequency
Ω	Rotor rotational speed

Suffices

$0, 1c, 1s, nc, ns$	Harmonics of a sine/cosine Fourier series
$0, 1c, 1s, nc, ns, d$	Degrees of freedom of the Fourier coordinate transformation
$(1), \ldots, (N)$	Blade degrees of freedom
0	Nominal
∞	Related to H_∞ control
con	Control

F	Flap
G	Plant
H	Actuator
K	Controller
L	Lag
m	Blade index
N	Normal
opt	Optimum
R	Radial
T	Tangential
x, y, z	x , y , z axis

Acronyms

BVI	Blade vortex interaction
IBC	Individual blade control
IBRC	Individual blade root control
imag	Imaginary part
LFT	Linear fractional transformation
MBC	Multiblade coordinates
MIMO	Multi input multi output
real	Real part
rev	Time unit rotor revolution
/rev	Frequency unit per rotor revolution
SBC	Single blade coordinates
SISO	Single input single output

Operators

$\dot{(\ )}$	$d(\ )/dt$ or $d(\ )/d\psi$
$(\ )'$	$d(\ )/dr$
diag( )	Diagonal matrix
rank( )	Rank
Ric( )	Symmetric, positive semi-definite stabilizing solution to the algebraic Riccati equation with the corresponding Hamiltonian matrix
$\rho(\ )$	Spectral radius

Abstract

This dissertation presents a control law for helicopters to reduce vibration and to increase damping using individual blade control. H_∞ control synthesis is used to develop a robust controller usable in different operating conditions with different helicopter flight speeds. The control design is applied in simulation to the four-blade BO 105 helicopter rotor, which is equipped with an individual blade control system, where the pitch rod links are replaced by hydraulic actuators, allowing blade pitch control to be superimposed to the swashplate commands.

Either oscillatory hub loads can be reduced or fuselage vibration can be targeted directly. As concerns hub loads, vibration can be cancelled (-99%) in three outputs simultaneously, e.g. in all three hub forces or in the vertical hub force and in the roll and pitch moments. A number of more than three outputs exceeds the number of three degrees of freedom available for vibration reduction of the four-blade rotor. Vibration can then only be reduced moderately, e.g. by -49%, for all three hub forces and for the two moments about the roll and pitch axis. Reducing hub vibration, however, does not necessarily lead to reduced vibration in the cabin. When individual blade control inputs, aimed at minimizing hub loads, are introduced, fuselage accelerations increase by a factor of up to three.

Therefore, a finite-element model of the flexible fuselage is coupled with the aeromechanical rotor model. The resulting coupled rotor-fuselage model allows vibration to be calculated and controlled at locations in the cabin, such as at the pilot and copilot seats and in the load compartment. In simulation, a simultaneous vibration reduction of -89% is achieved at the pilot and copilot seats.

The control law is developed with the constraint of no sensors and, consequently, no measurements in the rotating blades. However, to increase lag damping, the lag rates must be fed back. The use of a model-based control strategy enables lag damping to be enhanced from 0.5% to >3% critical damping by feeding back the observed lag rates, only requiring measurements of the hub loads.

In order to consider the periodicity of the plant in the controller design, a time-periodic gain-scheduled controller is developed. The results of the simulation confirm the common viewpoint that incorporating more knowledge about the plant into the controller, instead of designing a more robust and thus conservative controller, improves performance or robustness against other influences.

Kurzfassung

Vibrationen im Hubschrauber

Im Flugzeug werden die verschiedenen Aufgaben von einzelnen Komponenten übernommen, d.h. Triebwerke erzeugen Schub, Flügel produzieren Auftrieb und Ruder erlauben die Steuerung. Im Gegensatz dazu produziert der Rotor des Hubschraubers gleichzeitig Auftrieb sowie Vortriebskraft und ermöglicht die Steuerung, was zu einer hohen Komplexizität des Rotorsystems führt.

Zusätzlich zur Komplexizität des Systems befindet sich der Rotor auch in einer komplexen aerodynamischen Umströmungssituation. Abb. 1.1 fasst die Effekte im Zusammenhang mit der Hubschrauberaerodynamik zusammen. Die im stationären Fall periodischen, auf das Rotorblatt wirkenden aerodynamischen Lasten variieren beträchtlich während eines Rotorumlaufes. Im Vorwärtsflug ist die Anströmgeschwindigkeit der Rotorblätter von ihrer Azimutposition abhängig. Die rotationsbedingte Relativgeschwindigkeit der Luft und die Fluggeschwindigkeit des Hubschraubers addieren sich für das vorlaufende Blatt, wogegen das rücklaufende Blatt eine reduzierte Anströmgeschwindigkeit aufgrund der Subtraktion der Komponenten erfährt. Dies kann zu transsonischen Bedingungen am vorlaufenden und zu Rückanströmgebieten am rücklaufenden Rotorblatt führen. Diese veränderlichen aerodynamischen Effekte sowie Pilotenkommandos durch die Taumelscheibe und Blattwirbelinteraktionen (“blade vortex interactions”, BVI) sind Ursachen für Schwingungen in den elastischen Blättern, welche dann durch die Rotornabe weitergeleitet werden und zu Vibrationen in der Hubschrauberkabine führen.

Im stationären Flug sind die Blattlasten und Blattbewegungen identisch. Wird keine Rotorunwucht angenommen, löschen sich die Kräfte der einzelnen Blätter an der Rotornabe aus, mit Ausnahme der harmonischen Lasten mit ganzzahligen (p) Vielfachen der Frequenz N pro Umdrehung (pN pro Umdrehung, “pN per revolution, pN/rev”) und $pN \pm 1$/rev im rotierenden System, welche als pN/rev Lasten in das nichtrotierende System übertragen werden [43], wobei N für die Rotorblattanzahl steht. Der Rotor wirkt damit als Frequenzfilter. Da die Vibrationen der ersten harmonischen Blattfolgefrequenz (“blade passage frequency”) N/rev $(28.264\,\text{Hz})$ dominant sind, wird in der vorliegenden Arbeit ausschließlich diese Frequenz betrachtet. Abb. 1.2 zeigt ein typisches Amplitudenspektrum der Vibrationen eines BO 105 Hubschraubers im Reiseflug.

Im Schwebeflug ist die Umströmungssituation des Rotors nahezu achsensymmetrisch und die Vibrationen sind niedrig. Generell steigt das Vibrationsniveau mit zunehmender Fluggeschwindigkeit an, was auf die zunehmende Asymmetrie der Strömung und die zunehmende harmonische Komponente der Blattschlagbewegung zurückzuführen ist [13]. Bei geringer Vorwärtsfluggeschwindigkeit, bei Fortschrittsgraden von $\mu \approx 0.1$, wird typischerweise ein Maximum in der Vibrationsamplitude aufgrund von Blattwirbelinteraktionen beobachtet. Blattwirbelinteraktionen verursachen deutlich größere höherharmonische Luftkräfte, welche durch die Rotornabe als Vibrationen weitergeleitet werden. Flugmanöver, wie beispielsweise eine Fluggeschwindigkeitsverringerung oder langsamer Sinkflug, durch welche der Rotornachlauf nahe bei der Rotorebene verbleibt, erhöhen die Vibrationen zusätzlich. Mit steigender Fluggeschwindigkeit entfernt sich der Nachlauf zunehmend von der Rotorebene und die nachlaufbedingten Vibrationen nehmen ab. Mit weiter steigender Fluggeschwindigkeit nehmen die Vibrationen wieder zu, hauptsächlich aufgrund höherharmonischer Lasten durch Strömungsabriss am rücklaufenden Blatt und durch Kompressibilitätseffekte auf der vorlaufenden Seite [43]. Abb. 1.3 zeigt einen typischen Verlauf der Vibrationsamplitude in Abhängigkeit von der Fluggeschwindigkeit.

Einzelblattregelung

Konzepte zur aktiven Vibrationsreduktion sind die höherharmonische Regelung (“higher harmonic control”, HHC) und die Einzelblattregelung (“individual blade control”, IBC). Die Zielsetzung beider Methoden ist die Erzeugung von Zusatzkräften und -momenten am Rotor mit gleicher Amplitude, aber entgegengesetzter Phase, zu den ursprünglichen Kräften und Momenten. Die Überlagerung führt zu destruktiver Interferenz und die ursprünglichen Vibrationen werden folglich reduziert oder idealerweise ausgelöscht. Bei HHC befinden sich die Aktuatoren unterhalb der Taumelscheibe, womit die Steuerung im nichtrotierenden System stattfindet [66], [81]. Das aktuellere Konzept der IBC hebt einige Einschränkungen im Zusammenhang mit HHC über die Taumelscheibe auf [33]. Bei IBC werden die Rotorblätter einzeln im rotierenden System angesteuert. Blattwurzelsteuerung (“individual blade root control”, IBRC) steht für die Veränderung der Anstellwinkel der Rotorblätter an der Blattwurzel. Dazu werden die umlaufenden Steuerstangen, welche die starre Verbindung zwischen Taumelscheibe und Blattanlenkhebel darstellen, durch hydraulische Aktuatoren ersetzt, womit eine der Taumelscheibe überlagerte Ansteuerung der Rotorblätter ermöglicht wird.

In dieser Arbeit wird der Vier-Blatt-Rotor eines BO 105 Hubschraubers betrachtet, welcher mit einer Blattwurzelsteuerungsanlage ausgestattet ist [85], [91], [106], vgl. Abb. 1.4. Die Aktuatorik besteht aus einer konventionellen Taumelscheibe und durch Hydraulikaktuatoren ersetzten umlaufenden Steuerstangen. Die primäre Flugregelung erfolgt konventionell durch die Taumelscheibe. Die sekundäre Vibrationsregelung nutzt die überlagerte Ansteuerung der Blattanstellwinkel durch die hydraulischen Aktuatoren im drehenden System.

Abb. 1.5 zeigt die Rotornabe mit dem IBC System des BO 105 Hubschraubers. Eine Nahaufnahme des hydraulischen Aktuators sowie das IBC Konzept wird in Abb. 1.6 gezeigt.

Ein Vorteil der Blattwurzelsteuerung gegenüber anderen Methoden der IBC, wie beispielsweise Klappen im Außenbereich der Rotorblätter, Verdrehung der gesamten Rotorblätter usw., besteht darin, dass keine Veränderung am Blatt selbst erforderlich ist. Folglich müssen die Rotorblätter nicht neu zertifiziert werden. Die Verwendung der Originalblätter bedeutet jedoch, dass keine Blattsensoren zur Verfügung stehen, und damit auch keine Messungen im rotierenden System möglich sind. Die alleinige Verfügbarkeit von Rotornabenlasten (und gegebenenfalls Zellenbeschleunigungen) bringt gewisse Einschränkungen für das Regelsystem mit sich.

Einsatzmöglichkeiten der Einzelblattregelung sind eine Flugbereichserweiterung und eine Steigerung der Akzeptanz des Hubschraubers durch die Besatzung, die Passagiere und die Bevölkerung. Dies wird erreicht durch eine Reduktion von

- Vibrationen,
- flugmechanischen und aeromechanischen/aeroelastischen Instabilitäten,
- Lärm und
- Leistungsbedarf.

Vibrationsreduktion steigert nicht nur den Passagierkomfort, sondern wirkt sich auch positiv auf die Lebensdauer von Struktur und Systemen des Hubschraubers aus. Damit steht die Vibrationsreduktion in direktem Zusammenhang mit den Kosten. Nach einer Studie von Sikorsky [86] führt eine Vibrationsreduktion um 30% zu einer Reduktion der direkten Betriebskosten um 20%. Die Ergebnisse einer von Westland durchgeführten Studie zeigen, dass eine einprozentige Vibrationsreduktion zu einer einprozentigen Reduktion der ungeplanten Instandhaltungskosten führt [86].

Der im Sinkflug auftretende Blattinteraktionslärm kann durch IBC reduziert werden [49], [98], [110]. Im schnellen Reiseflug kann durch IBC der auftretende Verdichtungsstoß destabilisiert werden, womit eine Reduktion des Hochgeschwindigkeits-Impulslärms möglich ist [55]. Eine Verzögerung oder Unterdrückung des dynamischen Strömungsabrisses (“stall delay”) ist eine weitere IBC Anwendung, welche zu einem reduzierten Leistungsbedarf führt [46], [48], [84]. IBC kann ebenfalls zur automatischen Blattlaufspureinstellung (“auto-tracking”) verwendet werden.

Lärm- und Vibrationsreduktion können widersprüchliche Anforderungen darstellen [41]. Diesem Konflikt könnte begegnet werden, indem während Start und Landung in dicht besiedelten Gebieten (in der Nähe von Krankenhäusern usw.) die Zielsetzung Lärmreduktion vorrangig verfolgt wird, wogegen im Reiseflug das Augenmerk auf die Vibrationsreduktion gerichtet wird.

Problemstellung

Die Hubschrauber-Vibrationsreduktion gehört zur Klasse der Vibrationsreduktionsaufgaben für Regelstrecken mit periodischen Koeffizienten. Hier ist die Periodizität eine Folge der Rotormechanik und damit unvermeidbar. Ein linear zeitperiodisches System antwortet auf eine Sinusanregung nicht wie bei linear zeitkonstanten Systemen nur mit einem Sinussignal der Anregungsfrequenz, sondern auch mit zusätzlichen Frequenzen. Folglich ist eine schmalbandige Störungsunterdrückung für periodische Systeme beträchtlich komplexer als für zeitkonstante Systeme und es ist zu erwarten, dass periodische Regler besser zur Regelung geeignet sind [23].

Die Analyse und Regelung von zeitdiskreten periodischen Systemen ist in der Literatur ausführlich behandelt (vgl. Übersicht in [10]). Häufig verwendet wird eine kanonische Beziehung zwischen einem zeitdiskreten periodischen System mit p Ausgängen, q Eingängen, n Zuständen und m-facher Periodizität und einem diskreten zeitkonstanten "lifted" System mit mp Ausgängen, mq Eingängen und n Zuständen [65], [45]. In der "lifted" Darstellung erhöht sich die Dimension der Ein- und Ausgangsvektoren, während die Zahl der Zustände unverändert bleibt. In der "cyclic" [32] Formulierung des Systems erhöht sich auch die Dimension des Zustandsvektors, was zu einem diskreten zeitkonstanten System mit mp Ausgängen, mq Eingängen und mn Zuständen führt. Der Vorteil der "lifted" und "cyclic" Formulierung ist die Verwendbarkeit von zeitkonstanten Analyse- und Synthesemethoden [23]. Dieser Ansatz führt jedoch zu erheblich vergrößerten Systemdimensionen und kann somit für komplexe System unpraktikabel werden. Die vorliegende Arbeit konzentriert sich daher direkt auf das periodische System, ohne vorherige Diskretisierung und anschließende zeitkonstante Umformulierung. Die Entwicklung eines zeitperiodisch verstärkungsangepassten Reglers ("time-periodic gain-scheduled controller") sowie die Erweiterung von zeitkonstanten Modellreduktionsverfahren auf den periodischen Fall stellen zwei der wichtigsten Beiträge dieser Arbeit dar.

Die schwach gedämpfte Schwenkbewegung der Rotorblätter ist anfällig für verschiedene aeroelastische und aeromechanische Instabilitäten. Daher haben die meisten Rotoren mechanische Schwenkdämpfer, welche eine künstliche Dämpfung zur Vermeidung dieser aeromechanischen Phänomene bereitstellen [54]. Die Einzelblattregelung kann ebenfalls zur aktiven Dämpfungserhöhung eingesetzt werden [38]. Der physikalische Mechanismus der Dämpfungserhöhung ist bekannt (vgl. Kapitel 6.4). Wenn jedoch der Vorteil der Blattwurzelsteuerung (d.h. die Verwendbarkeit unveränderter Rotorblätter) genutzt werden soll, werden Regelungskonzepte ohne Messung der Schwenkrate benötigt. Die detaillierte Analyse der Steuer- und Beobachtbarkeit des Systems vom nichtrotierenden System aus sowie die Entwicklung eines robusten beobachterbasierten Reglers zur Dämpfungserhöhung stellen weitere Hauptbeiträge dieser Arbeit dar.

Das Ziel der Hubschrauber-Vibrationsreduktion ist letztlich nicht die Reduktion von periodischen Lasten an der Rotornabe, sondern an bestimmten Positionen in der Zelle, wie der

des Piloten- und Kopilotensitzes sowie des Laderaums. Bei der Einsteuerung von höherharmonischen Signalen zur Reduktion von Nabenvibrationen wurde in [33] eine Erhöhung von Zellenvibrationen um einen Faktor von zwei bis fünf festgestellt. Dies zeigt, dass ein als Reglerentwurfsgrundlage dienendes Modell sowohl die Rotor- als auch die Zellendynamik enthalten muss. Die Kopplung eines Finite-Elemente-Modells des BO 105 Hubschraubers mit dem aeromechanischen Rotormodell und die Entwicklung von darauf basierenden Reglern zur Minimierung von Zellenvibrationen stellen weitere Hauptbeiträge dieser Arbeit dar.

Zielsetzung und Aufbau der Arbeit

Die Zielsetzung dieser Arbeit ist die Entwicklung eines Regelgesetzes für einen Hubschrauber mit Einzelblattsteuerung zur Vibrationsreduktion und Dämpfungserhöhung. Benötigte Steuergrößen sind Regelstreckeneingänge, die den Auftrieb der einzelnen Blätter beeinflussen. Dies kann generell durch beliebige Aktuatoren im rotierenden System erfolgen, z.B. durch Klappen im Außenbereich der Blätter, durch aktive Verdrehung des gesamten Blattes oder durch Blattwurzelaktuatoren. Hier wird der Reglerentwurf für den oben beschriebenen BO 105 Hubschrauber mit Blattwurzelsteuerung durchgeführt.

Der Aufbau der Arbeit ist wie folgt: Der Einleitung (Kapitel 1) folgt eine detaillierte Beschreibung und Analyse zweier unterschiedlicher Rotormodelle in Kapitel 2. Ein einfaches analytisches Modell wird entwickelt und zur Analyse grundsätzlicher Rotorphänomene herangezogen. Ein komplexes aeromechanisches Modell, welches als Grundlage für den Reglerentwurf dient, wird detailliert beschrieben und untersucht. In Kapitel 3 wird das Potenzial von IBC zur Vibrationsreduktion analysiert. Modellreduktionstechniken für lineare, zeitkonstante Systeme werden in Kapitel 4 auf den zeitperiodischen Fall erweitert. In Kapitel 5 werden Grundlagen des H_∞-Verfahrens und die Details des Reglerentwurfs beschrieben. Kapitel 6 präsentiert die Ergebnisse. Eine Zusammenfassung sowie ein Ausblick auf zukünftige Arbeiten ist in Kapitel 7 enthalten.

Modellbeschreibung und Analyse

Ein analytisches Modell eines N-Blatt-Rotors wird entwickelt[1] [52], [93], [43]. Das analytische Modell wird zur Analyse der grundlegenden Rotoreigenschaften, der Schlag- und Schwenkbewegung, der Lasten, der Vibrationen und des Filtereffektes des Rotors herangezogen. Grundsätzliche Aspekte der Zeitabhängigkeit der Regelstrecke werden untersucht und die Multiblattkoordinaten-Transformation [39] wird eingeführt.

Ein mit der kommerziellen Hubschrauber-Analysesoftware Camrad II entwickeltes komplexes aeromechanisches Analysemodell [42], [43], [44], welches detaillierte Rotoraerodyna-

1. Das Modell ist in nichtlinearer und linearer Form als C-Programm und in Zustandsraumdarstellung verfügbar, siehe Anhang A.2.

mik, Kinematik und Dynamik umfasst, wird sowohl im Zeitbereich als auch im Frequenzbereich in Hinblick auf die Reglerentwicklung untersucht. Ein Finite-Elemente-Modell der Hubschrauberzelle [100] wird verwendet, um elastische Bewegungsformen der Zelle zu ermitteln. Diese Bewegungsformen werden in das Camrad II Modell implementiert und mit dem Rotor gekoppelt [97], so dass Vibrationen an Positionen in der Kabine berechnet und geregelt werden können.

Von der Periodizität der Strecke herrührende Aspekte der Regelstrecke und deren Auswirkungen auf die Reglerentwicklung werden diskutiert. Hierbei erfährt das Zusammenspiel der Fourier Koordinatentransformation, der multiharmonischen Antwort des periodischen Systems und der Frequenzfiltereffekt des Rotors große Beachtung. Durch die Verwendung von Multiblattkoordinaten kann das System von dem Streckeneingang in Multiblattkoordinaten auf den Ausgang der Rotornabenlasten linearisiert werden. Beide Signale sind im nichtrotierenden System definiert. Dieses System kann zeitlich über einen Rotorumlauf gemittelt werden, ohne alle periodischen Einflüsse zu verlieren, da einzelharmonische Übertragungen der Frequenz 4/rev "intern" die physikalischen 3/rev, 4/rev und 5/rev Übertragungspfade des periodischen Systems enthalten. Dies erlaubt die Anwendung der großen Palette von zeitkonstanten Reglerentwurfsverfahren auf den zeitperiodischen Rotor.

Einfluss der Blattanzahl

Für eine Familie von fiktiven Rotoren unterschiedlicher Blattanzahl für ein und denselben Hubschrauber werden Reglerentwürfe mit unterschiedlicher Anzahl der zu regelnden Ausgangsgrößen durchgeführt. Zielsetzung dieser Analyse ist die Untersuchung des Einflusses der Blattanzahl auf das Vibrationsreduktionspotenzial von IBC. Die Regelung erfolgt mittels optimaler Ausgangsvektorrückführung.

Das Ergebnis der Untersuchung besagt, dass bei Rotoren mit drei oder vier Blättern drei Freiheitsgrade zur Verfügung stehen und damit Vibrationen in maximal drei unabhängigen Ausgängen ausgelöscht werden können. Ab einer Blattanzahl von fünf weist der Rotor fünf Freiheitsgrade auf, die zur Auslöschung von Vibrationen in maximal fünf unabhängigen Ausgängen verwendet werden können. Die Simulationsergebnisse werden durch Singulärwertbetrachtungen bestätigt.

Modellreduktion

Eine Modellreduktion ist erforderlich, da in der modellbasierten Reglerentwurfsmethode H_∞ die Ordnung des Reglers von der Ordnung des im Entwurf verwendeten Streckenmodells abhängt und eine möglichst niedrige Reglerordnung angestrebt wird. Generell können das Streckenmodell, der Regler selbst oder beide einer Modellreduktion unterzogen werden. Hier wurde die Ordnung des Streckenmodells reduziert, womit ein reduziertes Entwurfsmodell und ein nichtreduziertes Ausgangsmodell für Verifikationszwecke zur Verfügung steht.

Die periodischen Rotormodelle werden in Multiblattkoordinaten transformiert und die Zustandsraummatrizen in Fourier-Reihen entwickelt. Mittels klassischer Reduktionsverfahren wird aus dem konstanten Anteil des transformierten Systems eine Zustandsreduktion bestimmt. Diese Zustandsreduktion wird anschließend auf die Fourierkoeffizienten angewendet. Die so abgeleiteten periodischen, reduzierten Modelle erwiesen sich als funktionierende Grundlage für periodische Reglerentwürfe.

Die beiden Hauptzielsetzungen des Reglerentwurfs lauten Vibrationsreduktion und Dämpfungserhöhung. Aufgrund der getrennten Frequenzbereiche wird diese sekundäre Regelung als unabhängig von der primären Flugregelung angenommen.

Die Zielsetzung der Schwenkdämpfungserhöhung erfordert eine Rückführung der Schwenkrate der Blätter. Da keine Blattsensoren zur Verfügung stehen, wird eine beobachterbasierte Reglerarchitektur gewählt. Dies erlaubt die Rückführung der (beobachteten) Schwenkraten und damit eine Erhöhung der Dämpfung ohne dedizierte Sensoren im Blatt.

Um Abweichungen zwischen der physikalischen Strecke und deren mathematischer Beschreibung bereits im Entwurf zu berücksichtigen und um den Regler robust gegenüber der Fluggeschwindigkeit zu machen, wurde die H_∞-Regelung als Entwurfsmethode gewählt. Aufgrund der größeren Flexibilität wurde der Entwurf am geschlossenen Kreis durchgeführt.

Die Reglerentwurfsziele werden als Anforderungen an die maximalen Singulärwerte der Übertragungsfunktionen formuliert. Aufgrund algebraischer Einschränkungen können diese Anforderungen nicht über den gesamten Frequenzbereich erfüllt werden, so dass frequenzabhängige Gewichtungsfunktionen $W(s)$ oder "gewünschte" Verläufe der Übertragungsfunktionen $W(s)^{-1}$ verwendet werden. Die verwendeten Gewichtungsfunktionen beziehen sich auf die Störgrößenunterdrückung, die Modellierung von Eingangs- und Ausgangsunsicherheiten, die Limitierung der Regelautorität und die Dämpfungserhöhung in bestimmten Bewegungsformen.

Die Anpassung der Gewichtungsfunktionen stellt ein komplexes Problem dar, insbesondere bei gleichzeitiger Berücksichtigung von Signalaspekten und Unsicherheiten. Daher wird die Einstellung der Gewichtungsfunktionen als Optimierungsproblem formuliert. Die Verstärkungen der Gewichtungsfunktionen werden als zu optimierende Parameter definiert. Die zu maximierende Kostenfunktion setzt sich aus den primären Reglerentwurfszielen wie Vibrationsreduktion und Dämpfungserhöhung zusammen. Trotz des hohen benötigten Rechenaufwandes erwies sich der Ansatz aufgrund der Systematisierung des Problems und der vollständigen Automatisierung der Optimierung als effizienter als ein manuelles Einstellen der Gewichtungsfunktionen.

Die zu reduzierenden Vibrationen wirken als Störung der Blattfolgefrequenz 4/rev am Streckenausgang auf den geschlossenen Kreis. Eine elementare Fragestellung ist die Auswahl der zu regelnden Ausgänge. Zur Vibrationsreduktion muss der Regler ein zur Störung

gegenphasiges Signal erzeugen. Dass dies nicht für eine beliebige Anzahl von Ausgängen möglich ist, wird mittels einer Rangbetrachtung gezeigt.

Der Regler wird in Beobachterform mit Zustandsvektorrückführung realisiert. Dies erlaubt im zeitperiodischen Reglerentwurf eine zeitperiodische Anpassung der Verstärkungsmatrizen.

Ergebnisse

Der auf einem Modell reduzierter Ordnung basierende Regler wird im geschlossenen Kreis mit dem nichtreduzierten Verifikationsmodell sowohl im Auslegungsfall (hohe Reiseflugeschwindigkeit) als auch an einem anderen Arbeitspunkt im langsamen Sinkflug simuliert. Im Auslegungsfall löscht der Regler Vibrationen in drei ausgewählten Ausgängen vollständig aus (-99%). Obwohl die Leistung desselben Reglers im Nichtauslegungsfall etwas reduziert ist, findet im Langsamflug noch eine deutliche Vibrationsreduktion (-96%) statt, was die Robustheit des Reglers gegenüber der Fluggeschwindigkeit demonstriert. Im nächsten Schritt der Überprüfung wird der Regler mit dem zeitperiodischen Streckenmodell simuliert. Hier werden Vibrationen um -91% reduziert. Trotz leichter Leistungseinbußen gegenüber dem zeitkonstanten Auslegungsfall verdeutlicht dieses Ergebnis, dass die Robustheit des Reglers die Abweichungen zwischen zeitkonstantem Auslegungsmodell und zeitperiodischem Simulationsmodell abdeckt.

Zur Verifikation des Ansatzes, die direkte Lösung von zeitperiodischen Riccati Gleichungen im Reglerentwurf durch gleichmäßig über einen Rotorumlauf verteilte Lösungen von zeitkonstanten Riccati Gleichungen zu approximieren, wird die Floquet-Lyapunov Theorie herangezogen. Dazu wird zunächst die zeitperiodische Systemmatrix des geschlossenen Regelkreises, bestehend aus zeitperiodischem Regler und zeitperiodischer Strecke, gebildet. Die resultierenden Poincaré Exponenten des Floquet-Lyapunov-transformierten Systems werden dann mit den Erwartungen aufgrund der Eigenwerte des zeitkonstanten Systems verglichen. Die Übereinstimmung validiert die näherungsweise Berechnung des zeitperiodischen Entwurfsproblems.

Simulationsergebnisse mit dem zeitperiodisch verstärkungsangepassten Regler (“time-periodic gain-scheduled controller”) zeigen, dass die erzielte Vibrationsreduktion vergleichbar mit der des zeitkonstanten Reglers ist. Der periodische Regler verwendet jedoch die differenzielle Bewegungsform, welche im periodischen System (im Gegensatz zum zeitkonstanten System) nicht reaktionslos ist. Der durch die Berücksichtigung der Periodizität im Entwurf gewonnene zusätzliche Freiheitsgrad wird zur Steigerung der Robustheit des Reglers verwendet, was durch eine Fallstudie belegt wird.

Das Ziel der Hubschrauber-Vibrationsreduktion ist letztlich nicht die Reduktion von Vibrationen an der Rotornabe, sondern an bestimmten Punkten innerhalb der Zelle, wie beispielsweise der des Piloten- und Kopilotensitzes und des Laderaums. Simulationen mit dementsprechend auslegten Reglern zeigen, dass es möglich ist, Vibrationsreduktionen von

–89% am Piloten- und Kopilotensitz zu erzielen, wobei jedoch eine Vibrationserhöhung von +32% im Laderaum verzeichnet wird. Bei Konzentration auf die Laderaumposition kann eine Vibrationsreduktion von –80% erreicht werden, jedoch begleitet von einer Zunahme der Werte am Piloten- und Kopilotensitz um +81%. Die gleichzeitige Berücksichtigung des Piloten- und Kopilotensitzes sowie des Laderaums erlaubt eine durchschnittliche Vibrationsreduktion um –47%. Wie aufgrund der Tatsache erwartet, dass im letzteren Fall mehr Ausgangsgrößen ausgewählt wurden als Freiheitsgrade zur Verfügung stehen, ist die erzielte Vibrationsreduktion geringer als bei der Betrachtung einzelner Punkte.

Die Rotornabenlasten wurden durchschnittlich um +293% erhöht. Vergleichbare Resultate wurden in [33] beobachtet, wo die vertikalen Rotornabenkräfte um den Faktor drei bis sechs anstiegen, wenn HHC zur Vibrationsreduktion in der Zelle betrieben wurde. Dies verdeutlicht, dass eine Vibrationsreduktion mit der Zielsetzung, Zellenbeschleunigungen zu reduzieren, nicht zwangsläufig zu reduzierten Nabenvibrationen führt (und umgekehrt).

Das Reglerentwurfsziel Dämpfungserhöhung in den Schwenkeigenformen kann für die zyklischen Bewegungsformen ohne Schwierigkeiten erreicht werden. Im Gegensatz dazu kann eine Erhöhung der Schwenkdämpfung in der kollektiven Bewegungsform nur dann erzielt werden, wenn eine Messung des Antriebsmomentes M_z verfügbar ist. Mittels des zeitperiodischen Reglers kann auch eine Dämpfungserhöhung in der differenziellen Bewegungsform der Schwenkbewegung erreicht werden, welche im zeitkonstanten Fall reaktionslos und damit nicht beeinflussbar ist.

Zusammenfassung

Es wurde ein Regelgesetz zur Vibrationsreduktion und Schwenkdämpfungserhöhung für Hubschrauber mit Einzelblattsteuerung entwickelt. Das verwendete H_∞-Reglerentwurfsverfahren erlaubte die Entwicklung eines robusten Reglers basierend auf einem reduzierten Modell, welcher an Arbeitspunkten mit unterschiedlicher Fluggeschwindigkeit zur Vibrationsreduktion eingesetzt werden kann. Die erzielte Dämpfungserhöhung führt zu einer deutlich reduzierten Böenempfindlichkeit.

Ein einfaches analytisches Modell eines N-Blatt-Rotors wurde entwickelt, welches die grundlegenden Eigenschaften des Rotors sowie die Schlag- und Schwenkdynamik der Rotorblätter beschreibt. Dieses Modell wurde zur Untersuchung des Potenzials der Einzelblattsteuerung sowie des Einflusses der Blattanzahl verwendet.

Die Reglerentwürfe und Simulationen basieren auf einem umfangreichen aeromechanischen Analysemodell, welches komplexe Aerodynamik sowie detaillierte Kinematik und Dynamik umfasst und mit der kommerziellen Hubschrauber-Analysesoftware Camrad II berechnet wurde.

Werden Rotornabenlasten als Zielgrößen der Vibrationsreduktion betrachtet, ist eine Auslöschung der Vibrationen (–99%) in drei Größen gleichzeitig möglich, z.B. in allen drei

Rotornabenkräften oder der vertikalen Rotornabenkraft und den Rotornabenmomenten um die Roll- und Nickachse. Wird derselbe Regler, der für hohe Reisefluggeschwindigkeit ausgelegt war, an einem anderen Arbeitspunkt im langsamen Sinkflug eingesetzt, wobei Vibrationen aufgrund von Blattwirbelinteraktionen auftreten, konnten Vibrationen noch um –96% reduziert werden. Dies demonstriert die robuste Einsetzbarkeit des Reglers. Eine Auswahl von mehr als drei Zielgrößen zur Vibrationsreduktion übersteigt die Anzahl von drei vorhandenen Freiheitsgraden eines Vier-Blatt-Rotors und Vibrationen können nur noch teilweise reduziert werden, z.B. um –49% bei gleichzeitiger Betrachtung aller drei Nabenkräfte und der beiden Nabenmomente um die Roll- und Nickachse. Generell führt jedoch eine Reduktion der Vibrationen an der Rotornabe nicht zwangsläufig zu einem reduzierten Vibrationsniveau in der Hubschrauberzelle. Die Zellenvibrationen wurden stattdessen durch eine Vibrationsreduktion an der Rotornabe um einen Faktor von bis zu drei erhöht.

Ein Finite-Elemente-Modell der flexiblen Hubschrauberzelle wurde mit dem aeromechanischen Rotormodell über die Rotornabe gekoppelt. Das resultierende gekoppelte Rotor-Zellenmodell erlaubt die Berechnung und Regelung der Vibrationen an Positionen in der Hubschrauberkabine, wie die der Piloten- und Kopilotensitze und des Laderaums. Durch die direkte Berücksichtigung von Zellenlasten konnten die Vibrationen am Piloten- und Kopilotensitz um –89% reduziert werden, unter Inkaufnahme eines um +32% erhöhten Vibrationsniveaus im Laderaum. Bei gleichzeitiger Berücksichtigung des Piloten- und Kopilotensitzes und des Laderaums konnte eine durchschnittliche Vibrationsreduktion von –47% erreicht werden. Durch die Reduktion von Zellenvibrationen wurden die oszillierenden Rotornabenkräfte und -momente um einen Faktor bis zu vier erhöht.

Die Verwendung einer modellbasierten Reglerstrategie erlaubte eine Erhöhung der Schwenkdämpfung von 0.5% auf bis zu >3% ohne Verwendung von Sensoren in den Rotorblättern. Da die Schwenkgeschwindigkeit der rotierenden Blätter aus Messgrößen im nichtrotierenden System rekonstruiert wird, ergeben sich gewisse Einschränkungen. Die Dämpfungserhöhung in den zyklischen Bewegungsformen des Rotors ist unproblematisch, wogegen für eine Dämpfungserhöhung in der kollektiven Bewegungsform eine Messung des Antriebsmomentes an der Rotornabe erforderlich ist. Die Schwenkdämpfung in der differenziellen Bewegungsform kann nur durch eine periodische Regelung erzielt werden.

Um die Periodizität der Regelstrecke bereits im Reglerentwurf berücksichtigen zu können, wurde ein zeitperiodisch verstärkungsangepasster Regler entwickelt (“time-periodic gain-scheduled controller”). Durch Simulationen konnte die Theorie bestätigt werden, dass die Verwendung von Informationen über die Regelstrecke, im Gegensatz zu der Entwicklung eines robusteren und damit konservativeren Reglers, zu einer verbesserten Leistungsfähigkeit oder zu einer erhöhten Robustheit gegenüber anderen Einflüssen führt.

Sowohl zeitkonstante als auch zeitperiodische Regler wurden auf der Grundlage reduzierter Modelle entworfen. Existierende Modellreduktionsverfahren für zeitkonstante Systeme wurden für den zeitperiodischen Fall erweitert. Die so erzeugten zeitperiodischen Modelle erwiesen sich als geeignet für den Entwurf von periodischen Reglern.

Eine optimierungsbasierte Prozedur zur Einstellung von Gewichtungsfunktionen wurde entwickelt. Damit konnte die Anpassung von Gewichtungsfunktionen systematisiert und Aspekte der gleichzeitigen Berücksichtigung mehrerer Modelle ("multi-model design") berücksichtigt werden.

In der Analyse des zeitperiodischen offenen und geschlossenen Regelkreises wurde die Floquet-Lyapunov Theorie eingesetzt. Im Reglerentwurf dagegen erwiesen sich Floquet-Lyapunov-transformierte Systeme nicht als geeignete Grundlage zur Reglerentwicklung. Es stellte sich heraus, dass das Floquet-Lyapunov-transformierte System, welches zwar definitionsgemäß eine konstante Systemmatrix A hat, eine beträchtlich erhöhte Periodizität in den Zustandsraummatrizen B und C aufwies. Folglich war die Gesamtperiodizität der Zustandsraumdarstellung (und damit der Fehler bei Vernachlässigung der höherharmonischen Terme) deutlich größer. Deshalb wurde zum Reglerentwurf eine Approximation mit konstanten Koeffizienten eines Fourier-transformierten Systems herangezogen. Dessen einzelharmonische $4/\mathrm{rev}$ Übertragungsfunktion von Einzelblattansteuerungen im nichtrotierenden Koordinatensystem auf (nichtrotierende) Rotornabenlasten enthält "intern" die physikalischen $3/\mathrm{rev}$, $4/\mathrm{rev}$ und $5/\mathrm{rev}$ Übertragungspfade des rotierenden Systems und ist daher als Entwurfsgrundlage ideal geeignet.

Die folgende Liste fasst die Beiträge dieser Arbeit zur aktiven Hubschrauber-Rotorblattregelung zusammen.

- Entwurf von BO 105 Reglern für verschiedene Zielsetzungen der Vibrationsreduktion (Nabenlasten oder Piloten-/Kopilotensitz und/oder Laderaum), welche robust gegenüber Änderungen in der Fluggeschwindigkeit sind.
- Entwicklung eines gekoppelten Rotor-Zellenmodells, welches eine Reduktion von Vibrationen in der Kabine erlaubt, was durch eine Reduktion von Rotornabenlasten im Allgemeinen nicht erreicht wird.
- Aktive Schwenkdämpfungserhöhung ohne spezielle Sensoren in den Rotorblättern.
- Entwicklung eines periodischen Reglers zur Regelung der "reaktionslosen" Eigenform vom nichtrotierenden System aus.
- Erweiterung von Modellreduktionsverfahren für kontinuierliche, lineare, zeitkonstante Systeme auf den zeitperiodischen Fall.
- Systematische Analyse, inwieweit der Anzahl der Freiheitsgrade zur Vibrationsreduktion von der Rotorblattanzahl abhängt.

Ausblick

Flugversuche mit dem entworfenen Regelgesetz sind mit dem BO 105 Hubschrauber mit Einzelblattansteuerung geplant. Um ein schrittweises Vorgehen zu erlauben, sollen zunächst Regler experimentell erprobt werden, welche nur eines der beiden Ziele, Vibrationsreduk-

tion oder Dämpfungserhöhung, berücksichtigen. Im Gegensatz zu klassischen Eingrößenreglern, bei denen einzelne Rückführverstärkungen manuell im Laufe einer Flugtestreihe erhöht werden können, soll eine Familie von Reglern mit zunehmender Regelautorität nacheinander getestet werden.

Eine interessante Forschungsrichtung wäre die Anwendung der entwickelten Regelstrategie auf ein anderes System der Einzelblattansteuerung im rotierenden System, wie beispielsweise Rotorblätter mit Klappen. Es wird angenommen, dass der Reglerentwurf für eine andere Aktuatorik ohne wesentliche Änderungen wiederholt werden kann, da eine veränderte Aktuatorik im Wesentlichen lediglich die Matrizen B und D der Zustandsraumdarstellung beeinflusst.

Darüber hinaus wäre ein Reglerentwurf für einen Rotor mit mehr als vier Rotorblättern interessant, da die bei einem solchen Rotor höhere Anzahl an Freiheitsgraden genutzt werden könnte.

Chapter 1
Introduction

1.1 Helicopter

In the classical aeroplane, each component serves only one main purpose. The wings generate lift, the engines produce thrust, and rudder, tailplane, and ailerons provide control. In helicopters, on the other hand, the rotor generates lift, produces the propulsive force, and provides control. This leads to considerable complexity in the rotor system.

The rotor blades are, in effect, long rotating wings of small chord. The blades are mounted on a turbine-driven shaft. As they move through the air, they generate lift in the same way as a fixed wing. The obvious advantage of rotary-wing aircraft over fixed-wing aircraft is that the rest of the aircraft does not need to move relative to the air, and it can, therefore, hover, take off, and land vertically.

A major problem with rotary-wing aircraft is that when the aircraft flies forwards, the blades advance into the oncoming flow on one side, while on the other side they retreat from it. If corrective measures were not taken, the blades would generate more lift on the advancing side on account of the greater relative velocity. This in turn would mean that the whole aircraft would tend to roll.

The normal method for overcoming this problem is to allow the blades to flap up and down by hinging them at their roots, near the rotor axis. On the advancing side, the increased lift tends to cause the blades to flap up and as they do so, the effective angle of attack is reduced. On the retreating side, the blades flap down, increasing the effective angle of attack, thereby tending to restore the lift. In order to reduce bending moments on the blade roots, the blades are also equipped with lag hinges.

On conventional helicopters, in addition to the blades being allowed to flap and lag, the blades are also provided with cyclic pitch control, a mechanism which can be used to alter the geometric incidence (pitch) of the blades cyclically as they rotate. In addition to the cyclic pitch control, the rotor head is equipped with a collective pitch control mechanism, which alters the average blade incidence setting of all the blades collectively, so as to increase or decrease the overall lift.

The advancing blade moves through the air at a considerably higher speed than the speed of the helicopter. The blade, therefore, will approach the speed of sound when the helicopter is still travelling at well below this speed. Because blades continually move in and out of supersonic flow, considerable aerodynamic and structural problems occur. [5]

1.2 Rotor Induced Vibration

As mentioned above, the helicopter rotor operates in a complex aerodynamic flow field. Figure 1.1 summarizes the effects associated with helicopter rotor aerodynamics. The aerodynamic loads on a rotor blade vary considerably as it moves around the rotor disc, and in steady flight these loads are periodic. In forward flight, the speed of the incoming flow for the rotor blades depends on their azimuthal position. The relative speed of air caused by rotation and the flight velocity of the helicopter are added together for advancing blades, whereas a retreating blade experiences reduced incoming flow speed due to subtraction of the components. This can lead to transonic conditions on the advancing side and to regions of reverse flow on the retreating side. These changing aerodynamic effects, as well as pilot inputs via the swashplate, and interactions of blades and vortices of preceding blades are causes of oscillations in the flexible rotor blades, which are transmitted through the rotor hub and cause vibration in the fuselage.

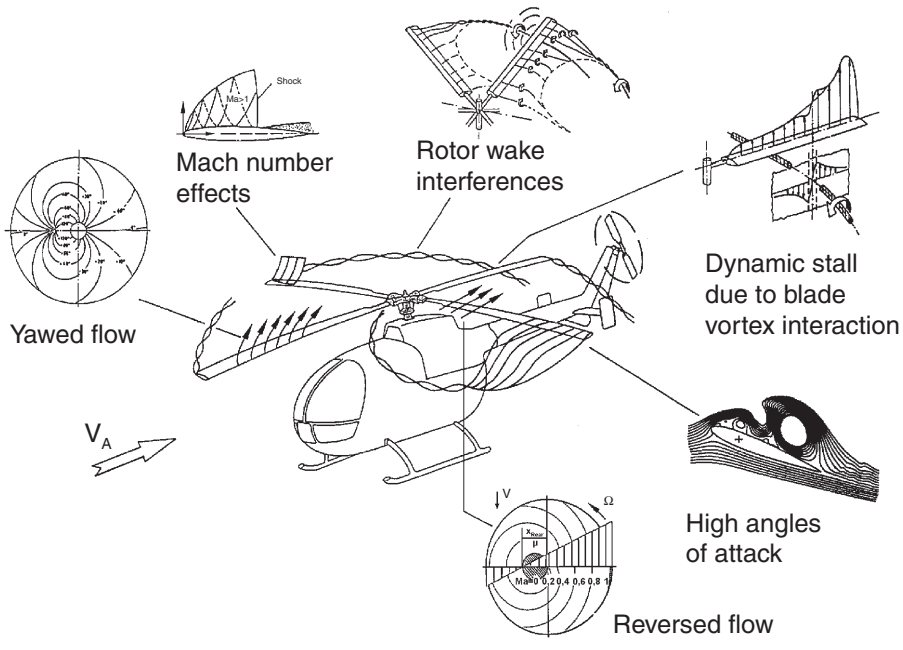

Figure 1.1 Aerodynamic effects associated with helicopter rotors [72]

In steady flight, the blades have identical loading and motion. Assuming there is no rotor imbalance, the forces from all the N blades cancel out at the hub, except for those harmonics at integer (p) multiples of the frequency N per revolution (pN/rev ; the rotor frequency

of the $N = 4$ blade BO 105 helicopter rotor is $1/\text{rev} = 7.066\text{Hz}$) and $pN \pm 1/\text{rev}$ in the rotating frame, which are transmitted to the helicopter fuselage as pN/rev loads in the non-rotating frame [43]. Thus, the rotor hub acts as a filter. Vibration at the first harmonic of the blade passage frequency N/rev (28.264Hz) is most dominant and it is this vibration that is targeted here for vibration reduction. Figure 1.2 shows a typical vibration amplitude spectrum of a BO 105 helicopter in a cruise flight condition.

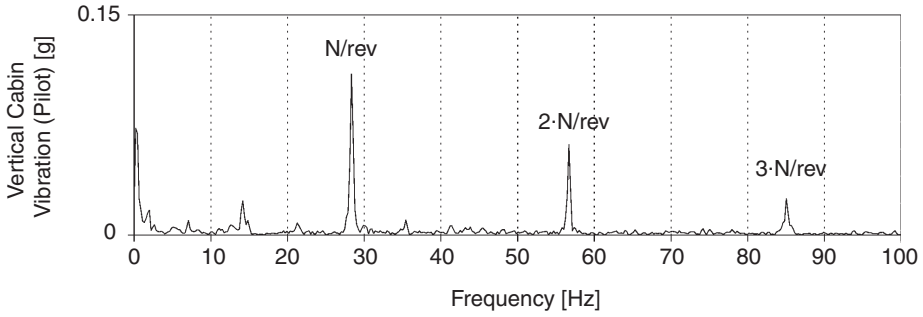

Figure 1.2 Vibration amplitude spectrum BO 105 in level cruise flight [29]

Helicopter vibration is low in hover where the aerodynamic environment is almost axisymmetric. The level of vibration generally increases with speed; this is attributed to the increasing asymmetry of the rotor thrust loading and the corresponding increase of the harmonic content in the blade flapping [13]. At low forward flight speeds, at advance ratios of around $\mu \approx 0.1$, there is typically a peak in the vibration level due to the wake-induced loads on the rotor, see Figure 1.3. Blade vortex interactions produce significantly higher harmonic airloading at the harmonics transmitted through the hub as vibration. The vibration is increased by maneuvers that retain the wake near the plane of the disk, such as decelerating or descending flight. As the speed increases, the wake is convected away from the disk plane and the wake-induced vibration decreases. At still higher flight velocities, the vibration again increases, primarily as a result of the higher harmonic loading produced by stall at the retreating blade and compressibility effects at the advancing side [43]. Figure 1.3 shows a typical vibration amplitude as a function of airspeed.

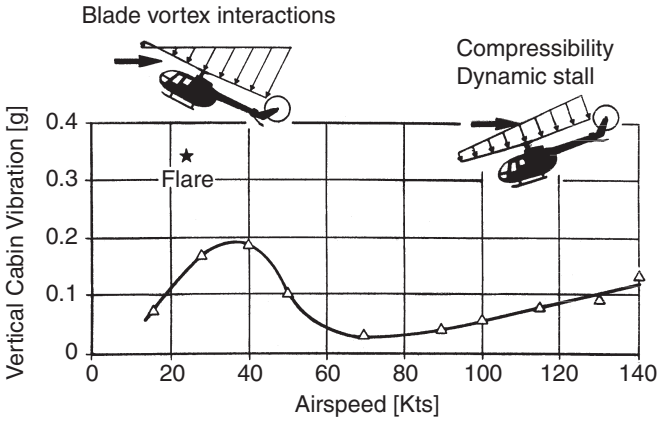

Figure 1.3 Vibration amplitude BO 105 as a function of airspeed [102]

Figure 1.4 BO 105 helicopter with individual blade root control system [88]

Figure 1.5 Rotor hub of BO 105 with individual blade root control system [88]

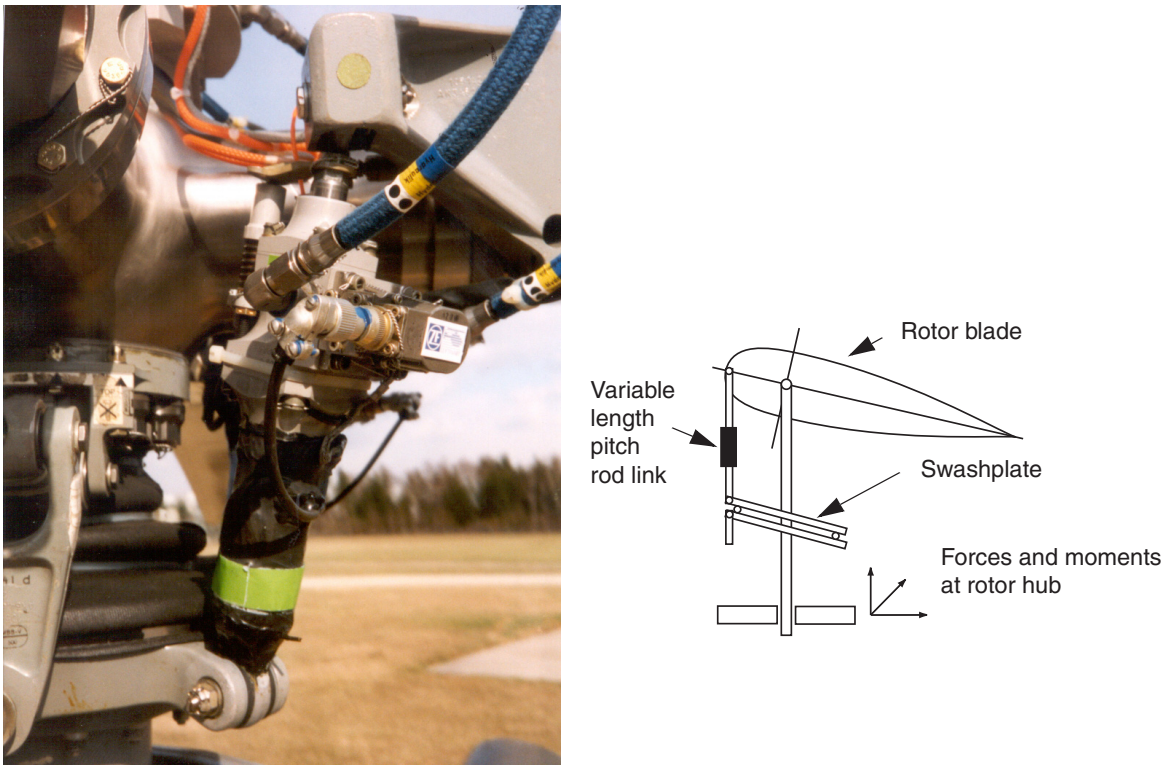

Figure 1.6 BO 105 individual blade root control actuator [88] and concept of individual blade root control

1.3 Individual Blade Control

Before individual blade control emerged, R. W. Tayler, in 1842, was the first to suggest a collective blade pitch adjustment for an air vehicle, whereas the first theory of cyclic blade pitch control was put forward by G. A. Crocco in 1906 [9]. In 1958, early insights into the possible use of higher harmonic rotor control were published by P. R. Payne [78].

Concepts for active vibration control are higher harmonic control (HHC) and individual blade control (IBC). Both methods aim at modifying existing and/or inducing additional forces and moments at the rotor that are opposite in phase and equal in amplitude with the original forces and moments, leading to destructive interference. The original vibration is consequently reduced and ideally cancelled out. In HHC, actuators are located below the swashplate, i.e. actuation takes place in the nonrotating system [66], [81]. The more recent concept of IBC removes some of the existing limitations on active control by means of the swashplate [33]. With IBC, the blades are individually controlled in the rotating frame above the swashplate [4]. An overview of rotor and actuation systems is given in [103], [101], [74]. One IBC method is the actively controlled flap that is located at the outer part of the rotor blade and that is used to change the lift of the blade [47], [17], [34], [69], [87]; an overview of this approach can be found in [68]. Issues related to implementation of actively controlled flaps are treated in [73]. Another way of influencing the lift of a rotor blade is to

control the twist of the blade [28], [7], [18], [19], [22]. This approach is described for a scaled helicopter in a wind tunnel test in [20]. Calculations and experimental results with active blade twist for a BO 105 model helicopter can be found in [12]. Individual blade control using smart structures is described in [77]. In the concept of individual blade *root* control (IBRC), the lift of the blade is varied by changing the pitch of the blade at its root. Therefore, the pitch link rods are substituted by hydraulic actuators, allowing blade pitch control to be superimposed to the swashplate commands. Investigations of an individual blade root control system for a BO 105 helicopter in the wind tunnel are described in [85] and in flight tests in [91]. An individual blade root control system for the CH-53G helicopter is developed in [50].

A four-blade BO 105 helicopter equipped with an individual blade root control system is considered here [106], [85], [91], see Figure 1.4. The actuation system consists of a conventional swashplate with the pitch rod links substituted by hydraulic actuators. The primary flight control works traditionally via the swashplate. The secondary anti-vibration control is superimposed via the hydraulic actuators in the rotating frame. Figure 1.5 shows the rotor hub with the IBC system of the BO 105 helicopter. A close-up of the blade pitch actuator and an illustration of the concept of individual blade root control is given in Figure 1.6.

One advantage of individual blade root control over individual blade control via flaps, twist, etc., is that no changes to the blade are necessary. Thus, the blades do not need to be recertified. The IBC system at the blade root has a retrofit capability, as proposed for the CH-53G helicopter [50]. As concerns overall clearance and certification, it is important to note that the system is fail-safe. In the event of a failure, the blade actuators are mechanically centered and act as a conventional pitch link [50]. Vibration control is supplementary to primary flight control, which again simplifies the clearance process.

However, if the original blades are used, no blade sensors are available and, consequently, no measurements are available in the rotating frame. The availability of only hub load (and possibly fuselage) sensors imposes certain restrictions on the design of the control law.

1.4 Benefits of Individual Blade Control

Benefits of IBC are the expansion of the flight envelope and an increase in acceptance of the helicopter by the crew, passengers, and society. This is accomplished by a reduction in:

- Vibration
- Flight mechanic and aeromechanical/aeroelastic instabilities
- Noise emission
- Required power

Vibration reduction does not only relieve human discomfort, but also helps to avoid or to delay fatigue damage of structural components. Thus, vibration reduction is directly related

to cost. Based on a study by Sikorsky, a vibration reduction of 30% can decrease direct maintenance costs by 20% [86]. The results of a study conducted by Westland show that a vibration reduction of 1% reduces unplanned maintenance costs by 1% [86].

Exterior helicopter noise can be reduced in descent and maneuver flight when blade vortex interaction (BVI) leads to BVI impulsive noise [98], [49], [110]. In high speed flight, IBC can influence the transonic shock that occurs at the advancing blade and, consequently, can help to reduce high speed impulsive noise [55]. Delay or suppression of dynamic stall is a further application of IBC that leads to a reduction in required power [48], [84], [46]. IBC might also be used for auto-tracking, as a substitute for the manual tracking procedure, which is costly, since it requires an iterative process of adjusting, starting, testing, landing, readjusting, and restarting, and so on.

Noise and vibration reduction can be contradictory objectives [41]. This conflict could be resolved by concentrating on noise reduction during take-off and landing in urban areas (e.g. near hospitals, etc.) where stringent noise emission restrictions apply and by focussing on vibration control during cruise flight.

1.5 State-of-the-Art

Control law designs for helicopter vibration reduction are described in [109], [92], [90], [105]. H_∞ control for helicopter flight control systems is presented in [83], [96], [82]. Collocated sensors/actors are used in [76], [57]. Linear quadratic control is used in [104] to control six hub forces and moments and in [11] to control the force in thrust direction using collective pitch only. Optimal output feedback control strategies are presented in [29], [56]. State-space interpolation for gain-scheduled controllers is presented in [99]. Aspects of periodic system control are presented in [3], [2], [112], [16], [53], [111], [94], [113]. An application of periodic model following control in the design of flight controllers can be found in [63]. A comparable approach is taken in [75] to reduce vibration. Active control of fuselage vibration is described in [115], [24], [25], [40], [21], [114]. The subject of system identification is treated in [107], [64], [58]. Methods for helicopter simulation are presented in [8], [37], [1].

1.6 Motivation

Helicopter vibration reduction belongs to the class of vibration control problems for plants with periodic coefficients. Here, periodicity is a result of the mechanics of the system and cannot be avoided. A linear time-periodic system responds to a sinusoidal input not only with a sinusoid at the excitation frequency, as linear time-constant systems do, but also at additional harmonic frequencies that are spaced by multiples of the plant-periodic frequency. This behavior results when the time-periodic system modulates the input frequency with the plant-periodic frequency. Thus, the narrowband disturbance rejection problem for

linear time-periodic systems is considerably more complex than its time-constant counterpart, and periodic controllers are expected to take better advantage of the system structure [23].

The analysis and control of discrete-time, linear periodic systems is well established in the literature, see [10] for a survey. Research relies heavily upon a canonical relationship between a discrete-time, linear, p-output, q-input, n-state, m-periodic system and a linear, mp-output, mq-input, n-state time-constant system; this linear time-constant system is called the "lifted" system [65], [45]. In the lifted reformulation, the output and input vectors are enlarged, while the dimension of the state vector is preserved. In the "cyclic" reformulation [32], the state space is also enlarged, resulting in a linear, mp-output, mq-input, mn-state time-constant system. The apparent advantage of the reformulated systems is that they allow to perform system analysis and controller synthesis using time-invariant techniques [23]. However, it must be noted that the approach leads to considerably larger systems that may become impractical for complex plants. Therefore, this study focuses on continuous-time periodic systems without discretization and without using a time-constant reformulation. The development of a time-periodic controller using gain-scheduling techniques, and the extension of time-constant model reduction methods to time-periodic systems represent two of the main contributions of this dissertation.

The lightly damped lag motion of the rotor blade is susceptible to various aeroelastic and aeromechanical instabilities. This is the reason why most rotors have mechanical lag dampers, which provide artificial damping to suppress the occurrence of such aeromechanical phenomena [54]. Individual blade control can also be used to actively increase damping [38]. The physical mechanism of damping enhancement is well-defined (see Section 6.4). However, if the advantage of individual blade root control, namely the usability of unchanged blades, is to be exploited, control strategies without lag rate sensing in the rotating blades are required. Another of the main contributions of this dissertation is the detailed plant analysis in terms of controllability and observability from the nonrotating system and the development of a robust observer-based controller to increase lag damping without blade sensors.

The final goal of helicopter vibration reduction is to reduce vibration, not necessarily at the rotor hub, but at specific points in the fuselage, e.g. at the pilot seat or in the load compartment. IBC inputs aimed at reducing hub loads may not necessarily lead to a simultaneous reduction in the accelerations at specific locations in a flexible fuselage. In [33], an increase in fuselage acceleration by a factor of two to five from its baseline value was observed when higher harmonic control inputs aimed at minimizing hub shears were introduced. This shows that the model on which the controller design is based is required to include both rotor dynamics and fuselage dynamics. Another of the main contributions of this dissertation is the integration of a finite-element model of the BO 105 helicopter with the aeromechanical model of the rotor as well as the development of controllers aimed at minimizing vibration at various locations in the fuselage.

1.7 Research Objective

The objective of this work is to develop a control law for an IBC helicopter in order to reduce fuselage vibration and increase damping. The control variables required are plant inputs that allow the lift of the individual blades to be influenced. This can be realized by means of any actuators in the rotating frame, i.e. flaps at the outer part of the blade, active blade twist, or blade root actuators. The control design here is applied in simulation to the BO 105 helicopter with an individual blade root control system.

1.8 Overview of Content

The study is organized as follows: The introduction (this chapter) is followed by a detailed description and analysis of two different rotor models in Chapter 2. A simple analytical model is used to analyze the basic features of rotor behavior and a complex aeromechanical model to be used for the final control law design is described. Chapter 3 addresses the potential of individual blade control. Model reduction techniques for linear time-constant systems are extended to time-periodic systems and are applied to the rotor in Chapter 4. In Chapter 5, the idea of H_∞ optimization and details of the controller design setup are outlined. The results are presented in Chapter 6. Finally, Chapter 7 summarizes the results and main contributions and gives directions for future research.

Chapter 2
Model Description and Analysis

In this chapter, two different rotor models are presented: a simple analytical model and a complex aeromechanical analysis model, including advanced rotor aerodynamics in addition to detailed kinematics and detailed dynamics derived with the commercial helicopter analysis software Camrad II [42], [43], [44].

The analytical model is used to analyze the basic features of rotor behavior, including flap and lag dynamics, loads, vibration, and hub filtering. Fundamental aspects of the time-periodicity of the plant are presented and multiblade coordinates are introduced. The properties of the rotor, in both frequency and time domain, are analyzed in detail using the complex aeromechanical model. Finally, a finite-element model of the helicopter fuselage is implemented resulting in a coupled rotor-fuselage model, allowing vibration to be calculated and controlled not only at the rotor hub but also at specific locations in the fuselage, such as at the pilot seat or in the load compartment.

2.1 Analytical Rotor Model

An analytical model of an N-blade helicopter rotor is developed[1] [52], [93], [43]. The structure of the rotor blades is modelled using mass and spring systems. In aerodynamics, blade element theory is used to determine the blade loading. Only rigid flap and lag motion is considered, with collective, cyclic, and, in case of even blade numbers, differential pitch control. The rotor is articulated with flap and lag hinge offsets. In general, small angles are assumed. The section aerodynamic characteristics are described by a constant lift curve slope and a mean profile drag coefficient. The effects of stall, compressibility, and radial flow are not included. A uniform induced velocity is used. The blade has constant chord and linear twist. Higher harmonics of flap and lag motion and the pitch degrees of freedom are neglected. The model parameters are chosen to resemble those of the BO 105 helicopter.

1. The model is available in nonlinear and linear from as C-code or as state-space matrices, respectively, see Appendix A.2.

While the basic features of rotor behavior are contained in the model described above, the model is far too limited for accurate quantitative results. Despite the fact that various effects are neglected and that structural and aerodynamic modelling is far too simple to predict vibrational loads, the model is assumed to allow a qualitative evaluation of the potential to influence vibration with IBC from a control law design perspective.

2.1.1 Flap and Lag Dynamics

The motion of a hinged blade ("articulated rotor") consists basically of rigid body rotation about each hinge, with restoring moments as a result of the centrifugal forces acting on the rotating blade. For a blade without hinges ("hingeless rotor"), the fundamental modes of out-of-plane and in-plane bending define the flap and lag motion. Because of the high centrifugal stiffening of the blade, these modes are similar to and can be approximated by the rigid body rotations of hinged blades, except in the vicinity of the root, where most of the bending takes place [43]. In addition to the flap and lag motion, it must be possible to change the pitch of the blade in order to control the rotor. Pitch motion allows the angle of attack of the blade to be controlled and hence the aerodynamic forces on the rotor. The blade pitch change is accomplished by movement about a bearing or occurs about a region of torsional flexibility at the blade root ("bearingless rotor").

An articulated rotor with a flap hinge offset from the center of rotation by a distance eR is considered, where e is the dimensionless distance and R the rotor radius. The radial dimensionless coordinate r is measured from the center of rotation. The blade motion is rigid rotation about the flap hinge with the degree of freedom β and the mode shape $\eta(r)$, such that the out-of-plane deflection is $z = \beta\eta$.

$$\eta = \begin{cases} 0 & r < e \\ \dfrac{r-e}{1-e} & r \geq e \end{cases} \tag{2.1}$$

The mode shape is normalized to unity at the tip such that β can be interpreted as the angle between the rotor disk plane and a line extending from the center of rotation to the blade tip, see Figure 2.1.

The forces acting on a blade mass element $m\,dr$, where m is the blade mass per unit length at the radial station r, are as follows and as shown in Figure 2.1:

- The inertial force $m\ddot{z} = m\eta R\ddot{\beta}$ opposing the flap motion, with moment arm about the flap hinge $(r-e)R$
- The centrifugal force $m\Omega^2 r$ directed outward, with moment arm $zR = \eta\beta R$ and the rotor rotational speed Ω
- The aerodynamic force $\tilde{F}_z$, with moment arm $(r-e)R$

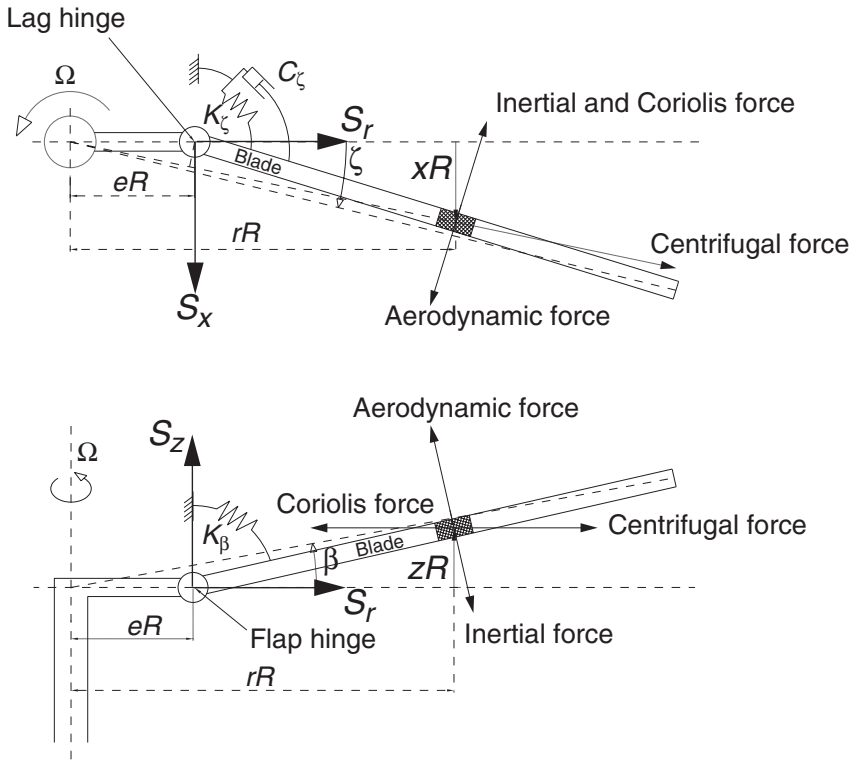

Figure 2.1 Forces acting on a blade section in lag and flap direction [52], [43]

- The Coriolis force due to the lag motion $2\Omega m\dot{x} = 2\Omega mR\eta\dot{\zeta}$ directed radially inward, with moment arm $zR = \eta\beta R$, the lag degree of freedom ζ, and the in-plane deflection $x = \eta\zeta$, assuming the mode shapes for flap and lag motion are identical.

Equilibrium of moments about the flap hinge, including a spring moment $K_\beta(\beta - \beta_p)$ with the precone angle β_p, gives the flap equation of motion expressed in dimensionless quantities

$$I_\beta^*(\ddot{\beta} + \nu_\beta^2\beta) - 2I_{\beta\zeta}^*\beta\dot{\zeta} = \frac{K_\beta\beta_p}{I_b(1-e)\Omega^2} + \gamma M_F \tag{2.2}$$

with the natural frequency of the flap motion

$$\nu_\beta^2 = 1 + \frac{3e}{2(1-e)} + \frac{K_\beta}{\Omega^2 I_b(1-e)^2} \tag{2.3}$$

the normalized generalized mass of the flap mode $I_\beta^* = 1 - e$, the normalized Coriolis flap-lag coupling $I_{\beta\zeta}^* = 1$, the blade lock number[2]

2. Representing the ratio of the aerodynamic and inertial forces on the blade.

$$\gamma = \frac{\rho a c R^4}{I_b} \tag{2.4}$$

where ρ is the air density, a the blade section lift-curve slope, c the blade chord, I_b the characteristic inertia of the rotor blade, and M_F the aerodynamic flap moment, which will be defined in Section 2.1.2.

The in-plane forces acting on a blade mass element and their moment arms about the offset lag hinge are as follows (see also Figure 2.1):

- The inertial force $m\ddot{x} = m\eta R\ddot{\zeta}$ opposing the lag motion, with a moment arm about the lag hinge $(r-e)R$
- The centrifugal force $m\Omega^2 r$ directed radially outward, with moment arm $(e/r)xR = (e/r)\eta R\zeta$
- The Coriolis force $2\Omega\dot{z}z'm = 2\Omega\dot{\beta}\beta\eta\eta' Rm$ opposing the lag motion, with moment arm $(r-e)R$
- The aerodynamic force $\tilde{F}_x$, with moment arm $(r-e)R$.

The operator $(\ )'$ is defined as $d(\ )/dr$. Equilibrium of moments about the lag hinge, including a spring moment $K_\zeta\zeta$ and a mechanical lag damper term $C_\zeta^*\dot{\zeta}$, gives the lag equation of motion that is expressed in dimensionless quantities as:

$$I_\zeta^*(\ddot{\zeta} + \nu_\zeta^2\zeta) + 2I_{\beta\zeta}^*\beta\dot{\beta} + C_\zeta^*\dot{\zeta} = \gamma M_L \tag{2.5}$$

The natural frequency of the lag motion is

$$\nu_\zeta^2 = \frac{3e}{2(1-e)} + \frac{K_\zeta}{\Omega^2 I_b (1-e)^2} \tag{2.6}$$

and the normalized generalized mass of the lag mode is $I_\zeta^* = 1-e$. The aerodynamic lag moment M_L is defined in Section 2.1.2.

The flap and lag equations of motion are coupled by nonlinear terms as a result of the blade Coriolis forces: $-I_{\beta\zeta}^* 2\beta\dot{\zeta}$ in the flap equation and $-I_{\beta\zeta}^* 2\beta\dot{\beta}$ in the lag equation. For linear analysis, these terms are linearized about the trim motion and approximated by

$$\begin{aligned} \Delta(\beta\dot{\zeta}) &= \beta_{\text{trim}}\Delta\dot{\zeta} + \dot{\zeta}_{\text{trim}}\Delta\beta \cong \beta_0\Delta\dot{\zeta} \\ \Delta(\beta\dot{\beta}) &= \beta_{\text{trim}}\Delta\dot{\beta} + \dot{\beta}_{\text{trim}}\Delta\beta \cong \beta_0\Delta\dot{\beta} \end{aligned} \tag{2.7}$$

where β_0 is the trim coning angle.

2.1.2 Aerodynamics

Blade element theory is used to calculate the aerodynamic forces acting on the rotor blade based on the assumptions given in the introduction to this section. The main influencing factors and the key results are given in the following; for a detailed derivation see [52] and the original source [43].

The helicopter has the forward velocity V and the disk angle of attack α. The rotor advance ratio[3] is defined as the in-plane forward velocity component normalized by the rotor tip speed:

$$\mu = \frac{V\cos\alpha}{\Omega R} \tag{2.8}$$

In a frame rotating with the rotor blade, the radial, tangential, and normal components of the velocity seen by the blade are given by:

$$\begin{aligned} u_R &= \mu\cos\psi \\ u_T &= r + \mu\sin\psi - \eta\dot{\zeta} - \eta'\zeta u_R \\ u_P &= \lambda + \eta\dot{\beta} + \eta'\beta u_R \end{aligned} \tag{2.9}$$

Equation (2.10), based on the theory of Glauert [43] to calculate the induced velocity in forward flight, can be solved for the rotor inflow ratio λ, with the thrust coefficient $C_T = T/\rho A(\Omega R)^2$, the thrust T, the air density ρ, and the rotor disk area A:

$$\lambda = \mu\tan\alpha + \frac{C_T}{2\sqrt{\mu^2+\lambda^2}} \tag{2.10}$$

The aerodynamic flap and lag moments appearing in the equations of motion (2.2) and (2.5) are

$$M_F = \int_{r=e_{\text{air}}}^{1} \tilde{F}_z \eta\, dr = \int_{r=e_{\text{air}}}^{1} \frac{1}{2}(u_T^2(\theta_{\text{con}} + \alpha_r r + \alpha_0) - u_T u_P)\eta\, dr \tag{2.11}$$

$$M_L = \int_{r=e_{\text{air}}}^{1} \tilde{F}_x \eta\, dr = \int_{r=e_{\text{air}}}^{1} \left(\frac{1}{2}(u_T u_P(\theta_{\text{con}} + \alpha_r r + \alpha_0) - u_T u_P) + u_T^2\frac{c_d}{2a}\right)\eta\, dr \tag{2.12}$$

3. Dimensionless forward speed of the helicopter.

where θ_{con} is the pitch control input, $\alpha_r r + \alpha_0$ the linear blade twist, a the blade section lift-curve slope, and c_d the drag coefficient. Integration is performed over the span, starting at the aerodynamically effective radius e_{air}.

2.1.3 Loads, Vibrations, and Hub Filtering

The forces and moments at the root of the rotating blades are transmitted to the helicopter airframe. The steady components of these hub reactions in the nonrotating frame are the forces and moments required to trim the helicopter. The higher frequency components cause helicopter vibration. Figure 2.2 shows the definition of the root shears and moments of the rotating blade and the forces and moments acting on the hub in the nonrotating frame.

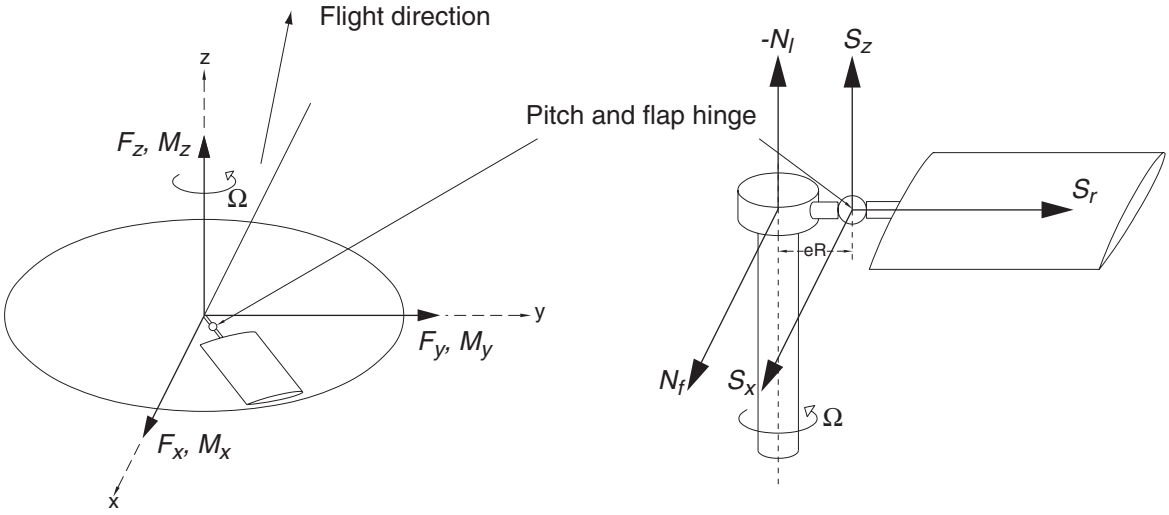

Figure 2.2 Forces and moments in the nonrotating and rotating system [52], [43]

The vertical shear force S_z generates the rotor thrust F_z and the in-plane shear forces S_x and S_r cause the rotor side and drag forces F_y and F_x. The flapwise root moment N_F produces the rotor pitch and roll moments M_y and M_x, whereas the lagwise moment N_L results in the rotor shaft torque $-M_z$.

The root forces of the rotating blades can be obtained by integrating the section forces, as in the derivation of the flap and lag equations of motion

$$S_z = \int_{r=e_{\text{air}}}^{R} \tilde{F}_z dr - \int_{r=e}^{R} m\eta R\ddot{\beta} dr \tag{2.13}$$

$$S_x = \int_{r=e_{\text{air}}}^{R} \tilde{F}_x dr - \int_{r=e}^{R} m\eta R\ddot{\zeta} dr + \int_{r=e}^{R} m\Omega^2 \eta R\zeta dr \tag{2.14}$$

$$S_r = \int_{r=e_{\text{air}}}^{R} F_r dr - \int_{r=e}^{R} 2\Omega m R \eta \zeta dr + \int_{r=e}^{R} m\Omega^2 r dr \tag{2.15}$$

with the aerodynamic forces:

$$\int_{r=e_{\text{air}}}^{1} \tilde{F}_z dr = \int_{r=e_{\text{air}}}^{1} \frac{1}{2}(u_T^2(\theta_{\text{con}} + \alpha_r r + \alpha_0) - u_T u_P) dr \tag{2.16}$$

$$\int_{r=e_{\text{air}}}^{1} \tilde{F}_x dr = \int_{r=e_{\text{air}}}^{1} \left(\frac{1}{2}(u_T u_P(\theta_{\text{con}} + \alpha_r r + \alpha_0) - u_T u_P) + u_T^2 \frac{c_d}{2a}\right) dr \tag{2.17}$$

$$\int_{r=e_{\text{air}}}^{1} F_r dr = \int_{r=e_{\text{air}}}^{1} \left(u_T u_R \frac{c_d}{2a} - z' \tilde{F}_z\right) dr \tag{2.18}$$

The moments N_f and N_l result from the shear forces S_x and S_r, with the hinge offset as moment arm and the hinge springs:

$$N_f = K_\beta(\beta - \beta_p) + S_z e R \tag{2.19}$$

$$N_l = K_\zeta \zeta + S_x e R \tag{2.20}$$

The forces and moments in the nonrotating frame are obtained by summing over all N blades, where the notation $^{(m)}$ stands for the m^{th} blade:

$$F_x = \sum_{m=1}^{N} (S_r^{(m)} \cos\psi_m + S_x^{(m)} \sin\psi_m) \tag{2.21}$$

$$F_y = \sum_{m=1}^{N} (S_r^{(m)} \sin\psi_m - S_x^{(m)} \cos\psi_m) \tag{2.22}$$

$$F_z = \sum_{m=1}^{N} S_z^{(m)} \tag{2.23}$$

$$M_x = \sum_{m=1}^{N} N_f^{(m)} \sin\psi_m \tag{2.24}$$

$$M_y = -\sum_{m=1}^{N} N_f^{(m)} \cos\psi_m \tag{2.25}$$

$$M_z = -\sum_{m=1}^{N} N_l^{(m)} \tag{2.26}$$

In steady-state forward flight, the root reaction of the m^{th} blade ($m = 1, \ldots, N$) is a periodic function of $\psi_m = \psi + m\Delta\psi$ with $\Delta\psi = 2\pi/N$. Therefore, all blades have identical loading and motion. When the loads are written in the rotating frame as Fourier series and the summations are evaluated, all loads cancel at the rotor hub, except for those appearing in the nonrotating frame as harmonics of pN/rev [43]. The rotor hub basically acts as a filter, transmitting to the helicopter only harmonics of the rotor forces at integer multiples p of N/rev. Table 2.1 summarizes the transmission of loads through the rotor hub. Filtering facilitates the task of vibration reduction, since only pN/rev frequencies have to be considered.

Table 2.1 Transmission of helicopter vibration through the rotor hub [43]

Nonrotating Frame		**Rotating Frame**
Thrust at pN/rev	from	vertical shear at pN/rev
Torque at pN/rev	from	lagwise moment at pN/rev
Rotor drag and side forces at pN/rev	from	in-plane shears at $pN\pm1$/rev
Pitch and roll moments at pN/rev	from	flapwise moments at $pN\pm1$/rev

2.1.4 Multiblade Coordinate Transformation

The equations of motion are derived in the rotating frame. However, the rotor responds as a whole to excitations (control inputs, gusts) from the nonrotating frame. This is the motivation to use coordinates in the nonrotating frame. Multiblade coordinates (MBC), which result from a linear Fourier coordinate transformation from single blade coordinates (SBC), are introduced, see Figure 2.3. The following equations describe the transformation from SBC to MBC. As an example, the flap motion is considered. $\beta^{(1)} \ldots \beta^{(N)}$ denote the flap angles in SBC, whereas the coordinates β_0 (collective mode), β_{nc} and β_{ns} (cosine and the sine modes), and β_d (differential mode, exists only for N even) are used in MBC. The blade index m ranges from 1 to N. The azimuth is $\psi_m = \psi + m \cdot \Delta\psi$ with the dimensionless

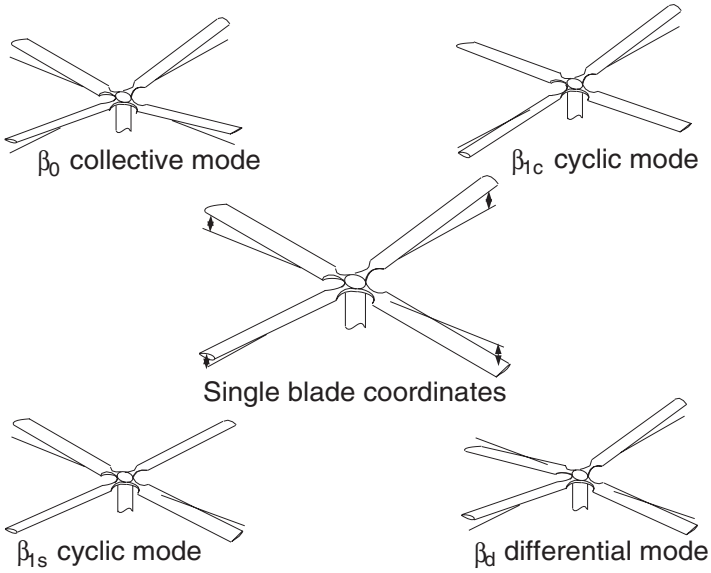

Figure 2.3 Fourier coordinate transformation, single blade coordinates (SBC), and multiblade coordinates (MBC)

time variable $\psi = \Omega t$ for constant rotational speed Ω and the equal azimuthal spacing between the blades $\Delta\psi = 2\pi/N$. The inverse coordinate transformation and the time derivatives are given in Appendix A.1.

$$\begin{aligned}
\beta_0 &= \frac{1}{N}\sum_{m=1}^{N}\beta^{(m)} \\
\beta_{nc} &= \frac{2}{N}\sum_{m=1}^{N}\beta^{(m)}\cos n\psi_m \\
\beta_{ns} &= \frac{2}{N}\sum_{m=1}^{N}\beta^{(m)}\sin n\psi_m \\
\beta_d &= \frac{1}{N}\sum_{m=1}^{N}\beta^{(m)}(-1)^m
\end{aligned} \tag{2.27}$$

2.1.5 Trimming

The trim task obtains the equilibrium solution of the system equations for a steady-state operating condition. This involves iteration on the controls to achieve equilibrium of the net forces and moments on the rotor or helicopter. The trim task yields the solution for the periodic motion and the steady trim variables. If just the rotor is considered, there are three control variables: collective, longitudinal cyclic, and lateral cyclic pitch. These controls may be

adjusted to trim three quantities, typically the rotor thrust and tip-path-plane tilt (e.g. for zero flapping relative to the shaft), or the thrust, propulsive force, and side force. Trimming three quantities is referred to as “wind tunnel trimming”. If the entire helicopter is considered, there are six control variables used to trim the six forces and moments on the helicopter: the pilot’s collective, longitudinal cyclic, and lateral cyclic stick, the pedal position, and the helicopter pitch and roll angles relative to the flight path. Trimming all six quantities corresponds to free flight. [42], [43]

The wind tunnel operating condition trimmed for thrust, propulsive, and side force is used here. This leads to a trim equation of the following form:

$$\min_{[\theta_0, \theta_{1c}, \theta_{1s}]} ((F_{x_0} - F_{x_{\text{meas}}})^2 + (F_{y_0} - F_{y_{\text{meas}}})^2 + (F_{z_0} - F_{z_{\text{meas}}})^2) \tag{2.28}$$

The variables F_{x_0}, F_{y_0}, and F_{z_0} stand for steady trim forces, i.e. the first coefficient of a Fourier series for the corresponding force at the rotor hub from (2.21) - (2.23), respectively. $F_{x_{\text{meas}}}$, $F_{y_{\text{meas}}}$, and $F_{z_{\text{meas}}}$ denote measured trim forces from flight tests. The trim variables θ_0, θ_{1c}, and θ_{1s} are the pilot’s collective, longitudinal cyclic, and lateral cyclic pitch commands. The pitch commands are transformed to SBC via the swashplate and enter the system as a pitch command per blade, denoted by θ_{con} in (2.11) and (2.12).

The use of wind tunnel trimming results in flight mechanical modes being neglected. This is justified, since the typical frequency range of primary flight control (approximately $0.3\,\text{rad/sec}$ - $12\,\text{rad/sec}$ [108], corresponding to $0.007/\text{rev}$ - $0.27/\text{rev}$ for the BO 105 helicopter) and the frequency range of interest for vibration control (around $3/\text{rev}$ - $5/\text{rev}$) are clearly separated.

2.1.6 Linearization

Linearization is typically performed about an operating condition, e.g. a trim state x^* and trim input u^*. Here, the system is linearized about a trim *trajectory* over one rotor revolution, resulting in a linear time-periodic system. The trim state trajectory $x^*(\psi)$ is obtained by means of nonlinear simulation and is written as a Fourier series, which, in the case of the analytical model, is truncated after the second-order terms:

$$x^*(\psi) = x_0 + x_{1c}\cos\psi + x_{1s}\sin\psi + x_{2c}\cos 2\psi + x_{2s}\sin 2\psi \tag{2.29}$$

The trim input trajectory $u^*(\psi)$ is defined by the collective and cyclic pilot inputs:

$$u^*(\psi) = \theta_0 + \theta_{1c}\cos\psi + \theta_{1s}\sin\psi \tag{2.30}$$

The system is transformed into state-space form:

$$\begin{aligned} \dot{x} &= A(\psi)x + B(\psi)u \\ y &= C(\psi)x + D(\psi)u \end{aligned} \tag{2.31}$$

Both state and input vectors are given in MBC:

$$x = \left[\dot{\beta}_0 \ \dot{\beta}_{nc} \ \dot{\beta}_{ns} \ \dot{\beta}_d \ \dot{\zeta}_0 \ \dot{\zeta}_{nc} \ \dot{\zeta}_{ns} \ \dot{\zeta}_d \ \beta_0 \ \beta_{nc} \ \beta_{ns} \ \beta_d \ \zeta_0 \ \zeta_{nc} \ \zeta_{ns} \ \zeta_d\right]^{\mathrm{T}} \tag{2.32}$$

$$u = \left[\theta_0 \ \theta_{nc} \ \theta_{ns} \ \theta_d\right]^{\mathrm{T}} \tag{2.33}$$

The harmonic index n goes from $n = 1$ to $(N-1)/2$ for N odd and from $n = 1$ to $(N-2)/2$ for N even. The differential degree of freedom (index d) only exists if N is even.

The output vector contains the hub loads in the nonrotating system:

$$y = \left[F_x \ F_y \ F_z \ M_x \ M_y \ M_z\right]^{\mathrm{T}} \tag{2.34}$$

The dimension of the plant is given by:

$$\left[\#\text{Outputs} \ \#\text{Inputs} \ \#\text{States}\right] = \left[6 \ N \ 4N\right] \tag{2.35}$$

2.2 Camrad II Rotor Model

The aeromechanical analysis software Camrad II [42], [43], [44] is used to derive a state-space model of a BO 105 helicopter rotor with four flexible blades [29]. This model very much resembles the simple analytical model in the previous section in terms of inputs and outputs, as well as in terms of time-periodicity and multiblade coordinates, but is of much higher complexity and accuracy, thus allowing quantitative results.

The rotor blades are modelled as beams by finite elements, allowing flap (out-of-plane), lag (in-plane), and torsion motion. Aerodynamics are calculated using blade element theory combined with experimental airfoil tables and a wake model. The structural blade modes considered are four flap modes, two lag modes, and the first torsion mode. Higher frequency structural and aerodynamical modes, as well as flight mechanical modes are neglected. Up until now, the BO 105 helicopter fuselage has been implemented as a rigid body in order to model the inertial properties of the helicopter. The implementation of the elastic airframe will be presented in Section 2.3. Aerodynamic effects of the fuselage and stabilizer are considered by table data. The tail rotor is treated as a rigid rotor without degrees of freedom.

The equations of motion are generally time-periodic and nonlinear. The equations of motion are trimmed and linearized about a time-periodic trim solution. The linearized equations of motion are of the form

$$M(\psi)\ddot{q} + C(\psi)\dot{q} + K(\psi)q = F(\psi)u \tag{2.36}$$

with degrees of freedom q (generalized coordinate). $M(\psi)$ is the generalized mass, $F(\psi)$ is the control term corresponding to the input u, and the spring and damping terms are denoted by $K(\psi)$ and $C(\psi)$, respectively. The coefficients associated with the aerodynamic terms vary with the rotor revolution, i.e. the matrices are periodic functions of the azimuth ψ, e.g. $M(\psi) = M(\psi + 2\pi)$. Azimuth and time are related by $\psi = \Omega t$, where Ω is the rotational speed. The input consists of the individual blade control commands in MBC:

$$u = \left[\theta_0 \ \theta_{1c} \ \theta_{1s} \ \theta_d\right]^{\mathrm{T}} \tag{2.37}$$

The equations of motion are transformed into state-space form:

$$\dot{x} = A(\psi)x + B(\psi)u \tag{2.38}$$

Time-constant equations of motion can be obtained by averaging the coefficients of the periodic system. The model consists of seven flexible modes, with the state variable $x = \left[\dot{q} \ q\right]^{\mathrm{T}}$ in MBC, resulting in 56 states. The modes are given in Table 2.2.

Table 2.2 Blade natural frequencies

Mode	Frequency [/rev]
1^{st} lag	0.68
1^{st} flap	1.10
2^{nd} flap	2.72
1^{st} torsion	3.95
2^{nd} lag	4.25
3^{rd} flap	5.01
4^{th} flap	7.97

The output equation is given by

$$y = C(\psi)x + D(\psi)u \tag{2.39}$$

with the output vector consisting of forces and moments at the rotor hub:

$$y = \left[F_x \; F_y \; F_z \; M_x \; M_y \; M_z\right]^{\mathrm{T}} \tag{2.40}$$

The baseline vibration is modelled as output disturbance d. Due to the mechanical filtering effect (see Section 2.1.3), the baseline vibration occurs at frequencies of $i \cdot N/\mathrm{rev}$, where i is an integer and $N = 4$ the number of blades. Vibration with $i = 1$ is the most dominant vibration and the only vibration considered here. The 4/rev Fourier coefficients can be calculated with Camrad II or flight test data can be used. The output equation including the disturbance term is given by:

$$y = C(\psi)x + D(\psi)u + d \tag{2.41}$$

2.2.1 Frequency Domain Analysis

In the following, singular values and pole maps are used to analyze the model in more detail. Figure 2.4 shows the pole map of the time-constant plant model. The poles of the model can be assigned to the rotor modes, as shown in the figure. For an N-blade rotor in the rotating frame (SBC), there are N pairs of roots per mode, all at the same location in the pole map corresponding to the frequency and damping of the mode. In the nonrotating frame (MBC), there are also N pairs of roots and these are at the same location as in the rotating frame for the collective and differential (for N even) form and at $\pm n/\mathrm{rev}$ for the cyclic cosine (nc) and sine (ns) form. Thus, the coordinate transformation leaves the real part of these roots unchanged and shifts the imaginary part by $\pm n/\mathrm{rev}$.

The lag modes show the smallest critical damping ratio and, therefore, are candidates for the control design goal of increased damping. A comparison of the pole locations for high

speed and low speed flight shows that flight speed has very little influence on the pole locations, except in the case of the well-damped and consequently less critical first flap and torsion mode.

Singular values are used to analyze transfer functions of the system. Figure 2.5 (a) shows a singular value plot of the transfer function from all IBC inputs to the in-plane hub quantities for the time-constant system where the weakly damped lag modes can be identified. Note that the collective forms are only observable in the output M_z. Consequently, even if M_z is not considered for vibration reduction, a measurement of M_z is required to control and thus increase damping in the collective forms. In the case of the progressive and regressive forms (frequency $\pm 1/\text{rev}$), it is sufficient to measure the in-plane hub forces. The differential form is not at all observable, since it is reactionless in the time-constant model. The transfer function for out-of-plane hub loads is shown in Figure 2.5 (b), where the flap modes can be noted. Figure 2.6 shows a comparison of the transfer function from all four IBC inputs to five hub loads (no M_z) for the time-constant system. Four singular values exist for this 5×4 system. The minimum singular value corresponds to the differential (input) mode and is reactionless (approximately $-90\,\text{dB}$ compared to the gain of collective and cyclic modes). In contrast to this, the minimum singular value of the time-periodic system, as an example evaluated at an azimuth of $\psi = 0°$ and $\psi = 45°$, is not reactionless.

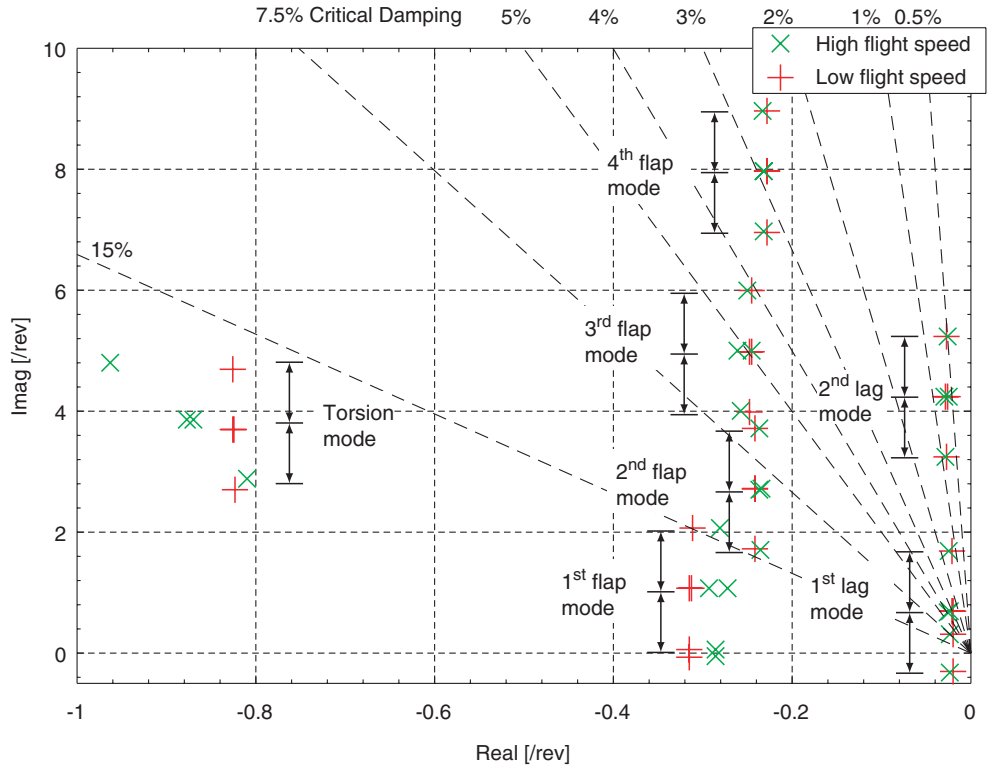

Figure 2.4 Pole locations of plant model at high (x) and low (+) flight speed

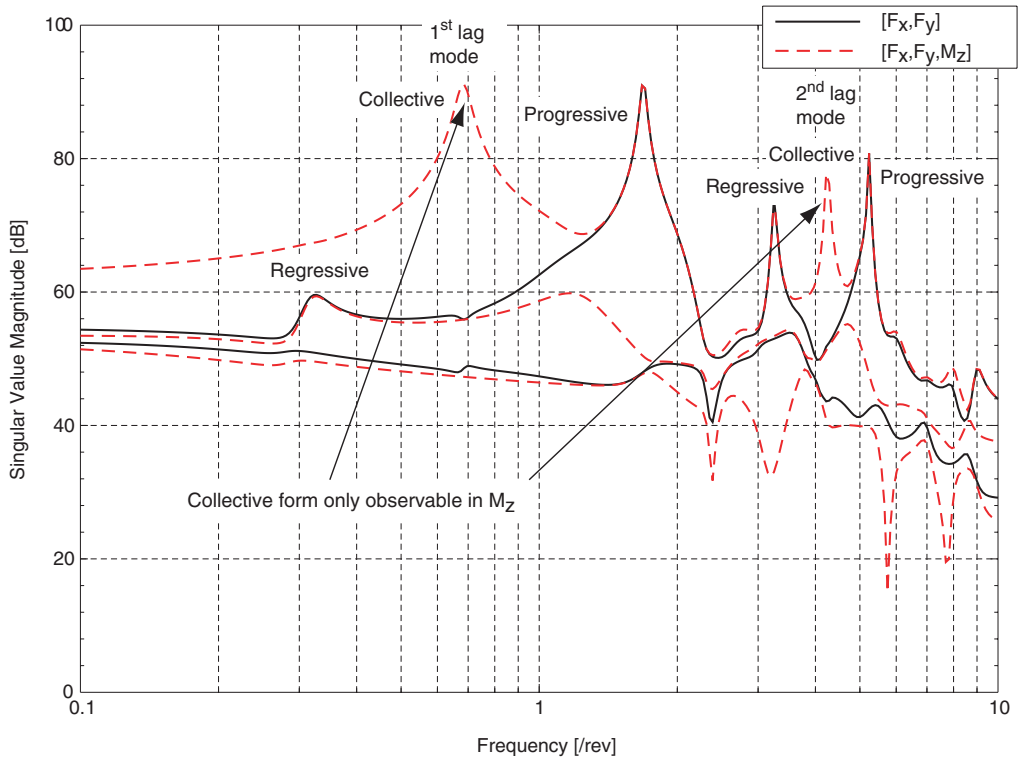

Figure 2.5 **(a)** Transfer function from IBC inputs to in-plane hub loads

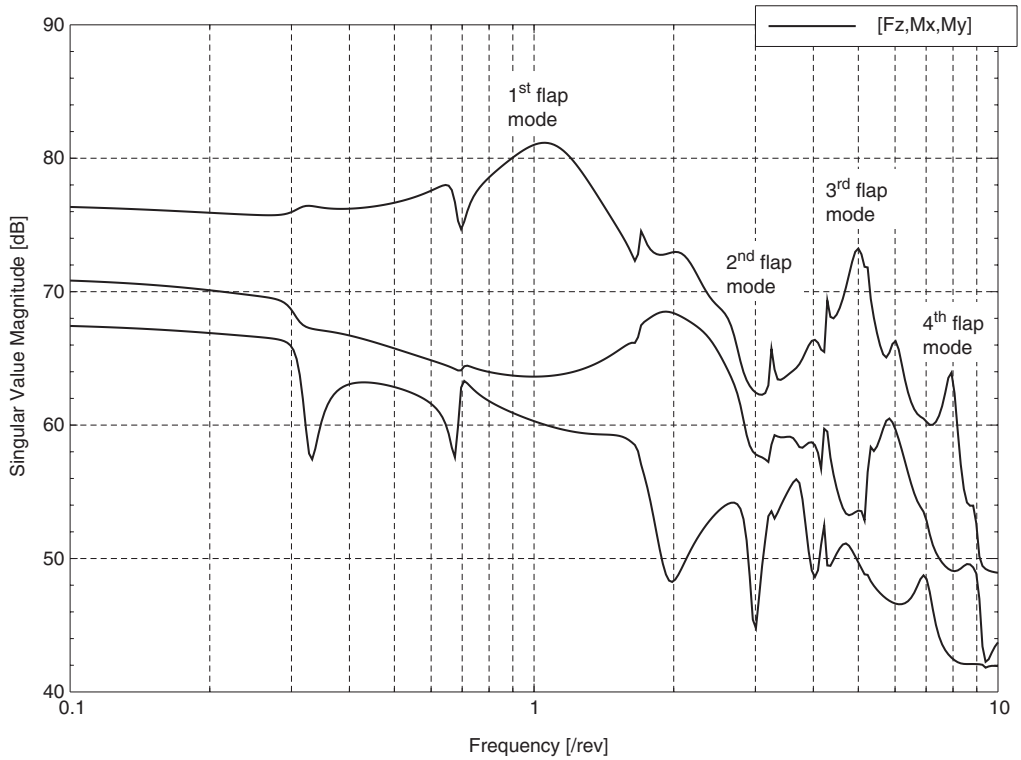

Figure 2.5 **(b)** Transfer function from IBC inputs to out-of-plane hub loads

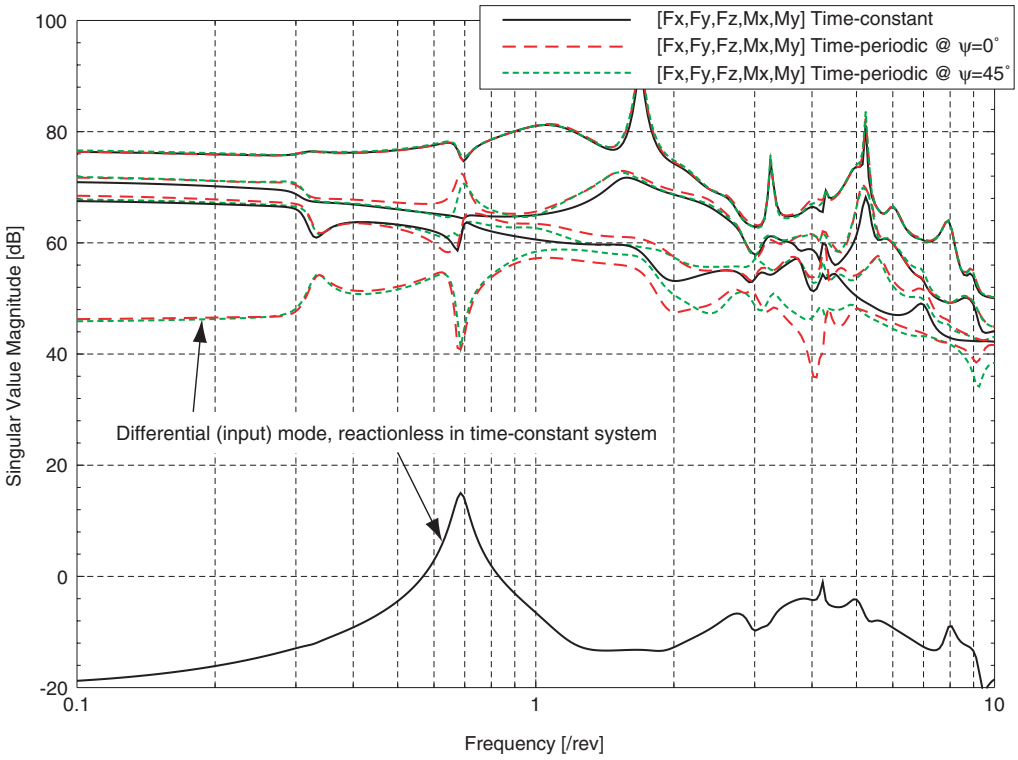

Figure 2.6 Transfer function from IBC inputs to in-plane hub loads, comparison of time-constant and time-periodic models

2.2.2 Time Domain Analysis

In order to analyze the effects of time-periodic and time-constant systems and the advantage of the coordinate transformation from SBC to MBC in more detail, a time domain simulation is presented in the following. Figure 2.7 shows the hub reactions and the time histories for the second lag mode for a collective impulse input. The response of the time-periodic plant is compared with the responses of the time-constant plant in SBC and MBC. The results for the hub reaction in F_z, dominated by the collective forms of the rotor modes, closely match time-periodic results for both time-constant simulations. However, the averaged coefficients in the time-constant model neglect the coupling between collective and cyclic modes, which leads to incorrect results in the cosine and sine form of the rotor modes and subsequently to incorrect hub responses in F_x, F_y, M_x, and M_y. The use of MBC preserves coupling between collective and cyclic modes, and the time histories for the cyclic modes and the hub responses closely match results of time-periodic simulations. The transformation of the system from SBC to MBC shifts information from the harmonic coefficients of the system matrices written as Fourier series towards the constant coefficient, i.e. the degree of periodicity of the system is reduced. The differential mode is only coupled in the time-periodic model, leading to incorrect results in the differential form of the rotor modes for both SBC and MBC time-constant simulations, as shown in Figure 2.7.

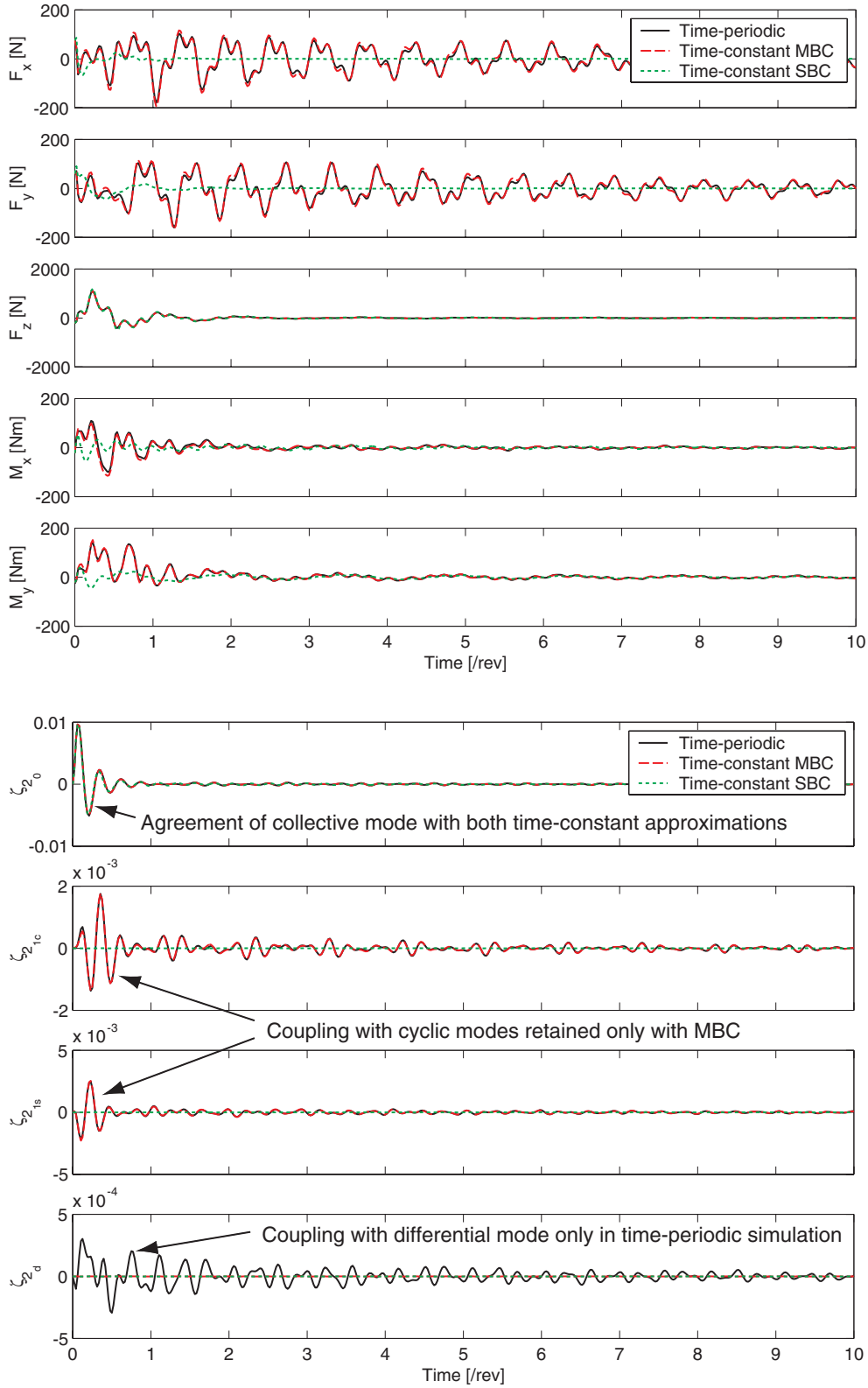

Figure 2.7 Collective impulse input, comparison of time-periodic and time-constant models in MBC and SBC

2.2.3 Actuator Dynamics

The actuators are modelled using first-order dynamics [29]. A frequency response is given in Figure 2.8.

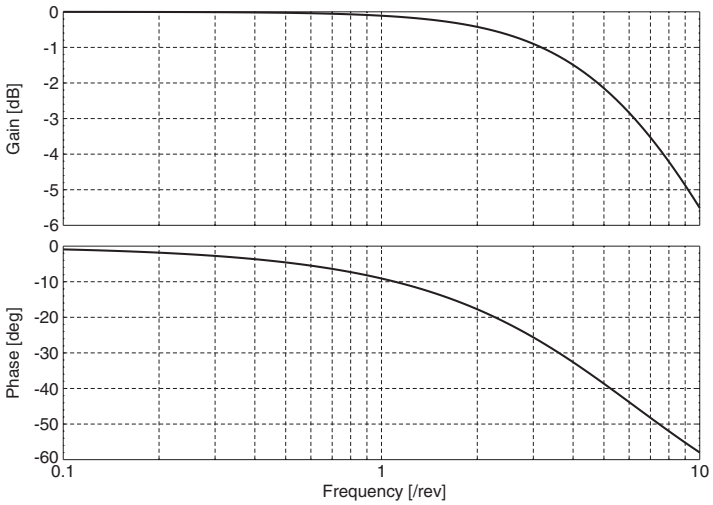

Figure 2.8 Frequency response of the actuator dynamics

2.3 Fuselage Model

This section will present the fuselage model used to calculate and control vibration at locations in the cabin, such as at the pilot and copilot seats and in the load compartment. An existing finite-element model of the fuselage [100] is used to obtain mode shapes of the flexible structure. The mode shapes are implemented [97] into the model in Camrad II, resulting in a coupled rotor-fuselage model.

The model was developed using the finite-element software Nastran [51]. The model consists of 812 points with three translatory and three rotatory degrees of freedom, resulting in a total number of 4872 degrees of freedom. Figure 2.9 shows the finite-element model. In Figure 2.10, specific points in the fuselage are defined, such as the pilot and copilot seat positions, the load compartment position, and the hub and swashplate points.

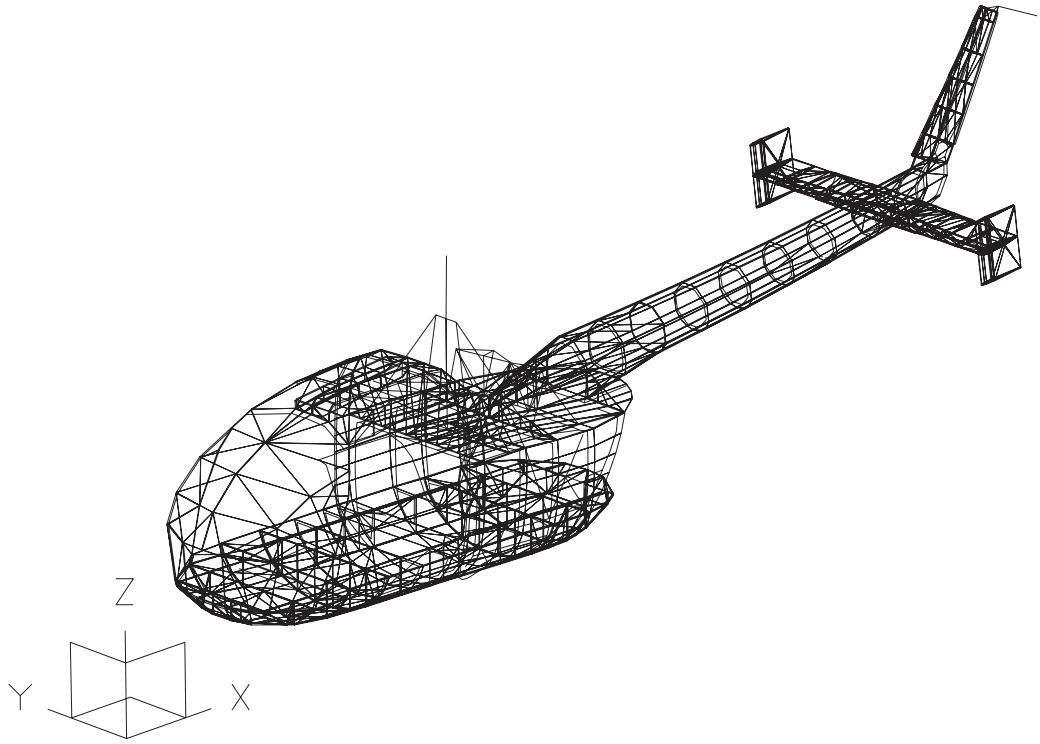

Figure 2.9 Finite-element model of the helicopter fuselage [100]

2.3.1 Implementation

In Camrad II, the rigid motion describes the center of mass motion of the helicopter. The rigid body degrees of freedom are orthogonal to the free-vibration modes [42]. The modes are calculated for a free body, including rigid motion. Small motion is assumed, consistent with the linear modes. Consequently, the center of mass motion does not affect the elastic modes and the elastic motion does not affect the inertial properties of the rigid modes.

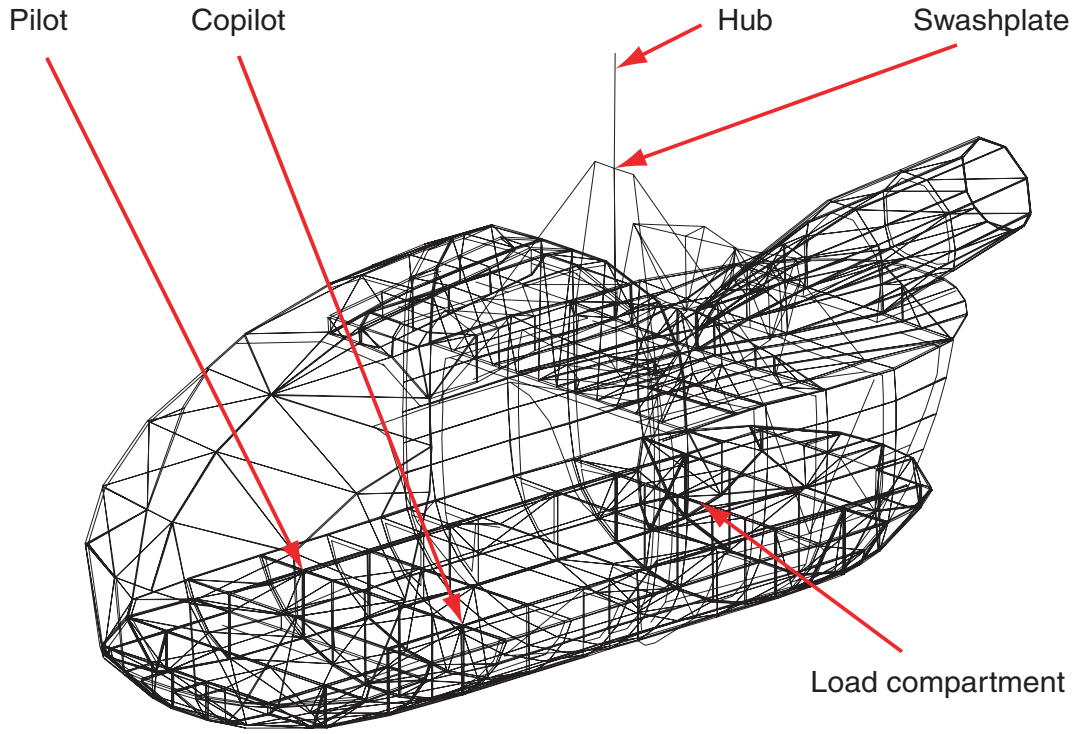

Figure 2.10 Definition of specific points in the fuselage [100]

In the Nastran model, the rotor is modelled with a point mass in order to calculate the center of mass and approximate the influence of the inertia on the modes. Only the elastic modes need to be imported from Nastran into Camrad II. The rigid body modes, therefore, must be truncated. Aerodynamics influences of the rotor on the damping and stiffness properties of the fuselage modes are neglected.

2.3.2 Structural Damping

The properties of the elastic modes consist of the generalized mass m, the frequency ω, the structural damping g, and the linear ξ and angular γ mode shapes. The generalized coordinate is denoted by q. F and M represent the forces and moments:

$$m(\ddot{q} + g\omega\dot{q} + \omega^2 q) = \xi^{\mathrm{T}} F + \gamma^{\mathrm{T}} M \tag{2.42}$$

The finite-element calculation does not yield values for the damping of the modes. Therefore, results from ground vibration tests [27] are used. In these tests, the structural damping of 29 modes, ranging from 5.52 Hz to 60.64 Hz, was measured. However, due to inaccuracies in the measurement of high frequency modes in the experiment, as well as deficiencies in the finite-element model, the results for frequencies above 40 Hz were considered to be unreliable. The average value of the critical damping ratio was 2.91%. In the frequency range of interest around 4/rev, the modes ranging from 17.64 Hz to 42.68 Hz have an average critical damping ratio of 3.02%. The smallest critical damping ratio in this frequency

range was 2.2%. To be safe, this value is used for all modes calculated using the finite-element method. In Camrad II, the structural damping (twice the critical damping ratio) is implemented as viscous damping.

2.3.3 Coupling and Mode Shapes

The rotor and fuselage are coupled via pitch/mast bending [42]. This is implemented by specifying the mode shapes (both linear and angular) at the hub. The contribution of the swashplate to coupling is ignored.

The elastic modes can be arbitrarily scaled. If the mode shapes are multiplied by a factor s (at all locations), the generalized mass should be multiplied by s^2 and the solution for the generalized coordinates divided by s. To compare the modes, the generalized mass is normalized to unity.

As coupling is via pitch/mast bending, the mode shapes of the individual modes determine how the fuselage and rotor modes are coupled. In order to examine this, the linear mode shapes are studied in more detail in the following. Translational displacement in z direction (coupling with the out-of-plane force) and the resulting translational displacement in x and y directions (coupling with the in-plane forces) are examined. A large translational displacement at the hub in the rotor plane is expected to coincide with strong coupling with the lag modes of the rotor, whereas a large degree of translational displacement in thrust direction indicates coupling with the flap modes. The second influencing factor is the frequency of both the fuselage and rotor modes.

Figure 2.11 shows translational displacement at the rotor hub out-of-plane (a) and in-plane (b). It can be noted that the values for displacement differ significantly. As an example, mode no. 6 shows a small degree of displacement in both in-plane and out-of-plane direction compared to other modes. Mode no. 7 has the largest degree of displacement in in-plane direction and a medium value in out-of-plane direction. Mode no. 22 has the largest degree of displacement in out-of-plane direction, with a comparatively small value in in-plane-direction.

Figure 2.12 (a) shows the shape of mode no. 6. It can be noted that this mode is dominated by a twisted tail boom with a small degree of displacement at the hub, whereas mode no. 7 is a bending mode of the entire structure, with a large degree of displacement at the hub, as shown in Figure 2.12 (b).

2.3.4 Pole Locations of the Coupled System

As previously noted, the rotor and the fuselage have been modelled as two subsystems with individual dynamic properties. By coupling the subsystems via pitch/mast bending, a new total system is created, which is expected to have changed dynamic properties compared to the two sub-systems. This section examines coupling between the modes. Camrad II offers

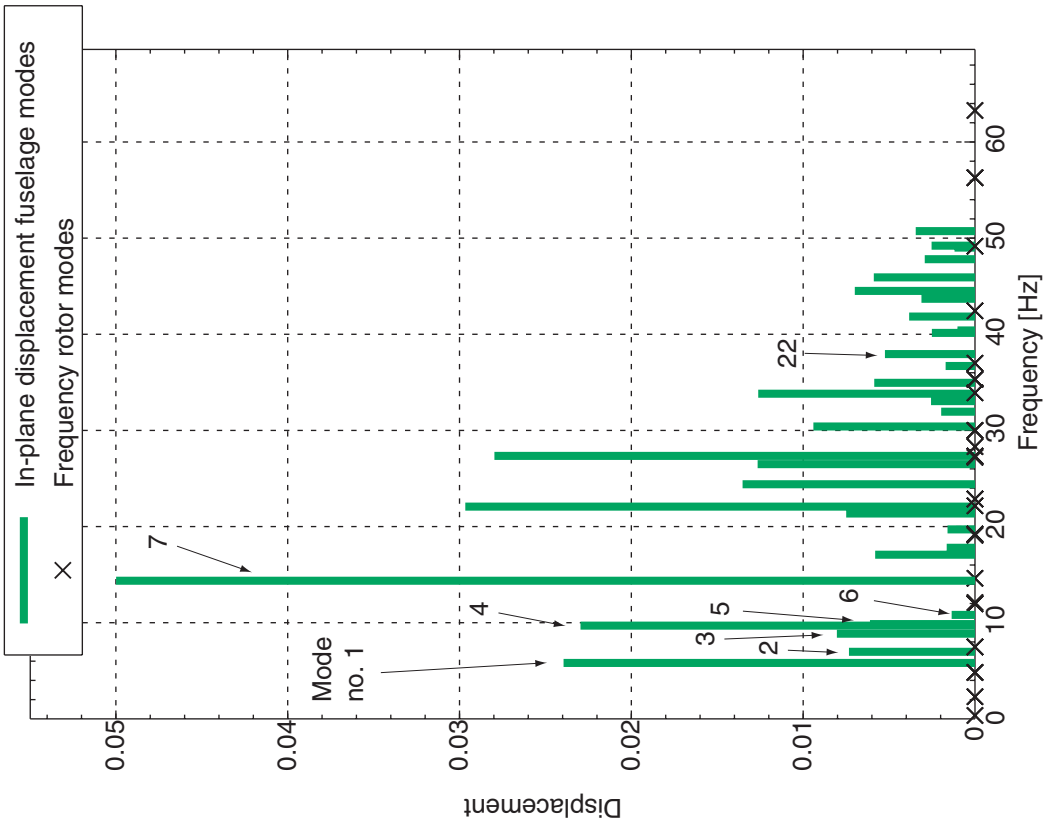

Figure 2.11 **(b)** In-plane linear fuselage mode shape at rotor hub [97]

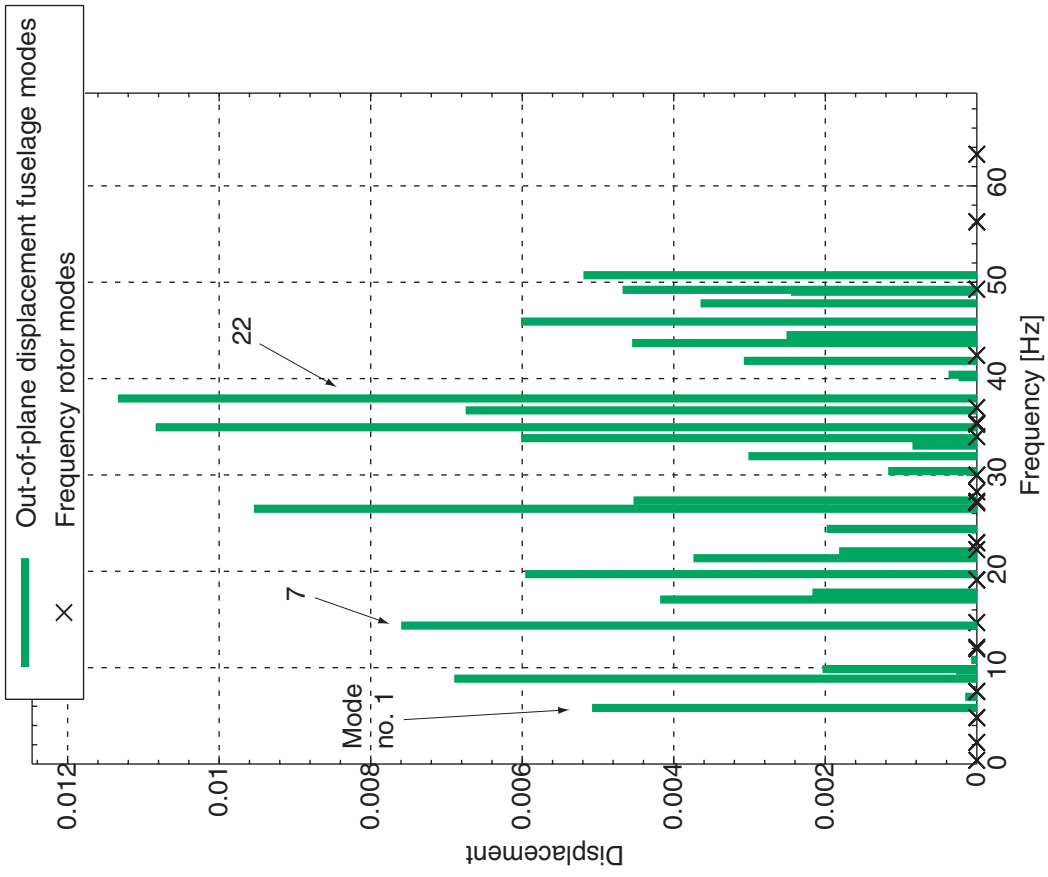

Figure 2.11 **(a)** Out-of-plane linear fuselage mode shape at rotor hub [97]

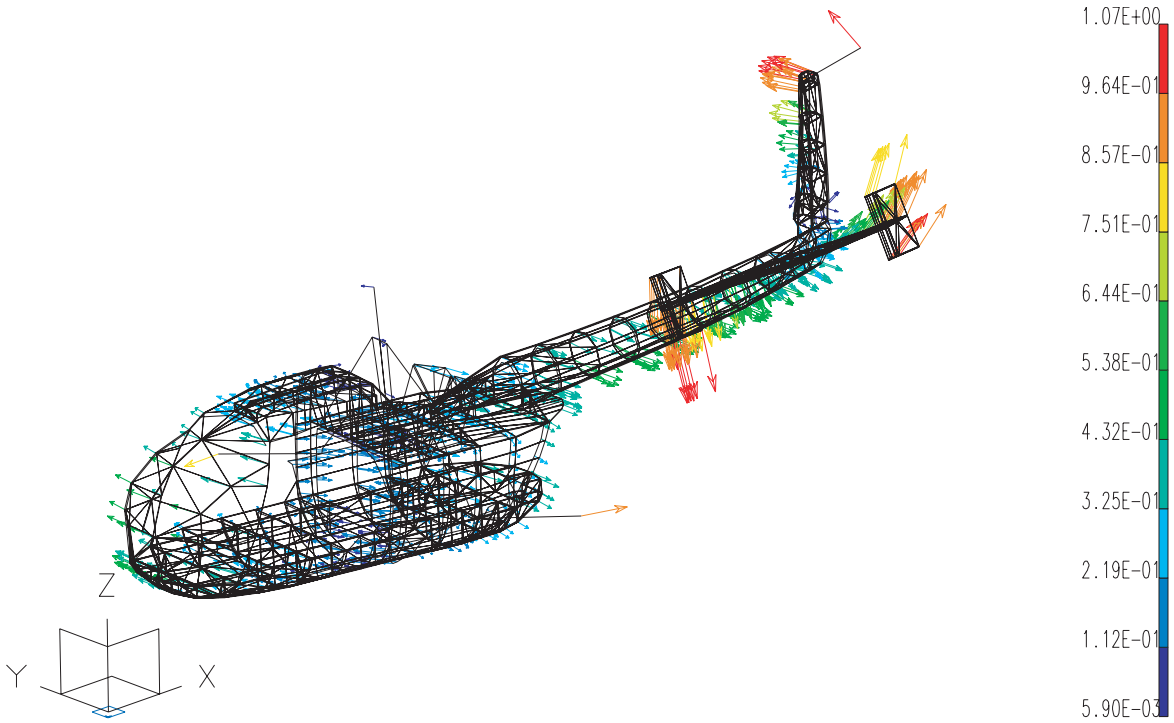

Figure 2.12 **(a)** Fuselage mode no. 6, frequency 10.81 Hz [100]

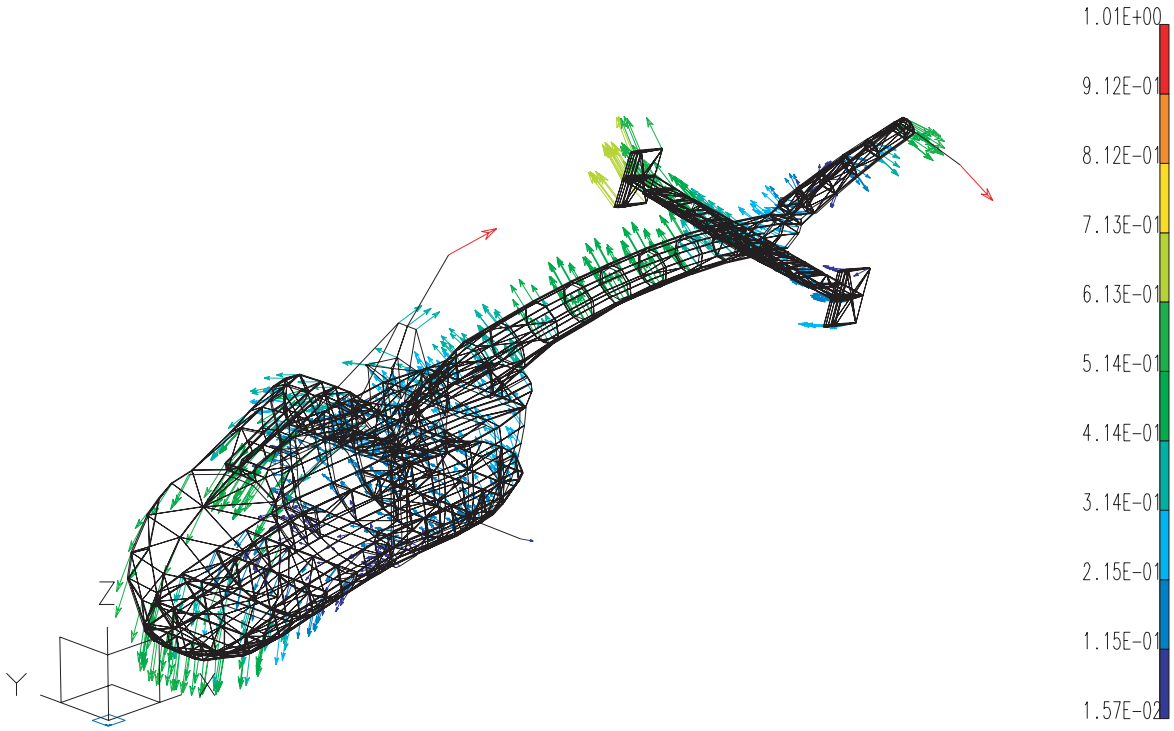

Figure 2.12 **(b)** Fuselage mode no. 7, frequency 14.37 Hz [100]

the possibility of declaring modes flexible or rigid on a mode-by-mode basis, i.e. to switch modes on and off. The following cases can be analyzed with the help of this feature:

- Flexible rotor with rigid fuselage
- Flexible rotor with only specific fuselage modes flexible
- Flexible rotor with flexible fuselage (all fuselage modes flexible).

To analyze the influence of specific fuselage modes, a coupled system of the flexible rotor and only one flexible fuselage mode is created and the pole locations are calculated. Fuselage mode no. 6 is shown as an example in Figure 2.13 (a). The rotor pole locations are unchanged, thus indicating no significant coupling between fuselage mode no. 6 and the rotor modes. In contrast to this, fuselage mode no. 7 is coupled with several rotor modes (Figure 2.13 (b)). A significant increase in the critical damping ratio from 1.5% to 3.2% can be observed in the progressive first lag mode. Furthermore, coupling with the first flap mode and minor influence on both second flap and second lag modes can be concluded from the changed pole locations. These results confirm the findings obtained by analyzing the mode shapes at the hub position in the last section. The pole locations for a model with a flexible rotor and 17 elastic fuselage modes are given in Figure 2.14. See Section 2.3.5 for a discussion of the number of fuselage modes to be considered.

A number of conclusions can be drawn:

- Coupling rotor and fuselage leads to an increase in damping for most lag modes
- The damping ratio of flap modes is partly reduced
- The torsional mode is not greatly affected
- Most of the fuselage modes are better damped in the coupled system.

2.3.5 Number of Fuselage Modes Required

While assembling the entire model, the question arises of how many fuselage modes are required to model the dynamics sufficiently. The most interesting frequency range for the purpose of vibration reduction is between approximately 20 Hz and 40 Hz, which is around the blade passage frequency of 4/rev (= 28.264 Hz). In the following analysis, an increasing number of fuselage modes are added, while the transfer behavior of the system is constantly monitored. The number of modes is assumed to be sufficient when adding further modes does not lead to further changes in the transfer behavior. Modes with a frequency close to 4/rev are first considered: mode no. 14 (26.49 Hz) and mode no. 15 (27.35 Hz). More modes are gradually added with close frequencies, higher or lower, centered around 4/rev: mode no. 16 (30.41 Hz), then mode no. 13 (24.4 Hz), and so on.

Transfer functions from collective and cyclic inputs at 4/rev are analyzed in order to monitor the transfer behavior of the system. Figure 2.15 shows the frequency responses (both gain and phase) at 4/rev for transfer functions from IBC inputs to accelerations at the rotor

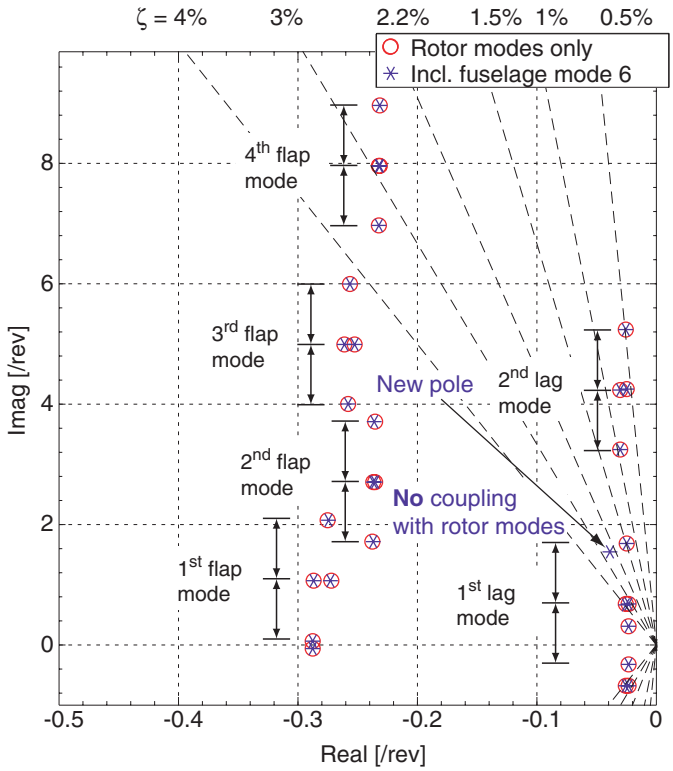

Figure 2.13 **(a)** Fuselage mode no. 6, no coupling, rotor pole locations unchanged [97]

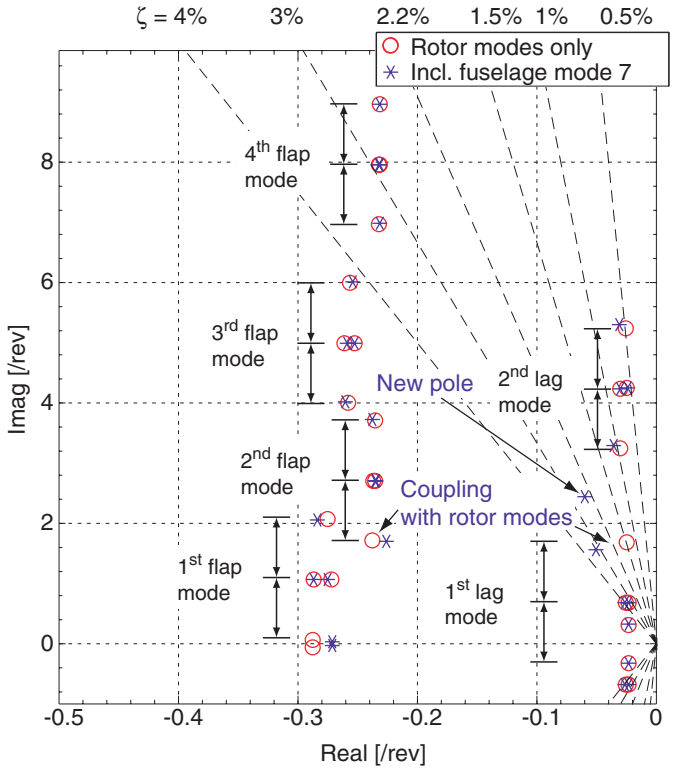

Figure 2.13 **(b)** Fuselage mode no. 7, coupled with 1st and 2nd flap and lag modes [97]

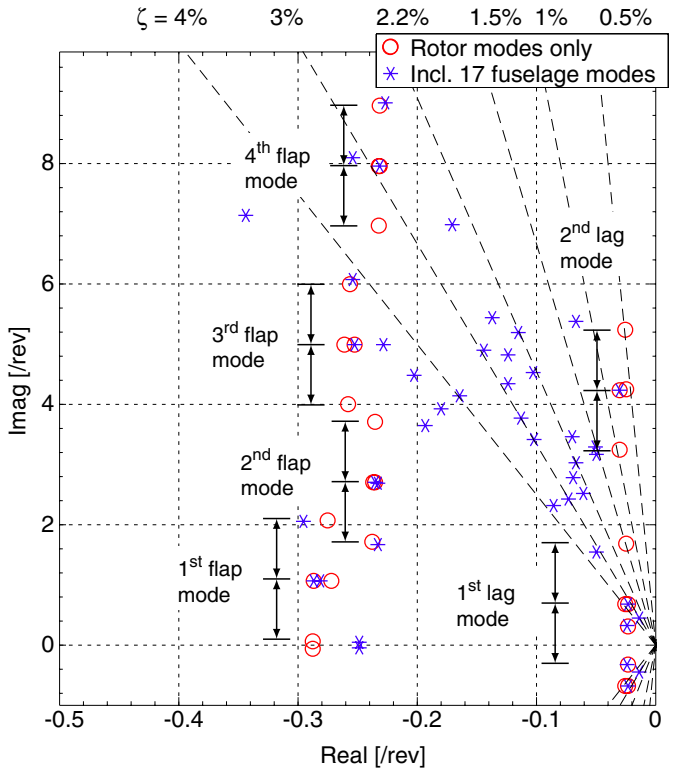

Figure 2.14 Rotor and 17 elastic fuselage modes (modes no. 7-23) [97]

hub. The results for a transfer function from IBC inputs to accelerations at a point in the fuselage (load compartment) are given in Figure 2.16. The results show that from 17 modes onwards, no significant changes occur in the frequency responses. This finding suggests that 17 modes are sufficient to model the dynamic properties of the fuselage in the frequency range of interest. The highest frequency (mode no. 23) is 40.14 Hz, thus the maximum of approximately 40 Hz (from where on mode calculations become less reliable (see Section 2.3.2)), is only violated marginally.

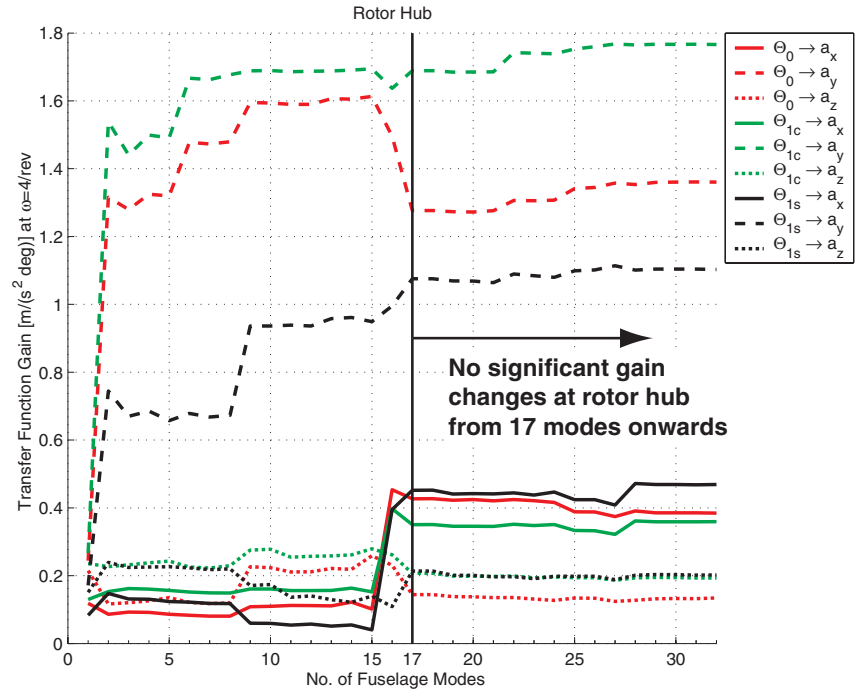

Figure 2.15 **(a)** Transfer function (gain) from IBC inputs to accelerations at rotor hub at 4/rev vs. number of fuselage modes considered [100]

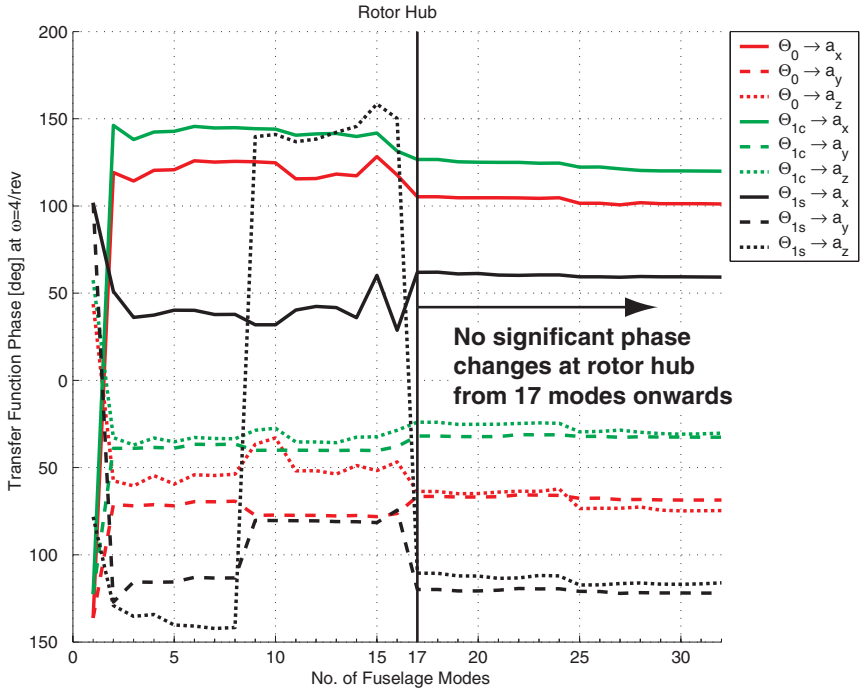

Figure 2.15 **(b)** Transfer function (phase) from IBC inputs to accelerations at rotor hub at 4/rev vs. number of fuselage modes considered [100]

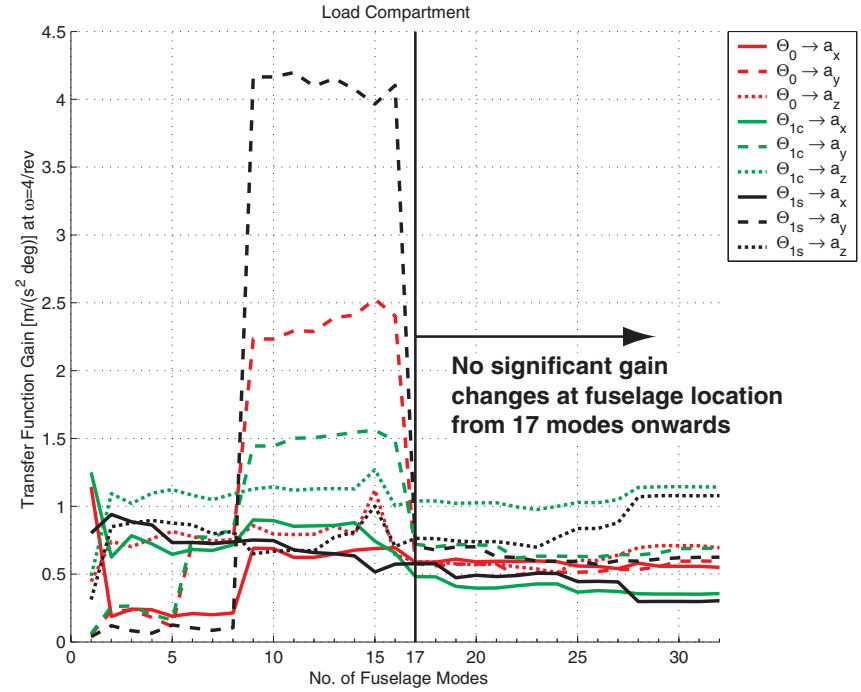

Figure 2.16 **(a)** Transfer function (gain) from IBC inputs to accelerations in the load compartment at 4/rev vs. number of fuselage modes considered [100]

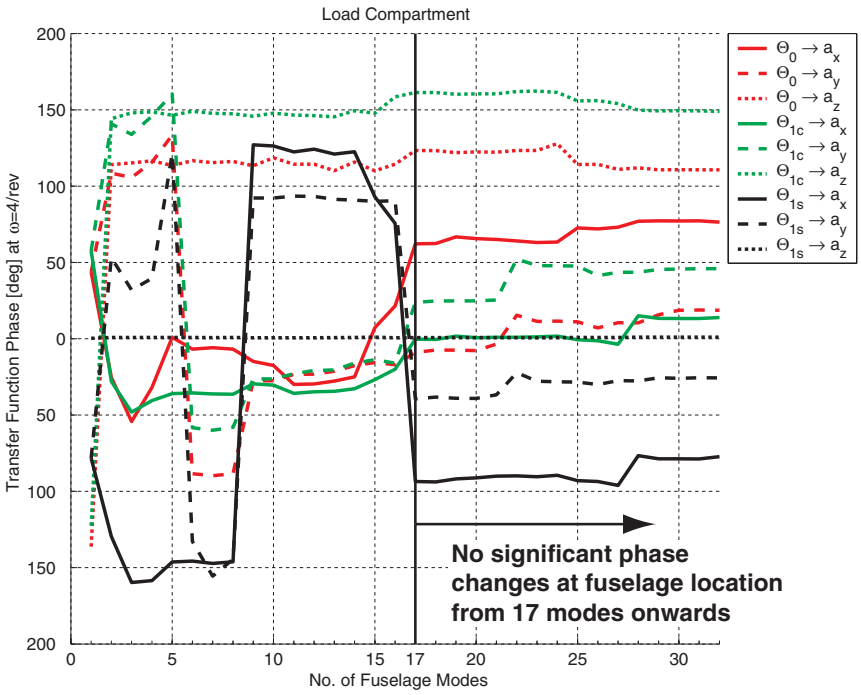

Figure 2.16 **(b)** Transfer function (phase) from IBC inputs to accelerations in the load compartment at 4/rev vs. number of fuselage modes considered [100]

2.4 Periodicity

This section presents aspects of the plant that arise from its periodicity and discusses some consequences for control law design. The interplay of the Fourier coordinate transformation, the multiharmonic response of the periodic plant, and the hub filtering effect of the rotor are analyzed in detail.

2.4.1 Multiharmonic Responses

An ordinary time-constant linear system, described with one or a set of linear differential equations with constant coefficients, responds to a single harmonic input with a single harmonic output of the same frequency. A system that can also be described with one or a set of linear differential equations but having time-periodic coefficients is called a "linear time-periodic system". The response of a linear time-periodic system to a single harmonic input is generally a multiharmonic output. The Fourier coefficients of the multiharmonic response depend on the system properties, i.e. on the periodicity of the coefficients of its differential equations. Figure 2.17 illustrates the fundamental difference between time-constant and time-periodic linear systems.

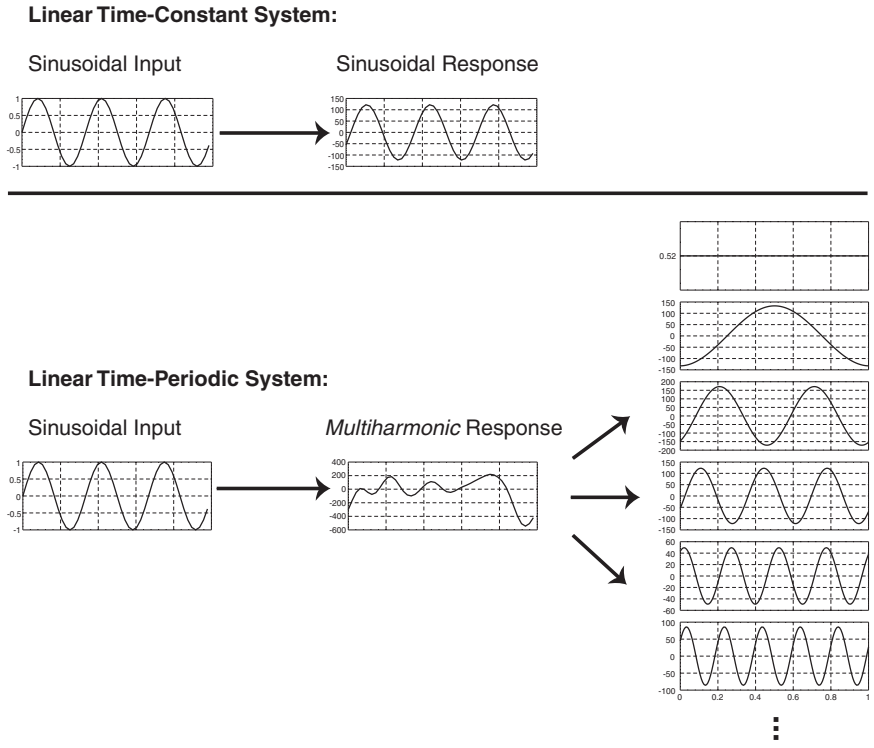

Figure 2.17 Multiharmonic response of a linear time-periodic system to a single harmonic input [48]

2.4.2 Transmissibility of Single Harmonic Blade Inputs

The following analysis is based on the comprehensive Camrad II model of the four-blade BO 105 helicopter. Open-loop simulations are performed with various single harmonic sinusoidal inputs with various frequencies but identical amplitudes of $1°$. The bar graphs in Figure 2.18 (a) represent the output amplitude of the Fourier coefficients and correspond to the input frequencies of $2/\text{rev}$ to $6/\text{rev}$. The amplitudes are given for different outputs: blade root moments for one blade in the rotating frame and rotor hub loads in the nonrotating frame. The Fourier coefficients are given for frequencies from $0/\text{rev}$ to $8/\text{rev}$. Note that the multiharmonic responses of the plant to the single harmonic input are caused by the time-periodic coefficients of the system, as described in the previous section. The input of the m^{th} blade ($m = 1$ to N) is a periodic function of $\psi_m = \psi + m\Delta\psi$, $\Delta\psi = 2\pi/\text{N}$. Therefore, all blades have identical loading and motion.

The blade root load outputs in the rotating frame respond to a single harmonic input with a multiharmonic output generally in all frequencies (only limited by the periodicity of the system). However, the response is dominated by frequencies close by, e.g. the response of a $2/\text{rev}$ input is typically dominated by $1/\text{rev}$, $2/\text{rev}$, and $3/\text{rev}$ sinusoidal components. The largest output amplitude is typically in the frequency of the input, whereas the amplitude of the "sidebands", i.e. the responses in frequencies different from the input frequency, typically decrease as the difference in frequency increases.

Figure 2.18 (b) shows the same simulation, but now with the time-constant rotor model in MBC. The rotating blade root outputs respond to single harmonic inputs with the frequencies $2/\text{rev}$ only with single harmonic outputs of $2/\text{rev}$. The same also holds for $6/\text{rev}$ inputs. By means of multiblade coordinates, however, the system responds to inputs with frequencies of $3/\text{rev}$, $4/\text{rev}$, and $5/\text{rev}$, with multiharmonic outputs in *all* three frequencies $3/\text{rev}$, $4/\text{rev}$, and $5/\text{rev}$, respectively. This is due to the fact that the multiblade coordinate transformation for the four-blade rotor introduces a progressive $(4+1)/\text{rev} = 5/\text{rev}$ and a regressive $(4-1)/\text{rev} = 3/\text{rev}$ cyclic mode. The multiharmonic response of the time-constant plant demonstrates how the transformation from SBC to MBC (partly) preserves the periodicity of the plant.

2.4.3 Hub Filtering

In order to determine the total influence of a rotor with N blades undergoing identical periodic motion, it is necessary to evaluate sums of harmonics, e.g.

$$\frac{1}{N}\sum_{m=1}^{N} \sin n\psi_m = f_n \sin n\psi \tag{2.43}$$

where $f_n = 1$ only if n is a multiple of the number of blades, otherwise $f_n = 0$ [43]. Again, the azimuth of the m^{th} blade is given by $\psi_m = \psi + m\Delta\psi$, $\Delta\psi = 2\pi/\text{N}$. This

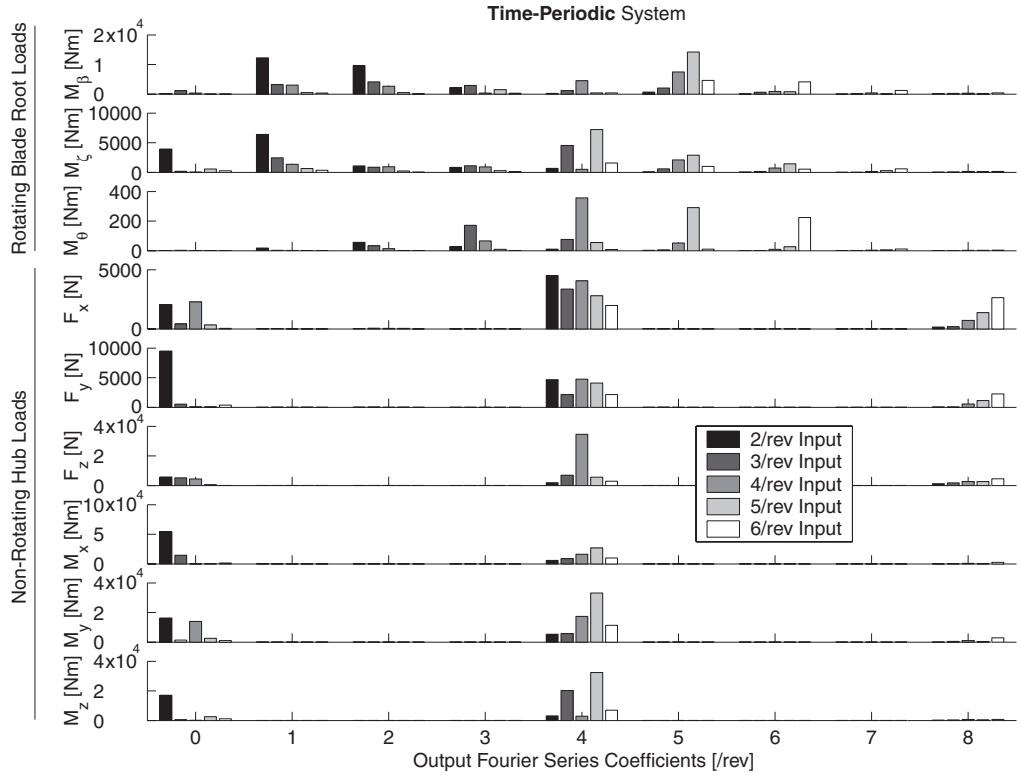

Figure 2.18 **(a)** Multiharmonic response of the periodic system at the blade root (rotating system) and at the hub (nonrotating system) to single harmonic inputs

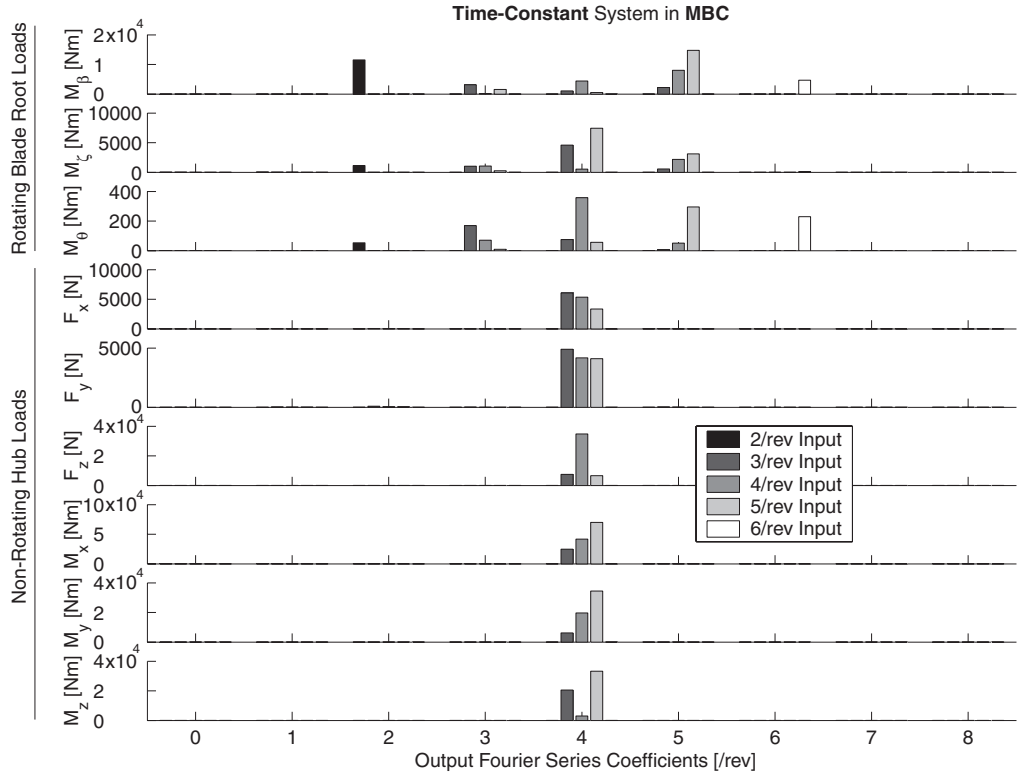

Figure 2.18 **(b)** Multiharmonic response of the constant system at the blade root (rotating system) and at the hub (nonrotating system) to single harmonic inputs

means that blade root loads with a frequency of N/rev are transmitted to the nonrotating frame. However, there are blade root loads that are multiplied by terms $\sin\psi_m$ (or $\cos\psi$), see (2.21), (2.22), (2.24), (2.25). By means of trigonometric relations, e.g.

$$\sin x \cdot \sin y = \frac{1}{2}(\cos(x-y) - \cos(x+y)) \tag{2.44}$$

it can be shown that $(N-1)$/rev, N/rev, and $(N+1)$/rev blade root loads yield N/rev terms in the summation and consequently are transmitted through the hub to the nonrotating system, see Table 2.1.

As regards transmission from individual blade commands in SBC to nonrotating hub loads, it can be stated that, in the periodic system, inputs of *any* frequency causing $(N-1)$/rev, N/rev, or $(N+1)$/rev blade root loads are transmitted to the rotor hub. Consequently, for a four-blade rotor, not only 3/rev, 4/rev, and 5/rev inputs, but also 2/rev and 6/rev inputs can be used to provoke 4/rev hub loads in the nonrotating system. However, whereas the 3/rev, 4/rev, and 5/rev inputs are "directly" transmitted to the rotor hub, the 2/rev and 6/rev inputs are only transmitted "indirectly" via the multiharmonic sideband responses of the blade root loads. These theoretical results are confirmed by experiments in [72].

Unfortunately, the Fourier coordinate transformation for the four-blade rotor translates 4/rev MBC inputs only into 3/rev, 4/rev, and 5/rev individual blade commands in SBC, leaving the 2/rev and 6/rev inputs inaccessible for controller designs based on a time-constant model. In contrast to this, periodic controllers based on the periodic plant can make use of the additional input frequencies; Figure 6.9 shows an example of where the periodic controller uses a 2/rev input. However, there are two drawbacks of 2/rev and 6/rev inputs: First, the effectiveness is reduced in comparison to 3/rev, 4/rev, and 5/rev inputs due to "indirect" transmission via sidebands only, as also reported in [72]. Second, the 2/rev input considerably affects 0/rev trim loads and the 6/rev input affects 8/rev hub loads in what could be an undesired way, see Figure 2.18 (a).

2.4.4 Periodicity of the Total System in MBC

As summarized in the previous sections, the total system consists of three subsystems with periodicity effects, see Figure 2.19. First, for a four-blade rotor, the N/rev input signal in MBC is split up into $(N-1)$/rev, N/rev, and $(N+1)$/rev signals in the coordinate transformation. Additional signals with $(N-2)$/rev and $(N+2)$/rev are created for rotors with $N = 5$ or 6 rotor blades[4]. The rotor blades considered to be the second subsystem respond to these input signals with multiharmonic responses. The resulting signals are dominated by

4. In the case of $N = 7$ rotor blades, third-order cyclic modes lead to additional frequencies of $(N-3)$/rev and $(N+3)$/rev.

frequencies of between $2/\text{rev}$ and $6/\text{rev}$. Finally, the hub filters frequencies with integer multiples of the number of blades, i.e. $0/\text{rev}$, mostly $4/\text{rev}$, $8/\text{rev}$, etc.

The system can be linearized from the input in MBC to the hub load output[5]. Both signals are given in the nonrotating frame. This system can be averaged, i.e. constant coefficients can be used, neglecting higher-order Fourier series terms. The resulting system is a linear time-constant system. This opens up the possibility of using a wide range of classical linear control law synthesis methods. The single harmonic $4/\text{rev}$ to $4/\text{rev}$ transfer function of the plant internally contains the $3/\text{rev}$, $4/\text{rev}$, and $5/\text{rev}$ physical transmission paths, making it an ideal choice on which to base control law designs.

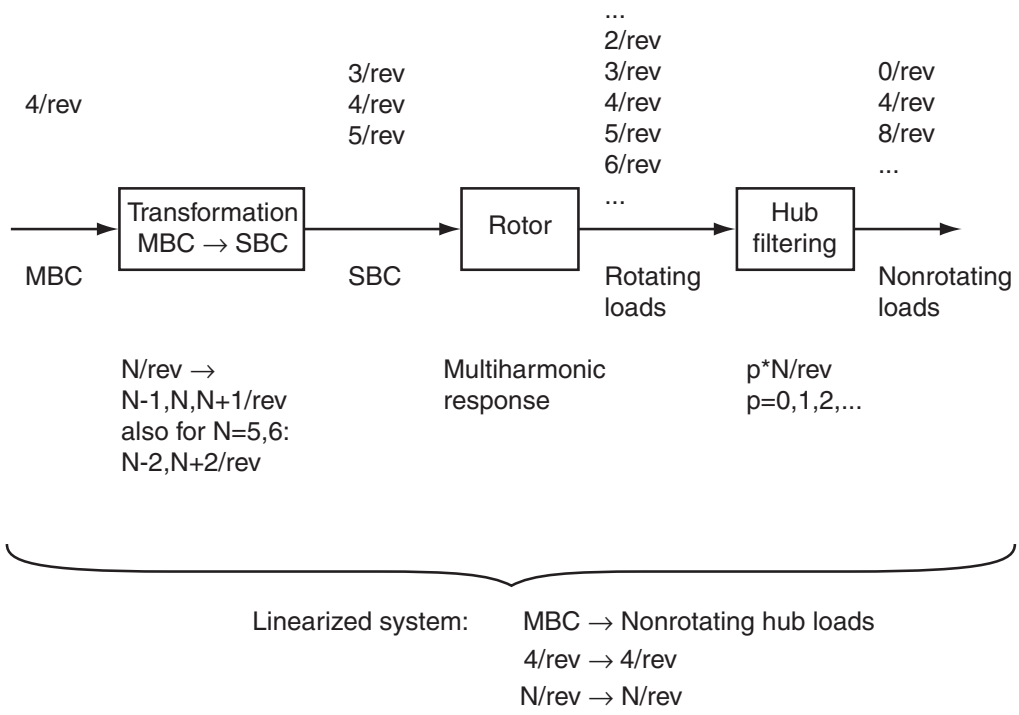

Figure 2.19 Transmission of signals through the coordinate transformation, rotor, and hub

2.4.5 Measuring Periodicity in State-Space Realizations

As noted previously, linear time-periodic systems can be realized in state-space. The matrix coefficients are periodic functions of time and can be written as Fourier series:

$$\begin{aligned} \dot{x} &= A(t)x + B(t)u \qquad t \in [0, T] \\ y &= C(t)x + D(t)u \end{aligned} \tag{2.45}$$

5. The coordinate transformation and the rotor are not realized as a series connection as shown in Figure 2.19, rather both inputs and states of the rotor are transformed to MBC, as described in Section 2.1.4.

As an example, the system matrix is given by:

$$A(t) = A_0 + A_{1c}\cos(\Omega t) + A_{1s}\sin(\Omega t) + A_{2c}\cos(2\Omega t) + \ldots \qquad \Omega = \frac{2\pi}{T} \quad (2.46)$$

The existence of higher harmonic terms A_n with $n > 0$ indicates that the matrix is time-periodic. This is a qualitative result. This, however, does not allow any conclusions to be drawn regarding *how* periodic the matrix or the system might be. A quantitative analysis is required in order to measure the periodicity of a matrix or a system.

For a single matrix element, a_{ij}, a comparison of the higher harmonic terms $a_{ij_n} = \mathrm{abs}(a_{ij_{nc}} + i \cdot a_{ij_{ns}})$, $n > 0$, normalized with the constant part a_{ij_0}, can give an indication of the relative significance of different higher harmonics. A comparison of the normalized higher harmonic terms a_{ij_n}/a_{ij_0} with unity ($a_{ij_0}/a_{ij_0} = 1$) helps to assess the importance of the higher harmonic terms relative to the constant part. Precautions must be taken if $a_{ij_0} = 0$, i.e. if a matrix element is periodic about zero, since, per definition, the relative higher harmonic term is infinite in this case.

The quantification of the importance of higher harmonics for a matrix (or a system) is more complex than for a single matrix element. The results are sensitive to scaling, since the state vector of a dynamic system can be arbitrary scaled, affecting the matrices A, B, and C. Normalization can be of help, although cases with zero constant parts typically yield misleading results.

Matrix norms can be used as a resort. The norm of higher harmonic matrices is normalized with the norm of the constant matrix $\mathrm{norm}(A_n)/\mathrm{norm}(A_0)$, $n > 0$. Here, the Frobenius[6] norm yielded good results. A comparison of normalized higher harmonic norms gives an indication of the relative importance of the different frequencies. The comparison of normalized higher harmonic norms with unity helps to assess the importance of the higher harmonic terms relative to the constant part, provided not all constant parts are zero (which is generally true for rotor models).

Figure 2.20 shows the normalized Frobenius norms of the higher harmonic matrix Fourier coefficients for the rotor model in different realizations. A comparison is made of all four system matrices A, B, C, and D. SBC and MBC are compared, as are Floquet transformed systems based on the system in SBC and MBC. Per definition, the matrix A of the Floquet transformed systems is constant, i.e. the normalized higher harmonic matrix norms are zero. The periodicity of the matrices B and C of both Floquet transformed systems is considerably increased in comparison to the original systems.

It would seem self-evident to use the approach of applying a Floquet transformation to the system and of using the resulting constant matrix A and the constant part of the periodic

6. The Frobenius norm of a matrix A is the square root of the sum of the squares of the individual elements of A. It is equivalent to the sum of the squares of the singular values of A.

matrices B and C for the control law design. The neglected periodicity in the matrices B and C could be modelled with input and output uncertainties. Although the Floquet transformed A matrix is constant (in contrast to a maximum higher harmonic norm of 0.14 in the original system), the periodicity in the B and C matrices is much higher (maximum higher harmonic norm of 0.73), thus the Floquet transformed system does not necessarily represent a good choice on which to base a control law design, since the total periodicity of the system (and, therefore, the error when neglecting higher harmonic terms) is significantly increased.

A comparison of SBC and MBC realizations of the rotor shows that the fundamental frequency of the MBC system is $1/2\text{rev}$, in contrast to 1rev for the physical plant in SBC [43], i.e. the odd Fourier coefficients are zero for the MBC system. Furthermore, the total periodicity of the system is reduced when MBC is used. This is particularly obvious in the D matrix with the maximum higher harmonic norm of 4.07 for SBC in contrast to 0.44 for MBC.

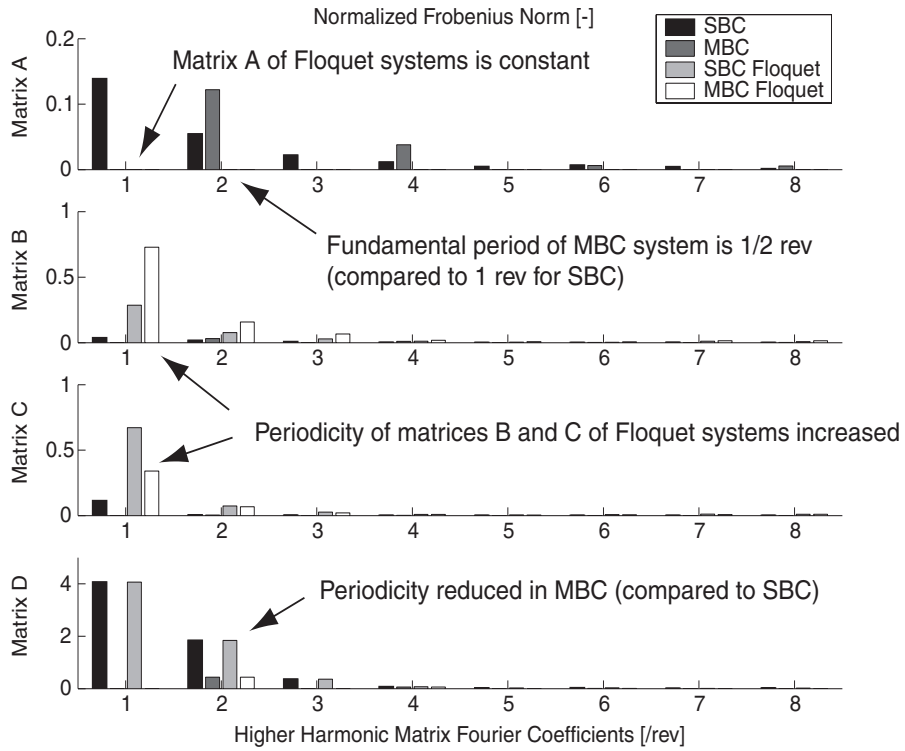

Figure 2.20 Periodicity of system matrices for realizations of the rotor system in SBC, MBC, and SBC and MBC-based Floquet transformation

Chapter 3

Control Law for the N-Blade Rotor

A control law for the N-blade rotor is developed in this chapter. The focus is on analyzing the potential of individual blade control and examining the dependence of the number of rotor blades. Optimal output feedback strategies are used to design control laws in order to reduce vibration. Aspects of simultaneous damping enhancement and robustness with respect to the flight speed are neglected for the moment but will be treated in Chapter 5.

3.1 N-Blade Rotor Effects

A straight forward approach to studying the influence of the number of rotor blades would be to compare different helicopters with different numbers of blades. A drawback of this approach is that the results would be affected by two factors: First, by the number of blades, as intended, and second by the fact that the different helicopters might have been designed for different missions, differ in size, mass, etc., whereby the second would make comparisons difficult, if not impossible. To overcome this problem, fictitious N-blade rotors are modelled for the four-blade BO 105 helicopter. In the four-blade rotor, all parameters of the rotor model are chosen to resemble the original BO 105 helicopter. For $N \neq 4$ blade rotors, the number of blades changes. If identical blades were used to those of the $N = 4$ blade rotor, the thrust and other forces and moments produced by the rotor would change. Therefore, the blade chord is scaled by the factor $4/N$. Consequently, the lift per blade is scaled and the total thrust is approximately independent of the number of rotor blades. This leads to approximately the same trim situation, i.e. the N-blade rotors produce the same trim forces and moments at the rotor hub for a given input of pilot collective and cyclic pitch. Choosing the blade chord as a parameter to be adapted to the number of blades means that the rotational speed, the rotor diameter, and fundamental blade properties, such as the natural frequencies of the flap and lag motion, remain unchanged, which helps to simplify comparisons [93], [62].

The different rotor models are trimmed at identical forward cruise flight conditions and are linearized about a trajectory about one rotor revolution, as described in Section 2.1.6. The result is a family of linear time-periodic models for rotors with N blades that differ in the

number of inputs (N, corresponding to N blades and N input modes in MBC) and states ($4N$, corresponding to flap and lag degrees of freedom and derivatives).

As described in Chapter 2, the most dominant vibration occurs at the blade passage frequency of N/rev . Amplitude and phase information is only available for the four-blade rotor from calculations using Camrad II or from flight tests. For the moment, it is assumed that the amplitude and phase is independent of N and only the excitation frequency is changed. Bramwell [13] gives a comparison of vibration for a four and five-blade helicopter. The results show that the amplitude of most hub loads is decreased with the five-blade rotor, except for the vertical shear in some cruise flight conditions. The above assumption is therefore simplifying. When comparing results, therefore, it has to be kept in mind that approximating N/rev vibration with 4/rev data underestimates true vibration for $N<4$ and overestimates vibration for $N>4$.

3.2 Optimal Output Feedback Control Law Design

The objective of the control law is to cancel vibration that enters the system as an output disturbance. The pitch of the individual blades can be controlled in order to change the lift (and drag) of the blades and consequently modify existing and/or provoke additional forces and moments at the rotor hub. By applying appropriate blade pitch commands, the baseline vibration can be reduced and ideally cancelled out at the rotor hub. The resulting hub loads are available to the controller as a measurement.

This disturbance rejection control problem is dealt with by implementing a servo-compensator. The servo-compensator is a dynamic compensator that is in resonance with the external disturbances acting on the plant [26], representing an internal model of the external disturbances. In the helicopter vibration problem, the external disturbances of sinusoidal type with the blade passage frequency N/rev are considered. The internal model of this external disturbance is an undamped oscillator tuned to the disturbance frequency. The oscillator is implemented as a second-order notch filter.

Standard optimal output feedback strategies are used to design the control law. A system of the form

$$\begin{aligned} \dot{x} &= Ax + Bu \\ y &= Cx + Du + d \end{aligned} \tag{3.1}$$

is considered, whereby x is the state vector, u the input vector, y the output vector, and d the output disturbance vector. The control law has the form:

$$u = -Ky \tag{3.2}$$

The gain-matrix K is to be chosen to minimize the performance criterion

$$J = \int_0^\infty (x^{\mathrm{T}} Q x + u^{\mathrm{T}} R u) dt \tag{3.3}$$

where $Q = \Gamma^{\mathrm{T}}\Gamma$ such that (Γ, A) is detectable and $R > 0$ [71].

The linear time-constant plant in MBC is augmented with the servo-compensator. The gain matrix is derived using an algorithm [71] for calculating optimal output feedback gains for the augmented system. Figure 3.1 shows the structure of the output feedback system with plant, servo-compensator, gain matrix, and with the baseline vibration acting on the system as output disturbances.

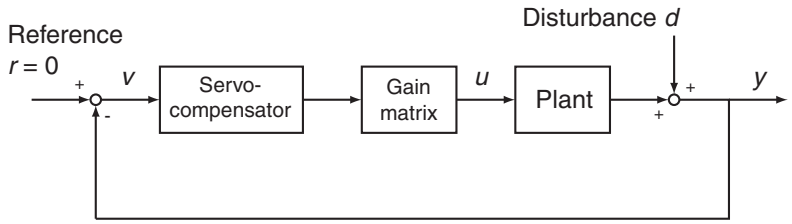

Figure 3.1 Disturbance rejection control structure

3.3 Vibration Reduction Results

For the family of N-blade rotors (here three to seven-blade rotors are considered), a set of controllers is designed using identical state and control weighting matrices in the cost functional, as described in the previous section. For each rotor, the number of outputs to be controlled are varied from three to six hub loads. The out-of-plane force and moments are chosen in the case of three hub loads. In the case of four outputs, the in-plane force F_x is added. In the case of five outputs, all three forces and the out-of-plane moments are considered. Finally, the entire force/moment vector at the rotor hub is considered when six outputs are controlled, see Table 3.1.

Table 3.1 Selection of outputs to be controlled

No. of	**3**	**4**	**5**	**6**
Selected Outputs	F_z, M_x, M_y	F_x, F_z, M_x, M_y	F_x, F_y, F_z, M_x, M_y	$F_x, F_y, F_z, M_x, M_y, M_z$

Table 3.2 shows the vibration reduction results for the different rotors and different numbers of outputs to be controlled. By following the first row of the table, a comparison can be made of the controllers designed for the same three outputs, but for different rotors. In all

cases, the vibration in the outputs considered can be reduced considerably (between –96% and –91%). A slight degradation can be observed when a rotor with an increasing number of blades is considered in the design. This is due to the higher blade passage frequency and the assumption of identical actuator dynamics, which leads to a smaller gain and a larger phase lag in the frequency response of the actuators for an increasing number of blades.

By taking into consideration the three-blade rotor and starting to increase the number of outputs to be controlled, the table shows that only three outputs can be reduced considerably. From four outputs onwards, the vibration can only be reduced by half of the original level (the shaded area in the table). A further increase in the number of outputs to be controlled further degrades vibration reduction. The results for the four-blade rotor are nearly identical to the results obtained with the three-blade rotor. The fourth blade does not lead to any additional degree of freedom being available for vibration control, since the rotor has a reactionless mode for an even number of blades. Thus, the vibration reduction potential is the same as it is for the three-blade rotor. The five and six-blade rotors allow a considerable vibration reduction (of between –92% and –88%) in five outputs. Although the results for up to five outputs are slightly better in the case of the seven-blade rotor, this rotor does not allow a considerable reduction in vibration (by around –90%) in all six forces/moments at the rotor hub, but only a value of –67% is achieved, which is a result comparable to the results of the five and six-blade rotors.

In summary, with three and four-blade rotors, three degrees of freedom are usable for vibration control, i.e. vibration can be reduced considerably in three outputs simultaneously. From five-blade rotors onwards, there are five degrees of freedom available for vibration reduction.

Table 3.2 Vibration reduction results for different numbers of blades and outputs

Resulting Vibration[a]	**3-Blade Rotor**	**4-Blade Rotor**	**5-Blade Rotor**	**6-Blade Rotor**	**7-Blade Rotor**
3 Outputs	-96%	-94%	-93%	-92%	-91%
4 Outputs	-49%	-43%	-94%	-91%	-93%
5 Outputs	-23%	-20%	-92%	-88%	-92%
6 Outputs	-36%	-32%	-74%	-72%	-67%

a. Example reading: For the four-blade rotor, the vibration in the three considered outputs are reduced on average by -94% of the original values of the three outputs considered. The vibration reduction (or, possibly, the vibration increase) in the outputs not considered is not included in the number.

3.4 Singular Value Analysis of the Plant

The linear time-constant model of the helicopter rotor in MBC is analyzed in the following. The MIMO transfer function from the IBC inputs to the hub loads is analyzed using singular values. Figure 3.2 shows the singular values for rotors with $N = 3$ to 7 blades. The frequency response is evaluated for a frequency from $1/\text{rev}$ to $10/\text{rev}$. The number of singular values coincides with the number of inputs (number of rotor blades, inputs in MBC). A comparison of the singular values of the three-blade rotor with those of the four-blade rotor shows that the largest three singular values (collective, progressive, and regressive cyclic modes) are almost identical, whereas the additional degree of freedom in the four-blade rotor corresponds to the differential mode with a gain some -100dB lower (reactionless) than the other modes. In the case of five rotor blades, first and second cyclic modes exist, resulting in five "usable" modes for active rotor control. As is the case for the four-blade rotor, the differential mode of the six-blade rotor is reactionless. Compared to the collective and the first and second cyclic modes, the third cyclic modes in the case of seven rotor blades have gains up to -50dB and -100dB lower, respectively. From a control law design perspective, this basically leaves five modes available for rotor control, as is the case for the five and six-blade rotors.

The findings confirm the results of the previous section where the number of degrees of freedom was examined by designing controllers with an increasing number of outputs to be controlled.

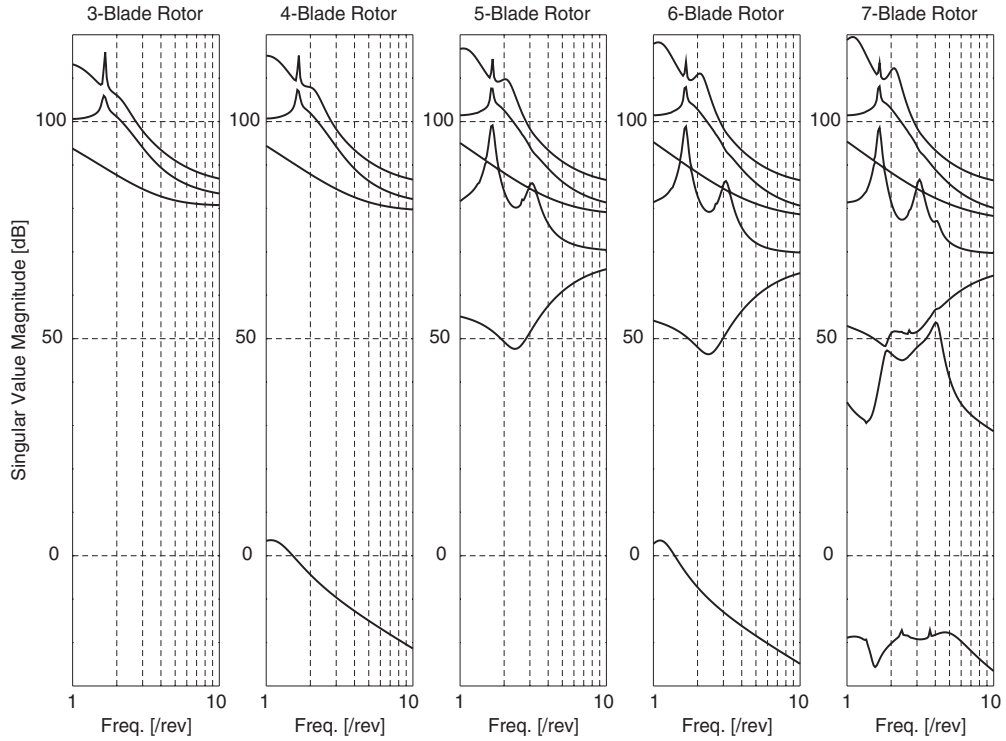

Figure 3.2 Singular values of the *N*-blade rotors

Chapter 4
Model Reduction

Model reduction is required, since in model-based H_∞ control the order of the controller depends on the number of states in the model used for design and the order of the controller is desired to be kept small. Either the model used for controller synthesis, or the controller itself, or both, can undergo model reduction. Here, the first approach will be taken, resulting in a reduced-order "design model" in contrast to the full-order original model that will be used for verification purposes. Existing model reduction techniques for continuous linear time-constant systems are extended to continuous linear time-periodic systems.

4.1 Reduction of Linear Time-Constant Systems

The reduction method applied to the model is the truncation of a balanced realization of the original system in state-space form. The algorithm actually utilized here uses Schur's method to calculate the reduced version of the system directly [89]. Hankel singular values are used to give an indication of the number of states to be retained in the reduced system.

It proved advantageous not to reduce the entire model as a whole, but to split it up first into sub-models. These sub-models are then reduced separately and are subsequently assembled to result in the desired reduced-order model. In order to determine suitable sub-models, the individual modes of the system are categorized into "critical" and "less critical" in terms of frequency and damping. Furthermore, the coupling between modes is considered. To examine the coupling between modes, the mode to be examined is truncated from the model. The poles of the remaining system are then compared with the poles of the original system. Changes in the pole locations of a mode indicate coupling with the truncated mode. Figure 4.1 shows this comparison for the second lag mode. The plot illustrates that the poles of the first lag and first and fourth flap mode do not change significantly, whereas the poles corresponding to third flap and torsion mode do change. From this it can be concluded that coupling exists between second lag and third flap and torsion modes.

As a result of the analysis, the model is separated into three sub-models. Table 4.1 gives details on the sub-models used and the degree of reduction. In total, the model was reduced

from 56 to 36 states. Figure 4.2 shows the poles of the original system compared with the poles of the reduced-order system.

Table 4.1 Details of model reduction

Sub-Model	Category	Contained Modes	No. of States	No. of States Retained
1	Less critical, low frequency	1st flap, 2nd flap	16	10
2	Critical	1st lag, 2nd lag, torsion, 3rd flap	32	24
3	Less critical, high frequency	4th flap	8	2
Total			56	36

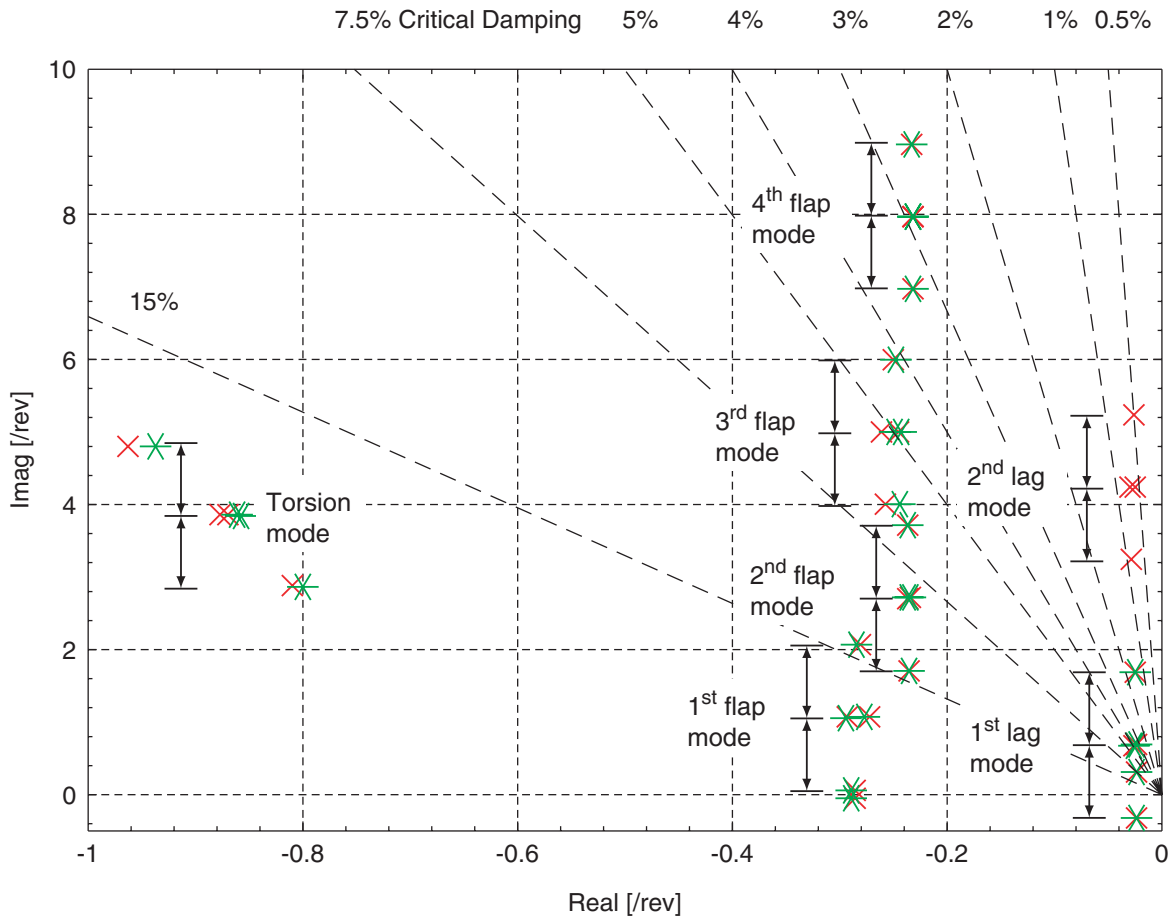

Figure 4.1 Pole locations original system (x) and system with the second lag mode removed (*)

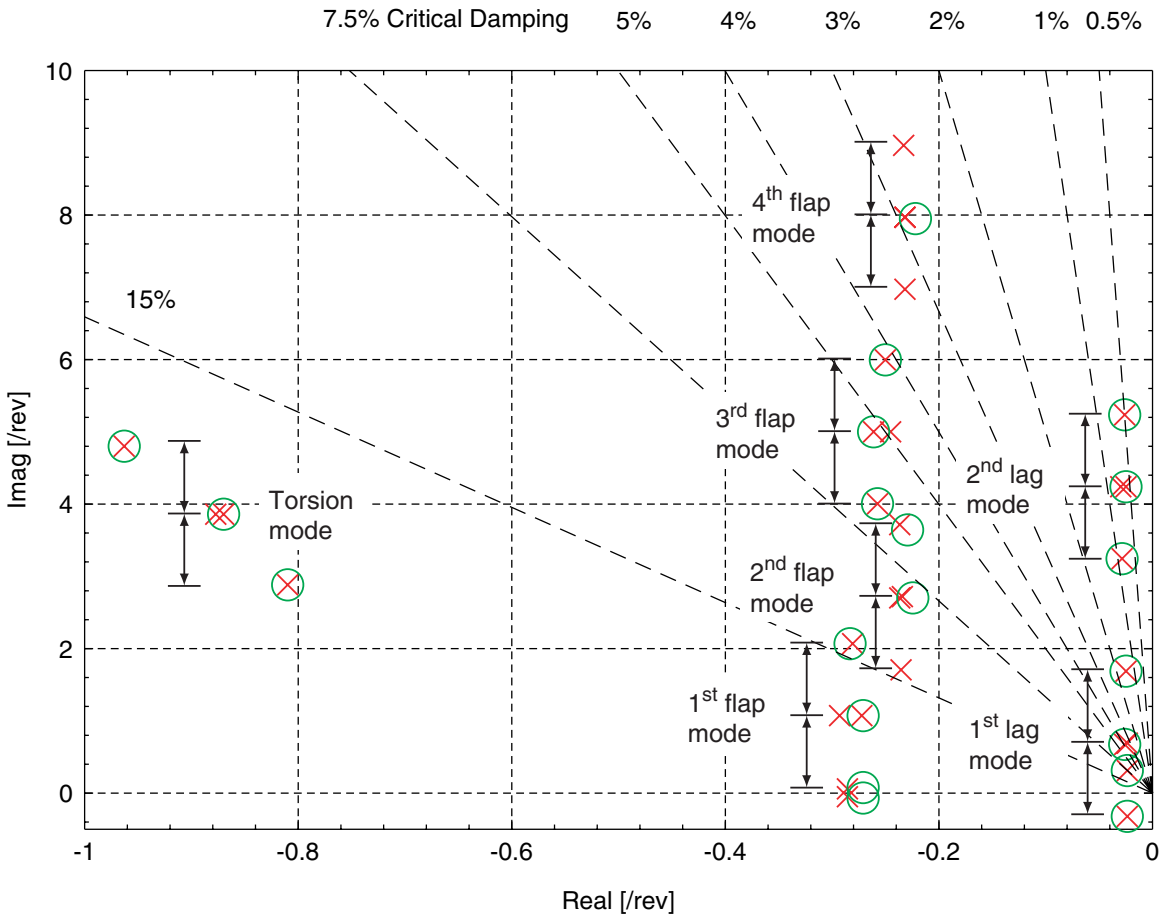

Figure 4.2 Pole locations original (x) and reduced-order system (o)

4.2 Extension to Linear Time-Periodic Systems

The model reduction technique demonstrated above is only applicable to linear time-constant systems. If periodicity has to be taken into account in the controller synthesis while using a reduced-order model for the design, the need for model reduction techniques suitable for linear time-periodic systems arises. The linear time-invariant method, therefore, is extended to linear time-periodic systems in the following.

The model is in the form

$$\dot{x} = A(t)x + B(t)u \qquad t \in [0, T] \tag{4.1}$$

$$y = C(t)x + D(t)u \tag{4.2}$$

with the matrices given for different values of t, e.g. for matrix $A(t)$

$$A(t_1), A(t_2), \ldots \qquad t_1, t_2, \ldots \in [0, T] \tag{4.3}$$

Applying the reduction techniques explained above to a constant system $A(t_n), B(t_n), C(t_n), D(t_n)$ at one specific time t_n and repeating this for all $t_1, t_2, \ldots$ results in reduced models

$$\dot{\bar{x}} = \overline{A}(t)\bar{x} + \overline{B}(t)u \qquad t \in [0, T] \tag{4.4}$$

$$y = \overline{C}(t)\bar{x} + \overline{D}(t)u \tag{4.5}$$

with the reduced matrices given for different values of t, e.g. for matrix $\overline{A}(t)$

$$\overline{A}(t_1), \overline{A}(t_2), \ldots \qquad t_1, t_2, \ldots \in [0, T] \tag{4.6}$$

This procedure gives the best model reduction in terms of the chosen algorithm and the number of states retained for each value of t, since the model reduction is applied to the actual system that corresponds to the value of t. As concerns Fourier series, however, this obvious advantage turns out to be a disadvantage. The reduction technique selects "the most important" states to be retained in the reduced-order model, and this selection may differ with different t due to the time-dependency of the model. Consequently, the remaining states and the remaining structure of the matrices are not consistent, which results in problems e.g. for Fourier series.

One way to overcome this problem is to perform the Fourier transformation first. The model can then be written in the form

$$\dot{x} = A(t)x + B(t)u \qquad t \in [0, T] \tag{4.7}$$

$$y = C(t)x + D(t)u \tag{4.8}$$

with the matrices given dependent on t, e.g. for matrix $A(t)$

$$A(t) = A_0 + A_{1c}\cos(\Omega t) + A_{1s}\sin(\Omega t) + A_{2c}\cos(2\Omega t) + \ldots \qquad \Omega = \frac{2\pi}{T} \tag{4.9}$$

The model reduction is then conducted with the constant (averaged values) system A_0, B_0, C_0, D_0, resulting in the reduced-order system with the state vector $\bar{x}$ and the transformation matrices S_l and S_r, derived with the algorithm described in [89]. The reduced-order system can be written as

$$\dot{\bar{x}} = S_l^{\mathrm{T}} A(t) S_r \bar{x} + S_l^{\mathrm{T}} B(t)u \qquad t \in [0, T] \tag{4.10}$$

$$y = C(t)S_r\bar{x} + D(t)u \tag{4.11}$$

with the matrices given dependent on t, e.g. for matrix $\bar{A}(t)$

$$\bar{A}(t) = S_l^{\mathrm{T}} A(t) S_r = S_l^{\mathrm{T}} A_0 S_r + S_l^{\mathrm{T}} A_{1c} S_r \cos(\Omega t) + \ldots \qquad \Omega = \frac{2\pi}{T} \tag{4.12}$$

Results of this method applied to the model are given in Figure 4.3 and Figure 4.4. The first singular value plot (Figure 4.3) shows a comparison of the original model with the reduced system, where the singular values of the reduced-order model closely match those of the original system. This indicates that the reduced-order model is suitable for controller design. This comparison was carried out for the averaged system, to which the reduction was applied, whereas Figure 4.4 shows the same comparison for the system influenced by the $\cos(2\Omega t)$ coefficients. Although this system was not reduced individually, but only by applying the transformation of the averaged system to the Fourier series coefficients, the singular values of the reduced-order system match those of the original system quite well. This finding indicates that the method can be used to create time-periodic reduced-order models.

The model reduction technique for continuous linear time-periodic systems can be summarized as follows:

1. The system undergoes a Fourier coordinate transformation from SBC to MBC.
2. The system matrices are developed into Fourier series.
3. A classical state reduction technique is applied to the constant part (averaged coefficients) of the system.
4. The resulting transformation is also applied to the higher harmonic Fourier series coefficients.

Based on the results of Section 2.4.5, the key idea of this process can be identified as: To first apply a transformation to the system that "shifts" as much as possible information into the constant part of the transformed system, and to next use the constant part of the *transformed* system to find optimal state reduction matrices for the entire system.

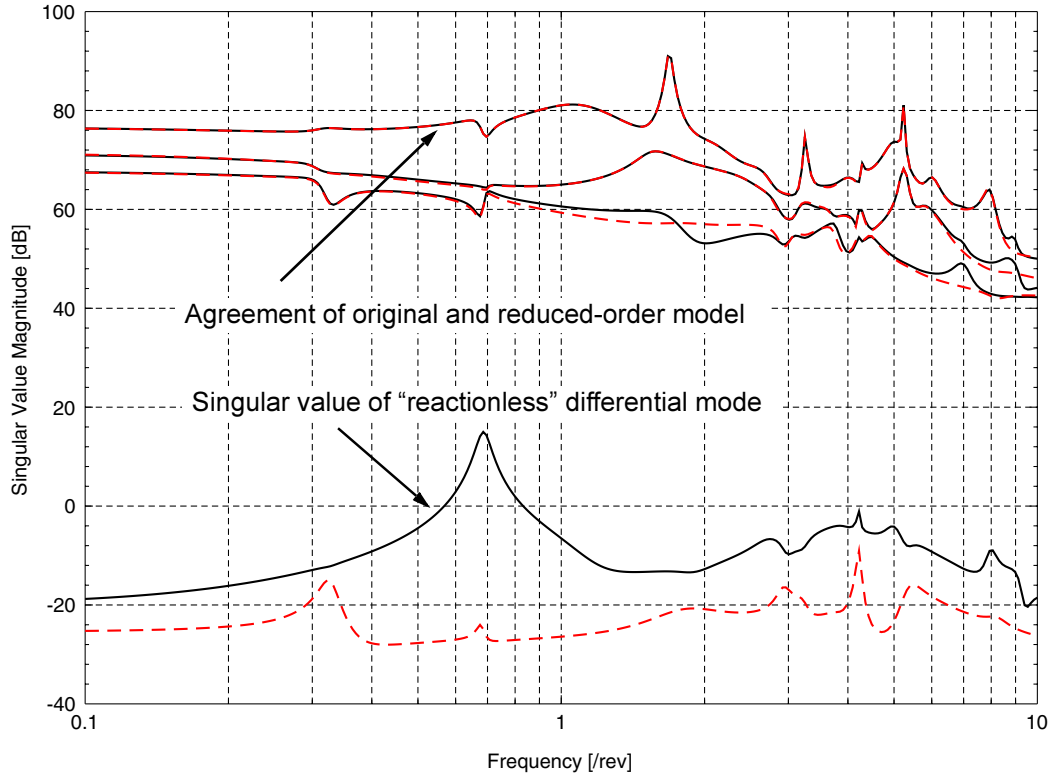

Figure 4.3 Singular values of averaged original system (solid) and averaged reduced-order system (dashed)

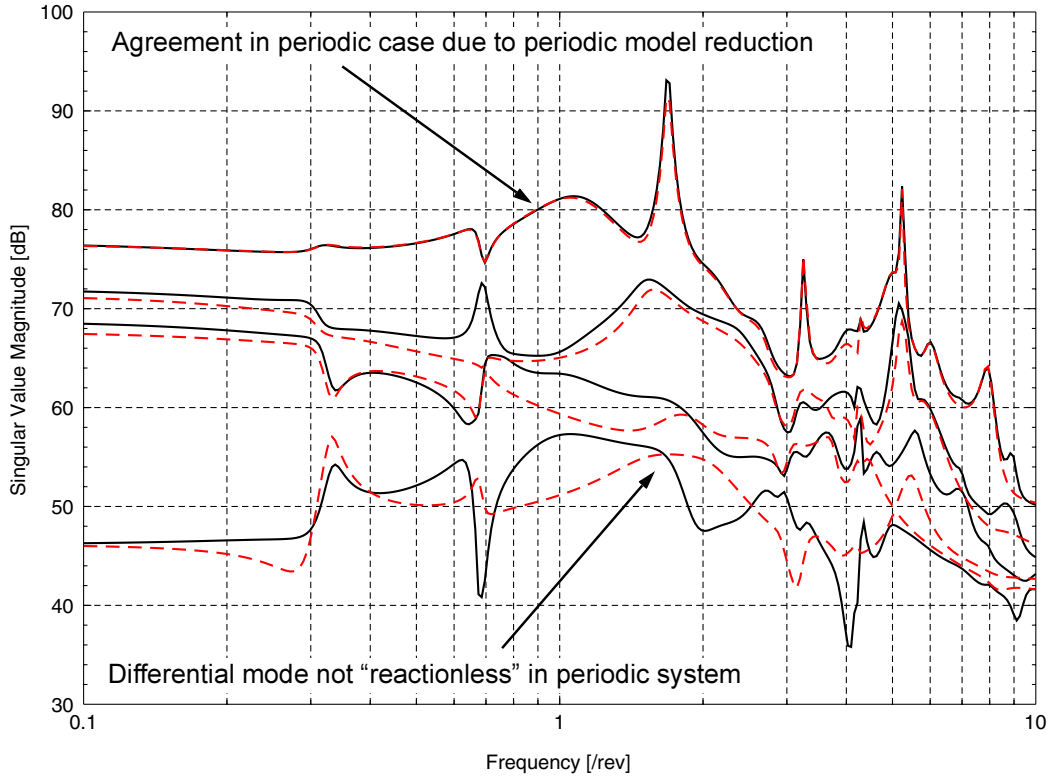

Figure 4.4 Singular values of original system (solid) and reduced-order system (dashed), both influenced by $\cos(2\omega t)$ coefficients

Chapter 5
Controller Design

In this chapter, the control objectives are defined, the idea of H_∞ optimization used to design the control law is outlined, and details of the controller design setup are presented. Time-periodic controllers are derived using time-periodic gain-scheduling. A method to systematize the process of adjusting weighting functions is developed.

5.1 Control Objectives

The two main objectives of the controller are:

- Vibration reduction
- Damping enhancement

In helicopter flight, forces and moments generated by the rotor act on the rotor hub and cause vibration in the fuselage. The anti-vibration controller is supposed to calculate suitable commands for the IBC inputs that modify existing and/or provoke additional forces and moments, that are equal in amplitude with but opposite in phase to the original forces and moments at the hub. If successful, the forces and moments cancel each other out. The sum of the original forces and moments and of the IBC-induced forces and moments transmitted to the fuselage is reduced, and the objective of vibration reduction is achieved. The second design purpose is to increase damping; this is demanded for the weakly damped lag modes. An increase in damping results in an improved transient response to disturbances.

Vibration control is assumed to be independent of primary flight control. This is justified, since the typical frequency range of primary flight control (approximately $0.3\,\mathrm{rad/sec}$ - $12\,\mathrm{rad/sec}$ [108], corresponding to $0.007/\mathrm{rev}$ - $0.27/\mathrm{rev}$ for the BO 105 helicopter) and the frequency range of interest for vibration control (around $3/\mathrm{rev}$ - $5/\mathrm{rev}$) are clearly separated. Experimental evidence for this is provided by the fact that during the BO 105 flight test series, non of the pilots reported any noticeable impact of higher harmonic control on helicopter trim or handling qualities [72].

5.2 Choice of Control Design Method

The objective of increased damping in the lag modes requires the lag rate of the blades to be fed back. Since no sensors in the blades, such as accelerometers in the outer part of the blade, are available, an observer-based control architecture is chosen. This allows one to feed back the (observed) lag rate and thus to increase damping without dedicated sensors.

To take into account deviations of the physical plant from the design model already in the design phase and to make the controller robust against changes in flight speed, H_∞ control methods are chosen for design. Closed-loop shaping is favored because of the flexibility in translating design requirements into weighting functions.

5.3 H_∞ Control Design

This section gives some important definitions from linear systems theory and briefly outlines the idea of H_∞ control. The treatment of H_∞ control design is by no means exhaustive, since the section focuses on problem-specific aspects. A full discussion can be found in [95], [6], [59].

5.3.1 The H_∞ Norm

The H_∞ norm of a stable linear time-invariant system $G(s)$ is defined as the peak value of the largest singular value over frequency of the frequency response $G(j\omega)$:

$$\|G(s)\|_\infty = \max_\omega \bar{\sigma}(G(j\omega)) \tag{5.1}$$

5.3.2 Linear Fractional Transformation

A plant P and a controller K are considered and are arranged as shown in Figure 5.1. If P is partitioned compatibly with K,

$$\begin{bmatrix} z \\ v \end{bmatrix} = P(s) \begin{bmatrix} w \\ u \end{bmatrix} = \begin{bmatrix} P_{11}(s) & P_{12}(s) \\ P_{21}(s) & P_{22}(s) \end{bmatrix} \begin{bmatrix} w \\ u \end{bmatrix} \tag{5.2}$$
$$u = K(s)v$$

the transfer function of the closed-loop system is then given by the lower linear fractional transformation (LFT):

$$\begin{aligned} z &= (P_{11} + P_{12}K(I - P_{22}K)^{-1}P_{21})w \\ &= F_l(P, K)w \end{aligned} \tag{5.3}$$

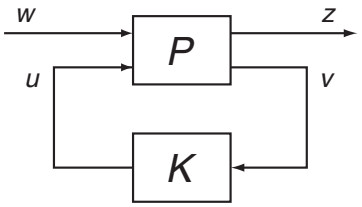

Figure 5.1 Lower linear fractional transformation

5.3.3 Frequency Domain Design Specifications

The transfer functions summarized in Table 5.1 can be defined by considering a feedback control system, as shown in Figure 5.2.

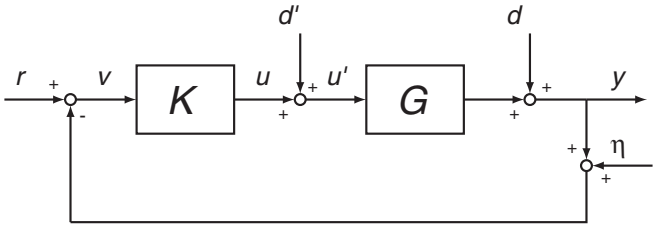

Figure 5.2 Feedback control system

Table 5.1 Transfer functions

Transfer Function		
Output sensitivity	$d \to y, r \to v$	$S_y = (I + GK)^{-1}$
Complementary output sensitivity	$r \to y, \eta \to y$	$T_y = (I + GK)^{-1}GK$
Input sensitivity	$d' \to u'$	$S_u = (I + KG)^{-1}$
Complementary input sensitivity	$d' \to u$	$T_u = (I + KG)^{-1}KG$
Controller activity	$r \to u$	KS_y
Plant with loop closed	$d' \to y$	S_yG

The control design objectives can be defined in terms of the maximum singular values of the transfer functions. Some of the most important requirements are:

- For good reference tracking and output disturbance rejection, $\bar{\sigma}(S_y) \ll 1$ is required
- To increase damping, e.g. of flexible modes, $\bar{\sigma}(S_y G)$ should be small
- For attenuation of measurement noise at the plant output, $\bar{\sigma}(T_y) \ll 1$ is required
- To limit control signals and hence avoid actuator saturation, $\bar{\sigma}(KS_y)$ should be small.

Further requirements arise for the objective of robustness:

- For robustness to additive uncertainty, $\bar{\sigma}(KS_y)$ should be small
- For robustness to input multiplicative uncertainty, $\bar{\sigma}(T_u)$ should be small
- For robustness to output multiplicative uncertainty, $\bar{\sigma}(T_y)$ should be small.

Due to algebraic restrictions,

$$\begin{aligned} S_y + T_y &= I \\ S_u + T_u &= I \end{aligned} \tag{5.4}$$

requirements cannot be met simultaneously over the entire frequency range, e.g. due to $S_y + T_y = I$ it is not possible to ensure $\bar{\sigma}(S_y) \ll 1$ for reference tracking and $\bar{\sigma}(T_y) \ll 1$ for noise attenuation simultaneously. To overcome this difficulty, frequency-dependent weighting functions $W(s)$ or "desired transfer function shapes" $W(s)^{-1}$ are introduced. As an example, it is sufficient to require $\bar{\sigma}(S_y) \ll 1$ for reference tracking in the low frequency range, whereas $\bar{\sigma}(T_y) \ll 1$ for noise attenuation is most important for high frequencies. Such requirements are "compatible", i.e. they can be met simultaneously.

For the series connection $W_{S_y} S_y$, $\left\| W_{S_y} S_y \right\|_\infty < 1$ may be required for all frequencies and hence S_y is shaped, as defined by W_{S_y}. Several requirements at the same time result in a combined criterion, e.g.:

$$\left\| \begin{matrix} W_{S_y} S_y & W_{S_y G} S_y G \\ W_{KS_y} K S_y & \cdots \\ \cdots & \cdots \end{matrix} \right\|_\infty < 1 \tag{5.5}$$

An example for a feedback control system augmented with weighting function is given in Figure 5.3.

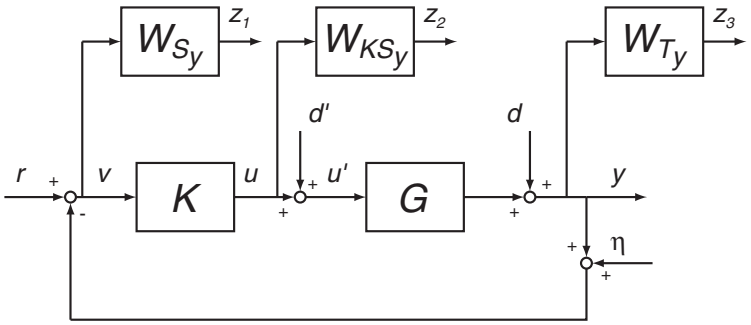

Figure 5.3 Feedback control system augmented with weighting functions

5.3.4 General Control Problem Formulation

The numerous possible control design setups can be arranged in the form shown in Figure 5.4. The generalized plant P consists of the plant G and the weighting functions W. The control variables are denoted by u, v represents the measurements to which the controller has access, w represents the exogenous inputs, such as reference signals and disturbances, and z represents the controlled outputs.

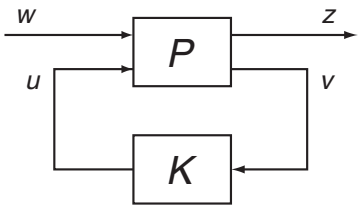

Figure 5.4 General control problem formulation

The standard H_∞ optimal control problem is to find an internally stable controller K that minimizes:

$$\left\| F_l(P, K) \right\|_\infty = \max_\omega \bar{\sigma}(F_l(P, K)(j\omega)) \tag{5.6}$$

In practice, the sub-optimal problem ($\gamma > \gamma_{\text{opt}}$) is solved:

$$\left\| F_l(P, K) \right\|_\infty < \gamma \tag{5.7}$$

The optimal solution is approached by reducing γ iteratively. The algorithm used to calculate the sub-optimal controller is outlined in Appendix A. The order of the resulting controller is the same as that of the generalized plant P.

5.4 Controller Design Setup

Only output feedback is possible for the structure of the controller, since the state variables are not measurable. Furthermore, the output disturbance is not available directly to the controller, since only the superposition of baseline vibration and IBC-induced vibration can be measured. Figure 5.5 shows the closed-loop structure, set up for disturbance rejection. The reference signal from Figure 5.2 is set to $r \equiv 0$ and is omitted in Figure 5.5. The signal d stands for output disturbances that cannot be influenced by the controller output u. The output disturbance is the periodic baseline vibration. These quantities are summed up with the vibration y caused by IBC. The sum v corresponds to the overall vibration that acts on the helicopter. Uncertainties of the plant G are modelled as input and output uncertainties. The sum of controller output u and uncertainty d' represents the IBC input of the plant in MBC.

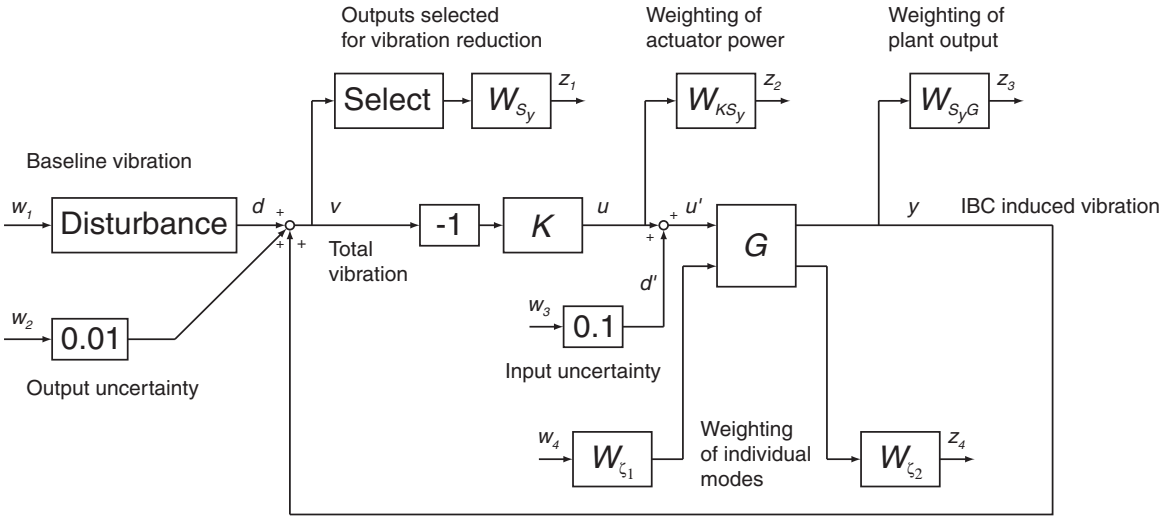

Figure 5.5 Closed-loop structure used for controller design

The reduced-order model described in Section 4.1 is used for design purposes. A comparison of the high and low flight velocity operating points showed that high flight velocity is more critical, e.g. lag damping is slightly lower. For this reason, the more critical high velocity model was used for design.

5.4.1 Modelling the Output Disturbance

The baseline vibration acts on the system as an output disturbance at the known frequency of 4/rev, determined by the number of blades and the rotational speed of the rotor. In the most general case, one element in the exogenous input vector w_1 is required per plant output, resulting in as many degrees of freedom (δ's) as plant outputs ($\dim(w_1) = \dim(d)$) to be controlled, i.e. allowing arbitrary directions in the disturbance vector d.

The directionality of the disturbance, however, can be modelled using the 4/rev coefficients of a Fourier series of the baseline vibration, resulting in one degree of freedom δ_1, $(\dim(w_1) = 1)$:

$$d = \delta_1 a_{4,\cos}\cos(4\Omega t) + \delta_1 a_{4,\sin}\sin(4\Omega t) \tag{5.8}$$

However, it is not sufficient to consider the Fourier series coefficients in one operating condition only, since the coefficients vary with flight speed. Instead, the average $(\bar{a})$ and the difference (Δa) of coefficients at two different operating points considered here can be used. This enables a disturbance ranging between the two operating points to be modelled using two degrees of freedom, δ_1 and δ_2, $(\dim(w_1) = 2)$:

$$d = \left(\delta_1 \bar{a}_{4,\cos} + \delta_2 \cdot \frac{\Delta a_{4,\cos}}{2}\right)\cos(4\Omega t) + \left(\delta_1 \bar{a}_{4,\sin} + \delta_2 \cdot \frac{\Delta a_{4,\sin}}{2}\right)\sin(4\Omega t) \tag{5.9}$$

The question as to whether to use the directionality information (less conservative) or to allow for arbitrary 4/rev disturbances (more conservative) is a trade-off between performance and robustness. Since the prediction of helicopter vibration is a difficult task, and is not entirely successful even with sophisticated analytical models [43], the directionality is not used in the controller designs presented here. This leads to a dimension of the disturbance vector equal to the number of outputs to be controlled.

In the frequency domain, a second-order Butterworth notch filter with resonance frequency 4/rev is used as a weighting function (see Figure 5.6), with both the filter output and its derivative for sine and cosine. The disturbance model and notch filters are denoted by "Disturbance" in Figure 5.5.

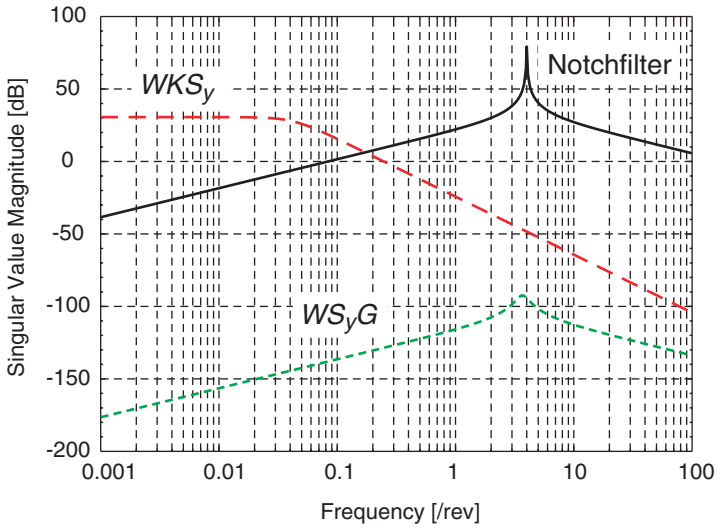

Figure 5.6 Frequency response of the weighting functions

5.4.2 Selection of Outputs to be Controlled

An elementary issue in helicopter vibration control is the selection of outputs to be controlled. For the design goal of vibration reduction, the controller has to induce a signal y that is ideally completely out of phase in comparison with the disturbance signal d. In general, this is not possible for an arbitrary degree of freedom. This can be shown with the complementary sensitivity function:

$$T_y = (I_{n\times n} + GK)^{-1} GK \tag{5.10}$$

The term GK has an upper limit for its rank,

$$\operatorname{rank}(GK) \leq \min(m, n) \tag{5.11}$$

where the dimension of the plant G is $n \times m$, the dimension of the controller K is $m \times n$, the number of IBC inputs is m, and the number of plant outputs is n.

This means that a maximum number of $n = m$ independent output signals can be generated with an m-blade rotor. When the number of rotor blades is even, this number is reduced to $n = m - 1$ due to the reactionless mode in the constant coefficient approximation, see Section 2.2. Typically, for a four-blade rotor, three hub forces/moments are chosen [29], e.g. the force vector $\begin{bmatrix} F_x & F_y & F_z \end{bmatrix}$ or a combination of the force in thrust direction and the roll and pitch moment $\begin{bmatrix} F_z & M_x & M_y \end{bmatrix}$. The jaw moment M_z is not usually considered in helicopter vibration control [67]. Although it appears self-evident to use the tail rotor to control vibration in M_z direction, the increased complexity can become prohibitive as a result of the flexibility of the tail boom and the dynamics of the drive train.

Instead of using a selection of three hub loads, a consideration of the symmetry in the helicopter rotor could be of help in selecting the outputs to be controlled. In hover flight, all blades experience identical aerodynamic conditions over one rotor revolution, except for influences of the fuselage and the tail rotor. These identical aerodynamic conditions lead to symmetry in the hub loads, i.e. the in-plane forces F_x and F_y differ only in a phase shift of $90°$ azimuth. The same holds for the moments about the roll and pitch axes M_x and M_y. These loads, as an example for the in-plane forces, can be interpreted as a rotating load that is observed in F_x and F_y with a phase shift of $90°$. Instead of individually concentrating on F_x and F_y, this rotating "fundamental" in-plane load could be targeted for vibration reduction. This leads to three outputs: $[F_x, F_y]$, $[M_x, M_y]$, and the single force F_z. Figure 5.7 shows singular values of transfer functions in hover flight. Comparing transfer functions at the blade passage frequency 4/rev from IBC inputs to individual outputs with the transfer function of the full MIMO system enables the in-plane forces F_x and F_y to be interpreted as corresponding to one singular value. Similarly, the out-of-plane moments M_x and M_y can be assigned to the second singular value and F_z corresponds to the third singular value. This coincides with the physical interpretation of F_x and F_y and also applies to M_x and M_y

differing only in a phase shift. In forward flight it is still possible to assign $[F_x, F_y]$, $[M_x, M_y]$, and F_z to the singular values (Figure 5.8), but it increasingly becomes an approximation, since an increase in forward flight speed causes differing aerodynamic conditions at the advancing and retreating blade and consequently less symmetry at the rotor hub. Results of the simulation for a controller design in line with this approach are given in Section 6.1.1.

The final goal of helicopter vibration reduction is to reduce vibration, not necessarily at the rotor hub, but at specific points in the fuselage, e.g. the pilot's seat or the load compartment [33]. The flexibility of the fuselage must then be included; see Section 2.3 for a description of the fuselage model and Section 6.3 for the results of the simulation.

The selected outputs are weighted with a second-order Butterworth notch filter with the frequency response shown in Figure 5.6.

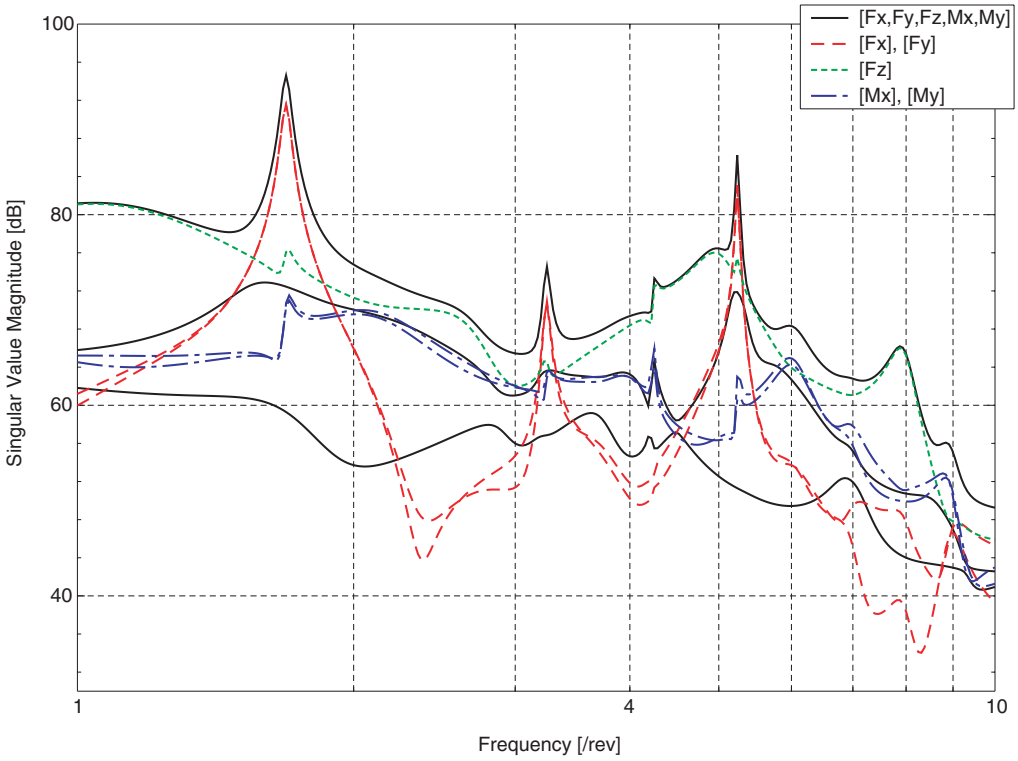

Figure 5.7 Assignment of in-plane forces, the out-of-plane force, and out-of-plane moments to the singular values in hover flight

5.4.3 Weighting of Individual Modes

The design goal of increased damping primarily concerns the lag modes. By transforming the system matrix to Jordan canonical form, the individual modes can be identified, as shown in the following extract of matrix A, where ω is the natural frequency and ζ is the critical damping ratio:

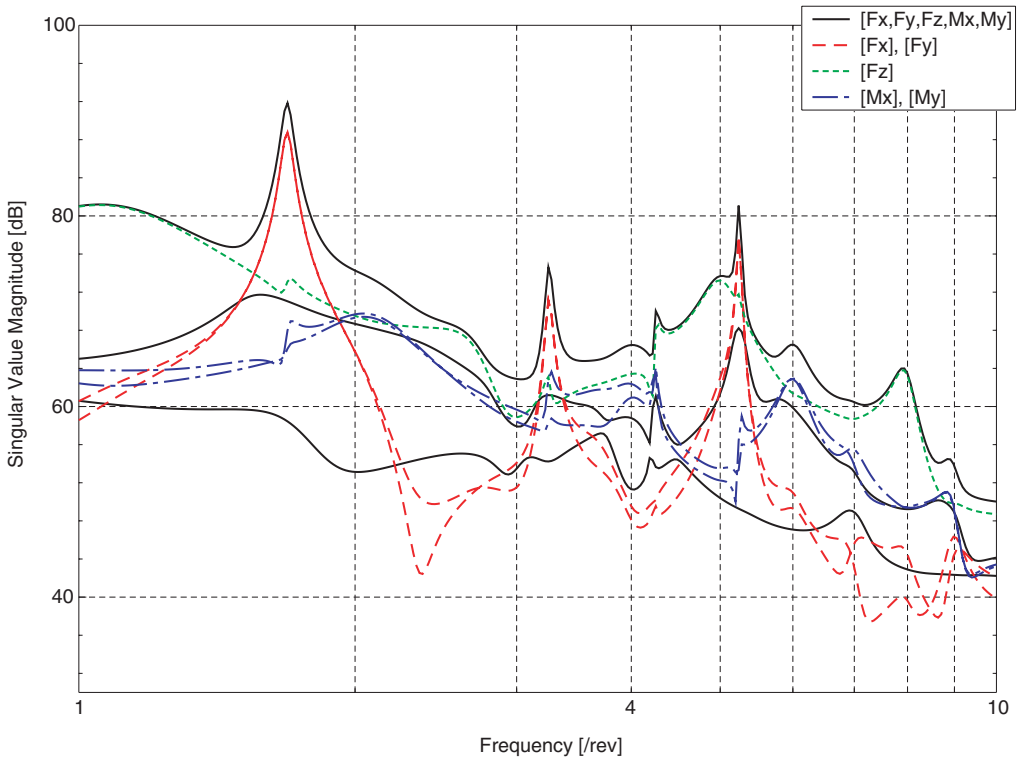

Figure 5.8 Assignment of in-plane forces, the out-of-plane force, and out-of-plane moments to the singular values in forward flight

$$A: \begin{bmatrix} \dots & \dots & \dots & \dots \\ \dots & 0 & 1 & \dots \\ \dots & -\omega^2 & -2\zeta\omega & \dots \\ \dots & \dots & \dots & \dots \end{bmatrix} \tag{5.12}$$

An additional plant input and output is introduced in order to excite and weight the velocity of this mode. This is realized by adding one column to matrix B and one row to matrix C, with one element set to unity at the position corresponding to the mode of interest:

$$B: \begin{bmatrix} \dots \\ 0 \\ 1 \\ \dots \end{bmatrix} \tag{5.13}$$

$$C: \begin{bmatrix} \dots & 0 & 1 & \dots \end{bmatrix}$$

This structured uncertainty modelling allows an increase in damping in selected modes only without using a weighting function with additional states, which would be required to restrict the effect on the intended frequency range. The scalar weighting blocks W_{ζ_1} and W_{ζ_2} in Figure 5.5 allow the degree of uncertainty (W_{ζ_1}) and the degree of weighting (W_{ζ_2}) of the individual modes to be adjusted [60].

5.4.4 Uncertainty Modelling

In addition to the structured uncertainty modelling of the damping of the lag modes, the plant's uncertainty is modelled with unstructured uncertainties. The input w_3 represents a multiplicative uncertainty at the plant input (Δ_u), which allows for deviations of the physical plant G from the nominal plant G_0. The design is then based on the uncertain plant

$$G_0(I + \Delta_u) \tag{5.14}$$

The H_∞ norm minimization carries the risk of producing inverting controllers that are based on cancellation of zeros and poles. An inverting controller, however, works only in the nominal case but not for deviations of the physical plant from the nominal design model. This leads to poor results for lightly damped modes. It is therefore desirable to avoid inverting controllers. The right-inversion $\|GG^{-1}\|$ is prevented by the input uncertainty. The input w_2 models an additional multiplicative uncertainty at the plant output (Δ_y). This prevents a left-inversion $\|G^{-1}G\|$ of the plant, since the uncertain plant

$$(I + \Delta_y)G_0(I + \Delta_u) \tag{5.15}$$

can be neither left nor right-inverted.

5.4.5 Low Frequency Control Authority

The question of low frequency control authority begins to play a role when it comes to nonlinear simulation or implementation. While the measurement signal v in the linear time-constant system and in steady flight only contains deviations from the trimmed condition and only 4/rev vibration, static offsets can either occur as a result of flight maneuvers or can be caused by 4/rev control inputs that provoke 0/rev responses from the time-periodic plant; see Section 2.4 for a discussion of this sideband effect.

The disturbance rejection controller should not be affected by static loads due to flight maneuvers, thus requiring low gain at low frequency. This is usually realized by introducing low frequency washout filters [29]. On the other hand, it would be desirable for the vibration reduction controller not to produce 0/rev responses, thus requiring tracking characteristics in the control law. An undesired static component in the measurement signal could then be distinguished from flight maneuver effects and appropriate action could be taken by

the controller. However, this would require a reference signal for forces/moments and/or accelerations at the hub and/or points in the fuselage from the primary flight control system, yet this reference signal is probably not available. Therefore, the controller is designed to have low gain at low frequency to avoid the need for the reference signal. In turn, small static influences from the vibration control law are accepted, which must then be compensated by adjusting the trim.

The transfer function KS_y, therefore, is weighted with a first-order lowpass filter with a frequency response shown in Figure 5.6. To adjust the controller authority to the available actuator power at the frequency 4/rev, an additional weighting function is applied with a constant gain of –40 dB.

5.4.6 Weighting the Plant Output

The output z_3 weights both transfer functions T_y and S_yG. Here, mainly S_yG is active. Penalizing S_yG allows one to influence the input disturbance rejection properties of the closed-loop. A weighting function with a constant gain of –110 dB is used for the first lag mode. A second-order bandpass filter is used in the frequency range of the second lag mode. The frequency response is shown in Figure 5.6.

5.4.7 Summary of Weighting Functions

Table 5.2 summarizes all the weighting functions and the input and output gains used in the controller design. Both constant and dynamic weighting functions are listed. The notation corresponds to the closed-loop structure given in Figure 5.5. A frequency response of the dynamic weighting functions is shown in Figure 5.6.

Table 5.2 Summary of weighting functions

Weighting	Type	Purpose
w_1	Notch	Disturbance rejection
w_2	Constant	Output uncertainty modelling
w_3	Constant	Input uncertainty modelling
W_{S_y}	Notch + constant	Disturbance rejection
W_{KS_y}	Lowpass + constant	Control authority
W_{S_yG}	Bandpass + constant	Damping enhancement
W_{ζ_1}	Constant	Damping enhancement of specific modes
W_{ζ_2}	Constant	Damping enhancement of specific modes

5.5 Periodic Controller

5.5.1 Observer-Based Realization

The controller can be realized as an observer with state feedback. The additional term $\gamma^{-2} B_1^{\mathrm{T}} X_\infty x_K$ can be interpreted as an estimate of the worst-case disturbance [95]. The state equation of the observer is given by:

$$\dot{x}_K = A x_K + B_1 \gamma^{-2} B_1^{\mathrm{T}} X_\infty x_K + B_2 u + Z_\infty L_\infty (C_2 x_K - y) \tag{5.16}$$

and the state feedback equation by:

$$u = F_\infty x_K \tag{5.17}$$

A, B_1, B_2, and C_2 are matrices from the augmented system's state-space realization, while F_∞, L_∞, X_∞, and Z_∞ are matrices and γ is a scalar of the controller (all in standard H_∞ control notation; see Appendix A.4 for details and the underlying assumptions).

5.5.2 Design at Equally Spaced Points Around the Azimuth

So far, the controller design has been based on a time-constant (reduced-order) system:

$$\begin{aligned} \dot{x} &= A_0 x + B_0 u \\ y &= C_0 x + D_0 u \end{aligned} \tag{5.18}$$

The index 0 stands for the averaged values of the periodic system matrices. In the closed-loop, however, the controller is confronted with the time-periodic plant:

$$\begin{aligned} \dot{x} &= A(t) x + B(t) u \qquad t \in [0, T] \\ y &= C(t) x + D(t) u \end{aligned} \tag{5.19}$$

As this is known prior to design, it seems appropriate to incorporate this knowledge about the plant into the controller.

The Riccati equations to be solved in the controller calculation procedure (see Appendix A.4) have so far been time-constant algebraic Riccati equations. With a time-periodic design model, these become time-periodic Riccati equations. The result that suggests that the positive semi-definite solution of the Riccati equation is unique under the stabilizability and detectability assumptions (Appendix A.4) also holds for time-periodic Riccati equations [3]. To enable standard H_∞ control algorithms to be used, the periodic solution is approximated as described in the following section. To validate this approximation, a Flo-

quet transformation is performed on the closed-loop of the periodic plant and periodic controller. The resulting Poincaré exponents are then compared to the closed-loop poles of a time-constant plant and controller. The results of this comparison are given in Section 6.2.1.

In order to approximate the solution of the periodic control problem, the periodic state-space matrices are evaluated at several equally spaced points around the azimuth $0 \le t_1, t_2, \ldots < T$, and individual controllers are designed based on these matrices. The design uses the periodic reduced-order model presented in Section 4.2.

The resulting controllers are gain-scheduled with respect to the time t. The realization follows that of the periodic plant: The controller matrices are developed into Fourier series, resulting in a gain-scheduled controller [61]:

$$\begin{aligned} \dot{x}_K &= A_K(t)x_K + B_K(t)y \qquad t \in [0, T] \\ u &= C_K(t)x_K \end{aligned} \tag{5.20}$$

Here, identical weighting functions have been used at 48 equally spaced points around the azimuth. Twelfth-order Fourier series were developed for the matrices. Figure 5.9 shows the realization of the controller as an observer with state feedback and the gain-scheduled matrices.

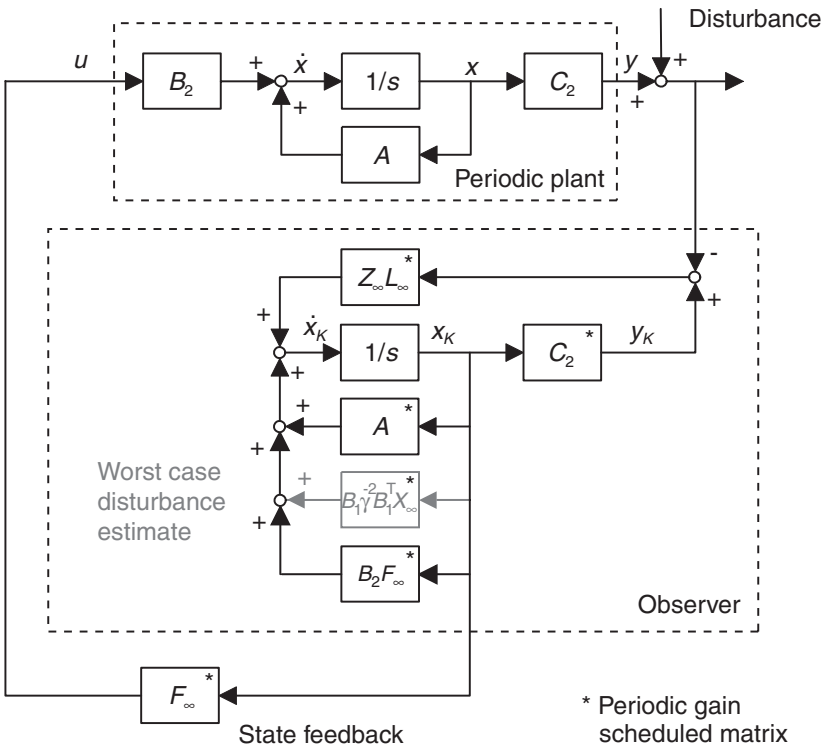

Figure 5.9 Observer-based realization of the controller

5.6 Systematic Adjustment of Weighting Functions

The selection of weighting functions in mixed sensitivity H_∞ control is a complex problem, especially if signal-based aspects and uncertainties have to be taken into account simultaneously. In the following, the selection of weighting functions is formulated as an optimization problem. The gains of the weighting functions are defined as parameters to be optimized in order to maximize a cost function representing the primary control objectives, such as vibration reduction and damping enhancement.

5.6.1 Performance Index

During the optimization process, the performance of the controller must be improved, i.e. the fulfillment of the primary design criteria must be improved while not violating possible constraints. To cast this into a form suitable for optimization, a performance index is defined. Several objectives contribute to this performance index. Thus, normalizing is required, e.g. 20 dB vibration reduction is "as important" as 2 % damping in the second lag mode. A characteristic curve is used to both normalize and act as a penalty function, i.e. to penalize significant non-fulfillment of criteria and violation of constraints. This ensures that the optimization process does not favor to improve one criterion by one or two percent at the expense of completely failing to fulfil other criteria, but concentrates on the required degree of criterion fulfillment in all aspects first before starting on desired improvements. Figure 5.10 shows how a logarithmic characteristic curve is used to translate "required" and "desired" into large and small contributions to the performance index.

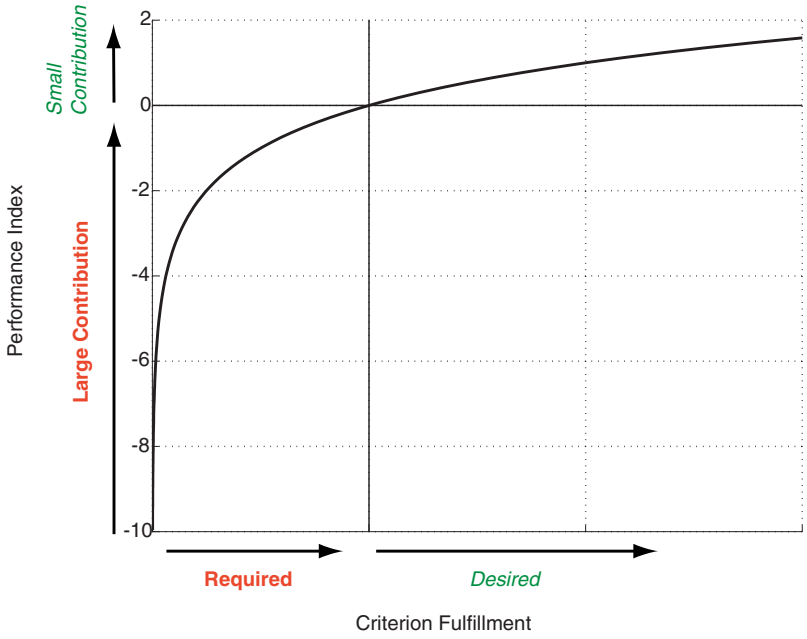

Figure 5.10 Definition of the performance index

The various design objectives taken into account in the optimization process are shown in Figure 5.11. 20 dB are aimed at for vibration reduction. From 25 dB onwards, further reduction does not further improve the performance index in order to emphasize other criteria. The aim of minimum damping in the lag modes is 2 %, but higher values are also appreciated. In order to limit the control authority and to ensure a low controller gain at low frequency, the penalty function aspect of the characteristic curve is used, see Figure 5.11. If a criterion is completely violated, e.g. a vibration "reduction" <0 dB (i.e. an increase in vibration), a critical damping ratio <0 % (i.e. an unstable system), or a control authority >2° occurs, the corresponding performance index is set to minus infinity[1]. A feasible initial guess of the parameters is required for the optimization process. Typically, a parameter combination yielding the criteria at least in the required range is available.

The total performance index is the sum of the various individual performance indices, which will then be maximized using optimization techniques. The use of multiple performance indices opens up the possibility of considering multi-model design aspects. As an example, the performance index related to vibration reduction was calculated for both high and low flight speed models. This was used successfully to improve robust performance properties for vibration reduction with respect to flight speed.

In multi-objective optimization, the requirements are typically conflicting, e.g. high vibration reduction and low actuator authority are conflicting objectives. Consequently, the optimization problem to be solved is a problem of Pareto optimality[2].

5.6.2 Optimization

The sum of performance indices is the objective function to be maximized. For the objective function to be evaluated, a controller must be calculated, which involves solving two Riccati equations in an iterative way. The objective function contains noise as a result of the tolerance in the iteration. Consequently, any optimization method relying on gradient information, which would have to be calculated using finite differences, is predetermined to fail.

As genetic algorithms do not need gradient information, a genetic algorithm using a float representation was applied to the problem [35]. A selection of weighting functions and disturbance inputs were chosen as parameters to be optimized. Here, the optimizer was allowed to vary the gains within ±10 dB. The final gains of the weighting functions and disturbance inputs used in the controller calculation at each optimization step are the sums of initial gains, roughly chosen manually, and the optimizer-chosen variations, denoted by

1. This discontinuity will most certainly cause problems with gradient-based optimization techniques. In the case of genetic algorithms, however, the approach works very well, since is marks the individual as "defective".

2. A parameter combination P_1 is said to be Pareto optimal if no other parameter combination P_2 dominates P_1 with respect to the set of objective functions. P_2 dominates P_1 if P_2 is better than P_1 in at least one objective function, and not worse with respect to all other objective functions.

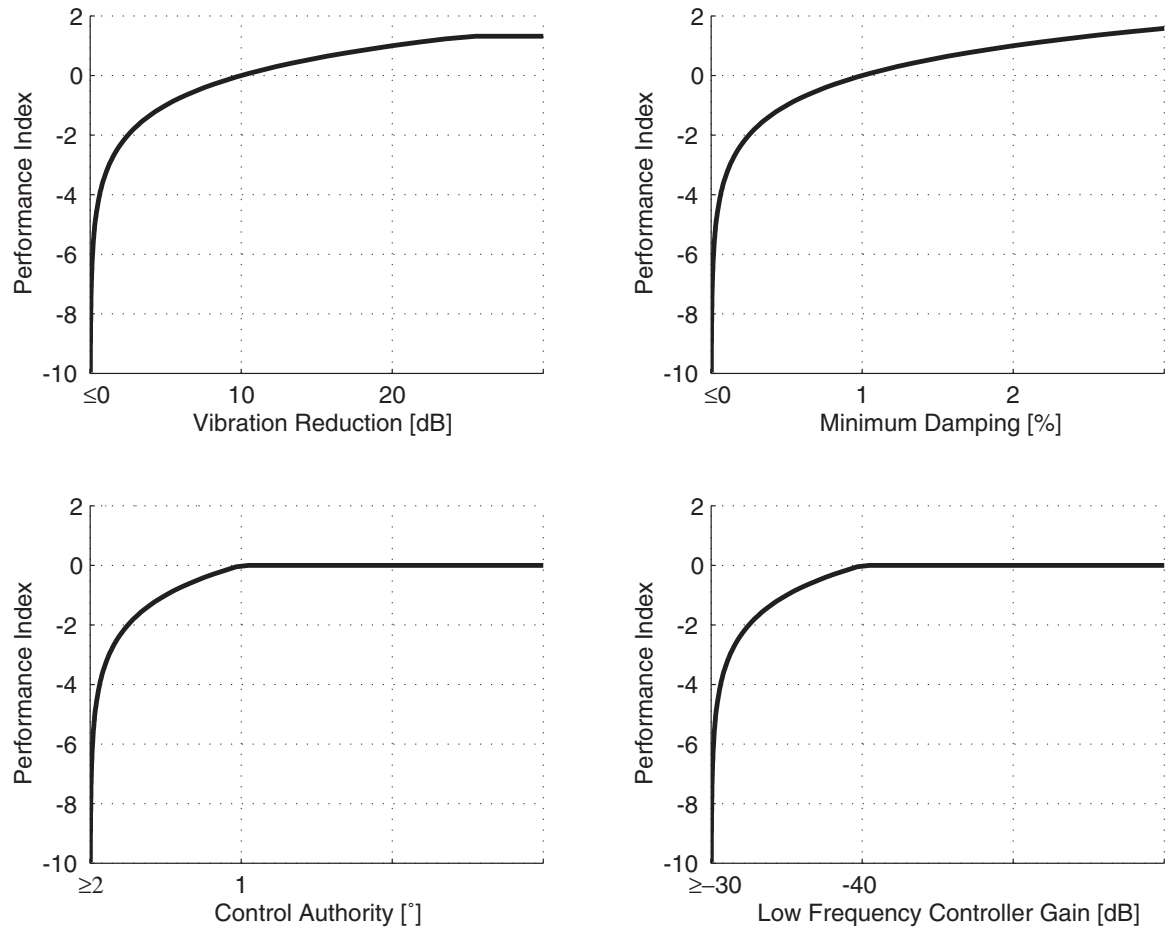

Figure 5.11 Performance indices for various design objectives

ΔW. The gains to be optimized comprise the disturbance inputs at the plant's input and output (d' and d), the notch input, the constant and notch-weighted sensitivity outputs (S_y and $S_{y,\,\mathrm{notch}}$), the constant and bandpass weighted complementary sensitivity outputs (T_y and $T_{y,\,\mathrm{bandpass}}$), and the constant and lowpass weighted control outputs (KS_y and $KS_{y,\,\mathrm{notch}}$).

Genetic optimization is based on the concept of individuals and generations, with a "survival of the fittest" strategy to determine the new generation from the individuals of the last generation. Here, an individual is a vector of parameters and the corresponding objective function is the measure of its "fitness". Figure 5.12 shows the evolution for a controller optimization with 65 individuals per generation and 100 generations. While the parameters are uniformly distributed in the intervals for the first generation (random seed as initial population), the optimum value for the parameters clearly emerges after some 30 to 50 generations. Thus, the optimization process allows optimal gains to be found, here within ±10 dB of the initial gains for the weighting functions, which had been roughly chosen.

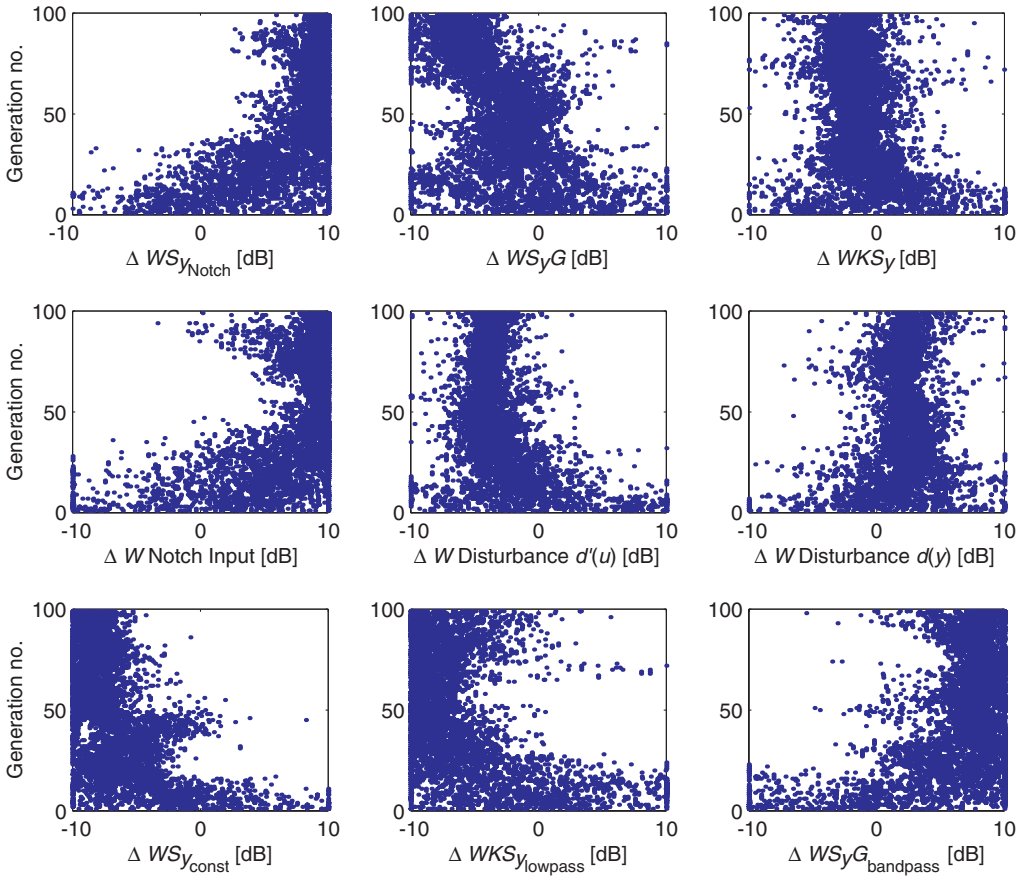

Figure 5.12 Evolution of optimized weighting function gains

5.6.3 Limitations

The genetic optimization approach has two main limitations. First, a sensible set of weighting functions has to be available as an initial guess for the optimization process. Not surprisingly, the structure of the controller must still be defined by the designer. Decisions, such as "the sensitivity function has to be weighted with a notch filter", remain to be taken by the control engineer. But once the structure is defined and a half-decent setting of the weighting functions is available, the optimization approach offers a systematic and efficient way to fine-tune the controller.

The second main limitation of the genetic optimization approach is the computational effort. The calculation of a controller and thus the evaluation of the objective function takes approximately one minute on a standard 0.5 GHz Pentium II PC. The total time required to calculate 100 generations with 65 individuals is approximately 108 hours. The algorithm has been modified to be suitable for parallel computing. This allowed the calculation to be completed overnight (twelve hours) on nine PCs. Alternatively, the calculation can be solved using two PCs over a weekend (54 hours). The computational burden could be eased by a factor of two or three by reducing the number of generations, since there was no sig-

nificant improvement after 30 to 50 generations. Although the computational effort is high, it was still found to be more efficient than manually “tuning” the parameters, since the procedure is fully automated. Furthermore, the continuously increasing computational power available in standard desktop computers increasingly facilitates matters.

Chapter 6
Results & Analysis

This chapter presents various controller designs with different objectives. The results for time-constant and time-periodic controllers are given. Different design objectives are considered in terms of outputs to be controlled. Possibilities and limitations for helicopter vibration reduction using individual blade control are presented. Robustness properties of the control laws are analyzed with respect to several aspects. The difference of reducing vibration at the rotor hub and in the fuselage is highlighted. Finally, the use of individual blade control to provide lag damping is assessed and the required actuator strokes are analyzed.

6.1 Constant Controller

Using the controller design setup described in the previous chapter, the controller is calculated using standard algorithms available in the μ control toolbox [30]. The resulting controller has 69 states, which arise from 36 states of the reduced-order model, 16 states from notch filters (second-order, five filters on the input for the hub quantities F_x, F_y, F_z, M_x, M_y, and three filters on the output of the quantities selected for vibration reduction, e.g. F_z, M_x, M_y), four states from the first-order lowpass actuator dynamics model, ten states from the second-order bandpass weighting functions W_{S_yG}, and three states from the first-order lowpass weighting functions W_{S_y}.

6.1.1 Frequency Domain Analysis

In Figure 6.1, the transfer function for the full-order, time-constant model at high flight velocity is plotted open-loop vs. closed-loop. Open-loop and closed-loop poles are given in Figure 6.2, where again only the upper half of the real-complex plane is shown. It can be noted that the lag modes show an increased damping in the closed-loop. The damping of the lag pole with the smallest damping is increased from 0.5% to >3% critical damping. The results are similar (not shown here) for the second operating point with low forward flight velocity. The differential lag pole is unchanged since the mode is not observable in the time-

constant system, see Section 2.2.1. A damping increase in the collective lag mode comparable to that achieved for the progressive and regressive modes is possible with a measurement of M_z, see Section 6.4. M_z, however, was not used in this controller design.

6.1.2 Time Domain Analysis

The controller is simulated in closed-loop with the full-order verification model at high flight velocity (design case) and at low flight velocity (off-design case). The baseline vibration from Camrad II acts on the system as a disturbance at the plant output. The controller cancels out vibration in the selected three hub quantities (-99%), as shown in Figure 6.3. The results of the simulation for low flight velocity are given in Figure 6.4. Although performance is slightly degraded in the off-design case, the controller still considerably reduces vibration in all three selected hub quantities (-96%). This demonstrates the robust usability of the controller at both operating points. Note that at low flight speed, the baseline vibration level is higher due to BVI effects (see Section 1.2), which leads to a larger required actuator stroke.

Next, the controller is tested with the time-periodic model at high flight velocity. The results in Figure 6.5 show slightly degraded performance, but the controller still provides considerable vibration reduction of -91%. This indicates that the robustness of the controller covers the variation between the time-constant design model and the time-periodic verification model. The residual vibration in the time-periodic simulation is dominated by 8/rev vibration. This, as well as the static offset (0/rev), is due to the multiharmonic response of the periodic plant, see Section 2.4.1. The controller does not compensate the static offset (0/rev) as low frequency authority was prevented in the controller design, see Section 5.4.5.

As described in the section on the selection of outputs to be controlled (Section 5.4.2), a combination of three hub forces/moments is typically selected for a four-blade rotor [29], e.g. the force vector $[F_x, F_y, F_z]$ or a combination of the force in thrust direction and the roll- and pitch-moment $[F_z, M_x, M_y]$. So far, results have been presented of the latter. In contrast to this, Figure 6.6 shows the results of the simulation for a controller designed to reduce vibration in the force vector $[F_x, F_y, F_z]$. Again, the vibration in the three outputs selected is cancelled (-99%). Note that the actuator stroke required for this design objective remains within a limit of $\pm 1°$. A drawback of selecting three outputs for vibration reduction is that vibration in the remaining quantities is typically increased, here by +159% when targeting $[F_z, M_x, M_y]$ and by +16% when targeting $[F_x, F_y, F_z]$.

Instead of controlling a selection of three hub forces/moments, three *directions* in the MIMO system can be targeted for vibration reduction. In Section 5.4.2, these three directions were identified as corresponding to the in-plane forces $[F_x, F_y]$, the out-of-plane force F_z, and the out-of-plane moments $[M_x, M_y]$. In order to analyze vibration reduction, the loop is closed with a controller designed in line with this output selection approach. The singular values of the output sensitivity (transfer function of the output sensitivity, describ-

ing the transmission of the baseline vibration through the rotor hub) at the blade passage frequency of 4/rev for five hub loads $[F_x, F_y, F_z, M_x, M_y]$ are calculated:

$$\sigma_{S_y(\omega = 4/\mathrm{rev})_{[F_x, F_y, F_z, M_x, M_y]}} = \left[-0.49 \;\; -4.29 \;\; -36.7 \;\; -40.1 \;\; -40.9\right] \mathrm{dB} \tag{6.1}$$

The result is as expected. Three directions are cancelled (around $-40\,\mathrm{dB}$), whereas the remaining two directions remain more or less unchanged. The output sensitivity of the individual outputs is considered next. Note that the singular value of the transfer function from all inputs to one output is calculated, e.g. $[F_x, F_y, F_z, M_x, M_y] \rightarrow F_x$. The results for the SISO transfer functions from one input to one output, e.g. $F_x \rightarrow F_x$, which are generally better (lower sensitivity) and sometimes quoted in the literature, are meaningless, since in the closed-loop all disturbance inputs act on the plant and the use of SISO transfer functions neglects the cross-transmission paths of the MIMO system:

$$\begin{aligned}
\sigma_{S_y(\omega = 4/\mathrm{rev})_{[F_x, F_y, F_z, M_x, M_y] \rightarrow F_x}} &= -3.3\,\mathrm{dB} \\
\sigma_{S_y(\omega = 4/\mathrm{rev})_{[F_x, F_y, F_z, M_x, M_y] \rightarrow F_y}} &= -3.0\,\mathrm{dB} \\
\sigma_{S_y(\omega = 4/\mathrm{rev})_{[F_x, F_y, F_z, M_x, M_y] \rightarrow F_z}} &= -11.4\,\mathrm{dB} \\
\sigma_{S_y(\omega = 4/\mathrm{rev})_{[F_x, F_y, F_z, M_x, M_y] \rightarrow M_x}} &= -6.2\,\mathrm{dB} \\
\sigma_{S_y(\omega = 4/\mathrm{rev})_{[F_x, F_y, F_z, M_x, M_y] \rightarrow M_y}} &= -7.9\,\mathrm{dB}
\end{aligned} \tag{6.2}$$

As predicted, the results for the in-plane forces F_x and F_y are almost identical, as is also the case for the out-of-plane moments M_x and M_y. In line with the expectations, the result for the single out-of-plane force F_z is the best result.

The average vibration reduction is -49%. Contrary to expectations, the vibration reduction is significantly lower than might have been concluded from the MIMO singular values. The reason for this might be that the assumption of symmetry (see Section 5.4.2) is strongly violated in forward flight. Moreover, there is no implicit guaranty that considerably reducing the fundamental directions leads to the individual outputs being reduced considerably.

6.2 Periodic Controller

6.2.1 Validation of the Gain-Scheduling Approach

This section presents results for the time-periodic controller. First, the calculation of controllers at points equally spaced around the azimuth as an approximation of the direct solution of the time-periodic problem is validated. The closed-loop system of the time-periodic

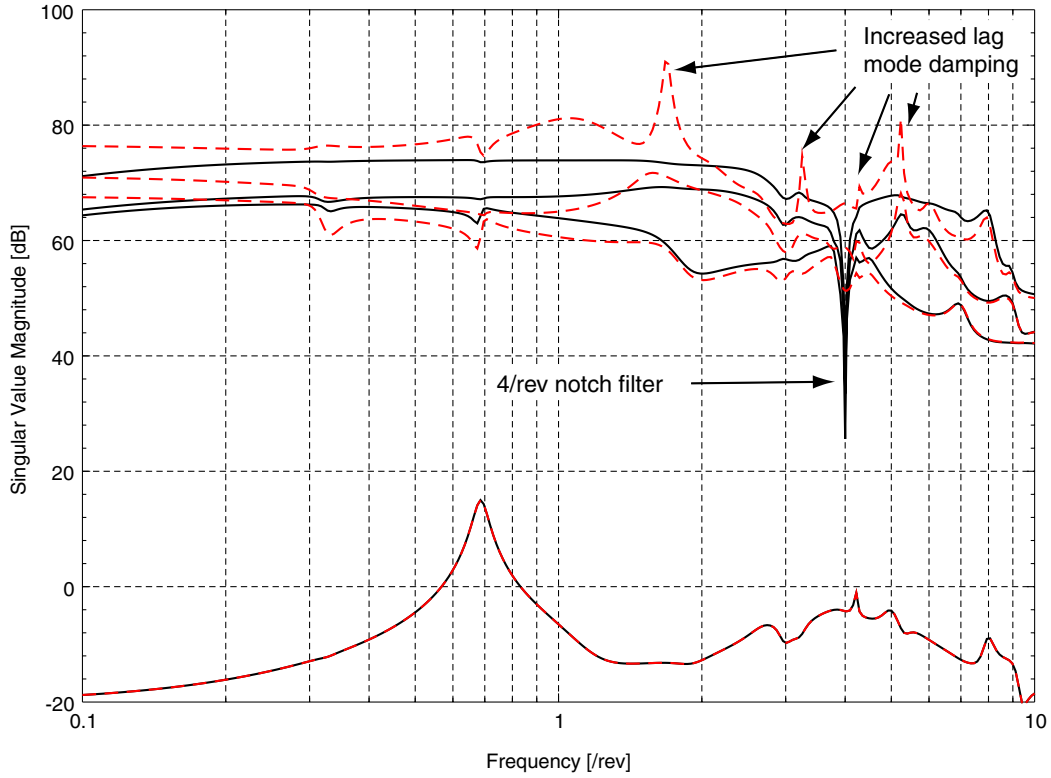

Figure 6.1 Input-output transfer behavior of plant with 56 states, high flight velocity: open-loop (dashed) vs. closed-loop (solid)

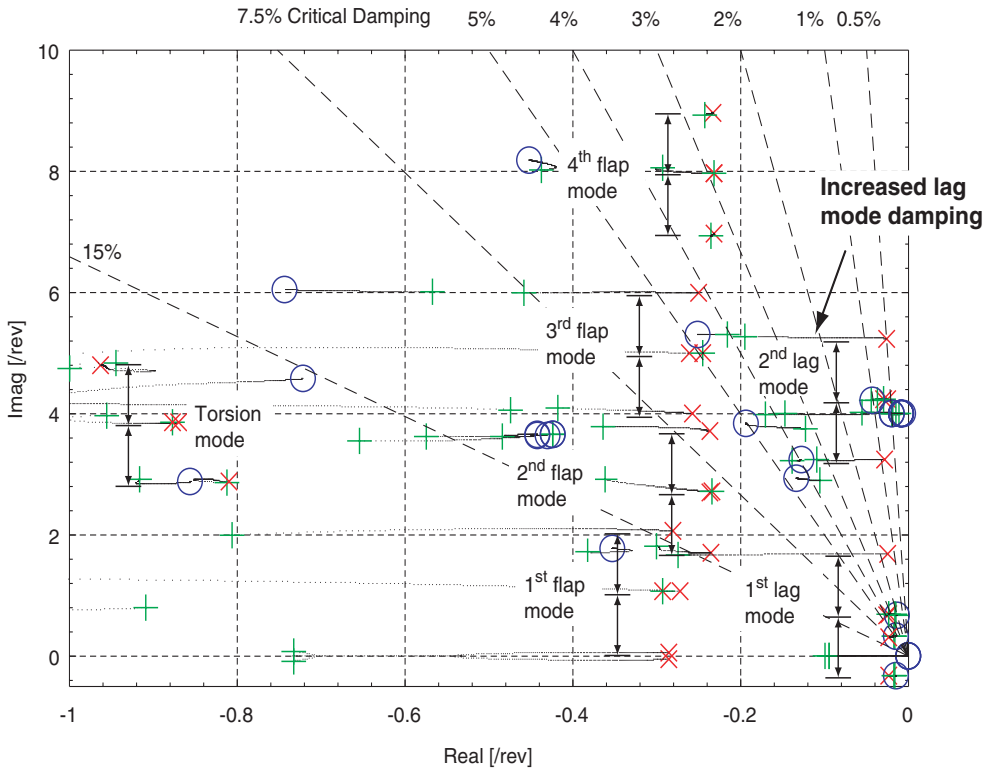

Figure 6.2 Pole locations open-loop plant (x) and controller (o) vs. closed-loop (+) for time-constant controller and 56 state time-constant model, high flight velocity

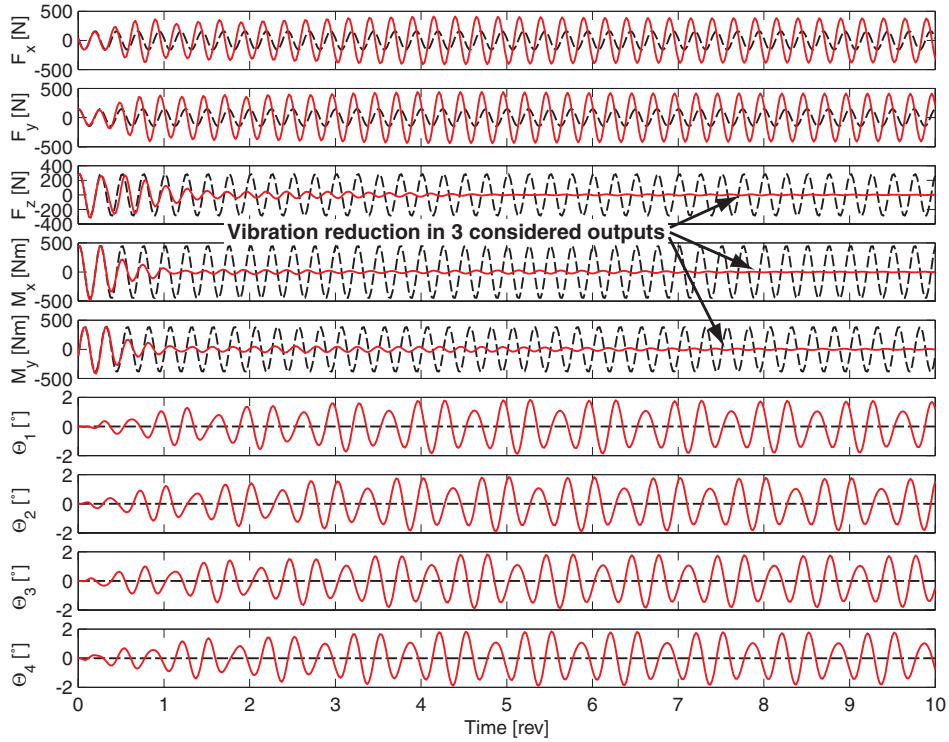

Figure 6.3 Vibration reduction with time-constant controller and 56 state time-constant model, high flight speed, baseline vibration (dashed) vs. controlled vibration (solid)

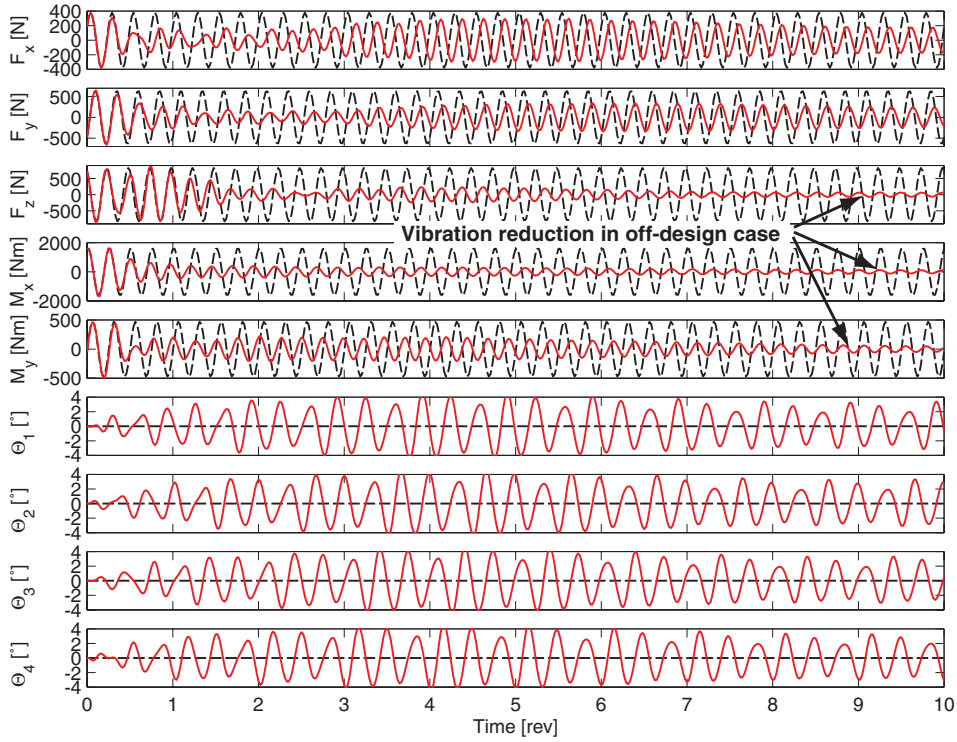

Figure 6.4 Vibration reduction with time-constant controller and 56 state time-constant model, low (off-design) flight speed, baseline (dashed) vs. controlled vibration (solid)

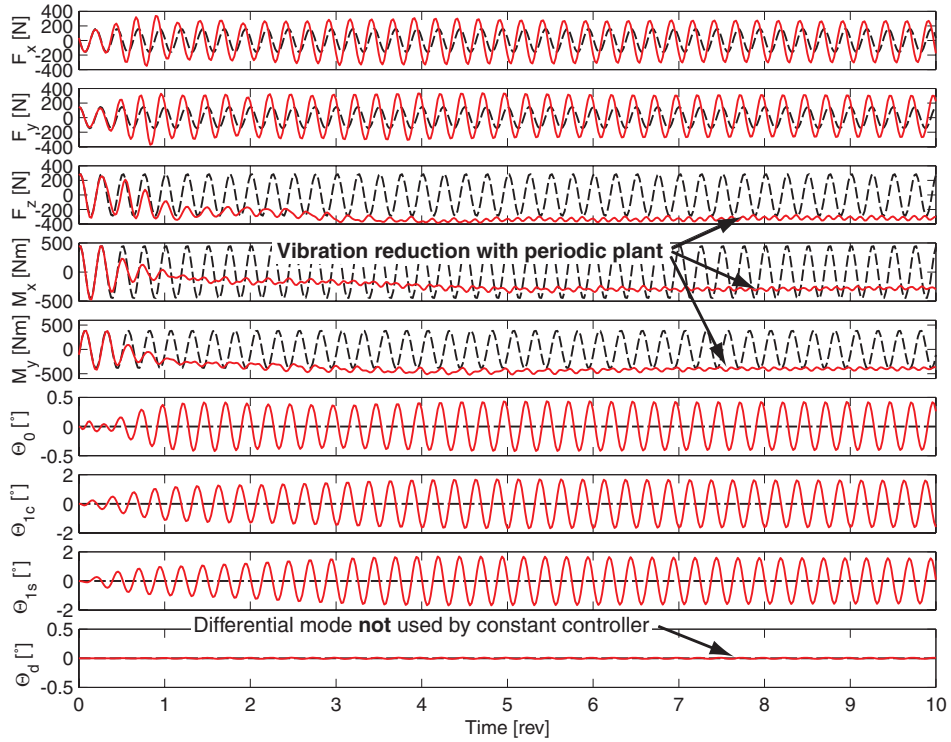

Figure 6.5 Vibration reduction with time-constant controller and 56 state time-periodic model, high flight speed, baseline vibration (dashed) vs. controlled vibration (solid)

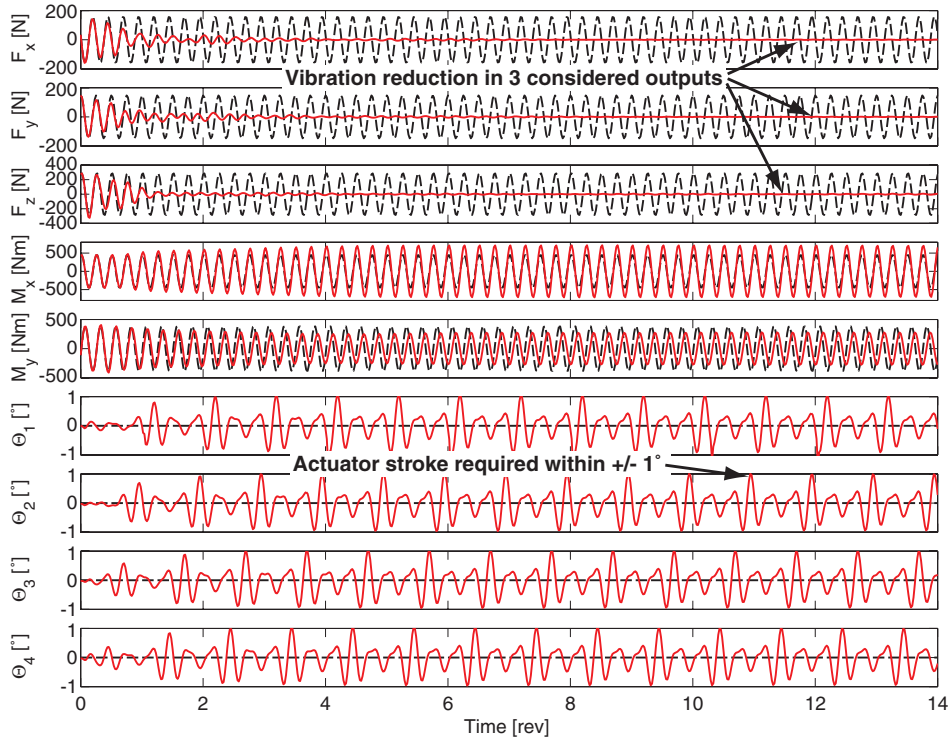

Figure 6.6 Vibration reduction in force vector with both time-constant controller and 56 state model, high flight speed, baseline vibration (dashed) vs. controlled vibration (solid)

controller K, the (time-constant) actuator dynamics H, and the (full-order) time-periodic plant G is arranged as shown in Figure 6.7.

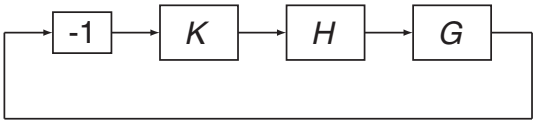

Figure 6.7 Closed-loop system with controller K, actuator dynamics H, and plant G

The systems have state-space representations of the form

$$\begin{aligned} \dot{x}_{K,H,G} &= A_{K,H,G}(t) \cdot x_{K,H,G} + B_{K,H,G}(t) \cdot u_{K,H,G} \\ y_{K,H,G} &= C_{K,H,G}(t) \cdot x_{K,H,G} + D_{K,H,G}(t) \cdot u_{K,H,G} \end{aligned} \tag{6.3}$$

with the indices K, H, G, corresponding to the time-periodic controller K, the time-constant actuator dynamics H, and the time-periodic plant G, respectively. Whereas the actuator dynamics have no direct feedthrough terms ($D_H = 0$), $D_K(t) \neq 0$ is assumed for generality for the controller[1]. With the interconnection equations

$$u_K = -y_G \qquad u_H = y_K \qquad u_G = y_H \tag{6.4}$$

the dynamics matrix of the closed-loop system can be derived:

$$A_{\text{closed-loop}}(t) = \begin{bmatrix} A_K(t) & -B_K(t)D_G(t)C_H & -B_K(t)C_G(t) \\ B_H C_K(t) & A_H - B_H D_K(t) D_G(t) C_H & -B_H D_K(t) C_G(t) \\ 0 & B_G(t) C_H & A_G(t) \end{bmatrix} \tag{6.5}$$

The time-periodic dynamics matrix is now analyzed using the Floquet transformation, allowing a stability analysis of the time-periodic closed-loop system. The resulting Poincaré exponents plotted in the pole map are given in Figure 6.8. The Poincaré exponents meet the expectations of the poles of the time-constant closed-loop system, validating the gain-scheduling approach for the time-periodic controller.

6.2.2 Time-Periodic Closed-Loop Simulations

The gain-scheduled time-periodic controller, based on the reduced-order, time-periodic plant is simulated in closed-loop with the full-order, time-periodic plant. The results are given in Figure 6.9. The performance of the gain-scheduled controller in terms of vibration reduction is comparable with that of the time-constant controller. Note that the periodic con-

1. This allows any very fast poles in the controller to be realized as direct feedthrough terms.

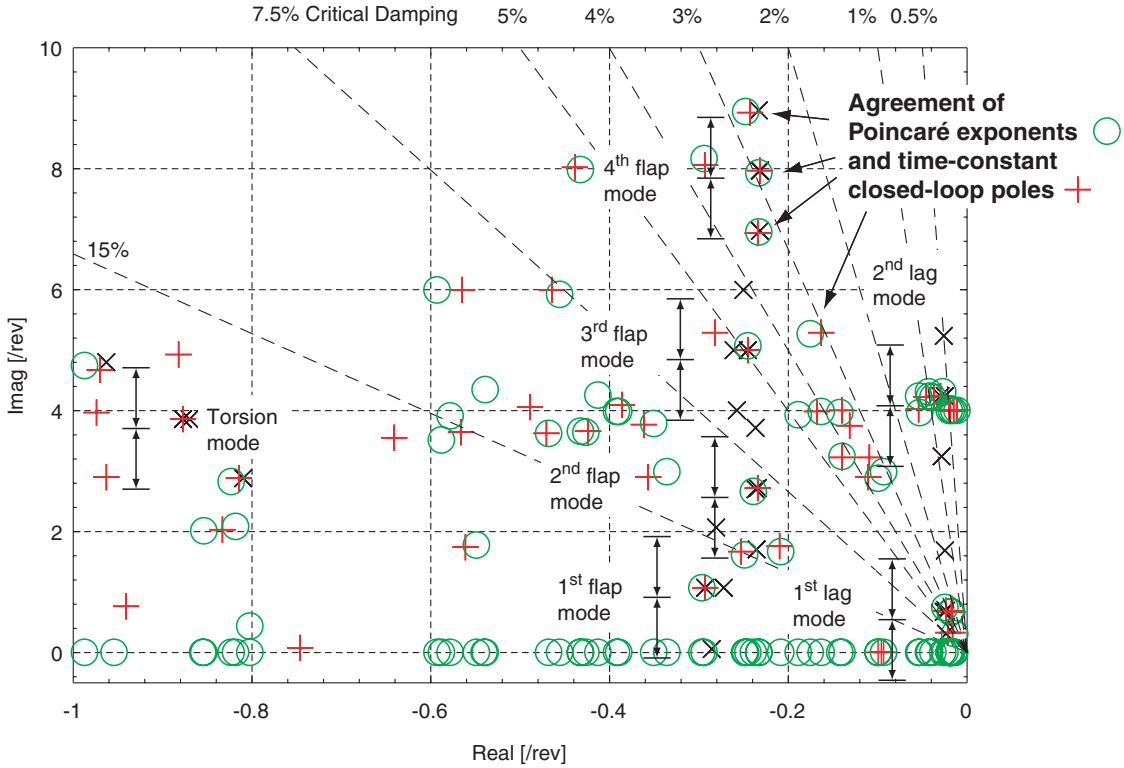

Figure 6.8 Open-loop plant poles (x) vs. time-constant closed-loop poles (+) vs. Poincaré exponents of time-periodic closed-loop system (o)

troller uses the differential mode of the plant input, which is no longer reactionless, unlike in the time-constant system (Figure 6.5). This means that one degree of freedom is gained, considering periodicity already in design. This advantage is used to improve the robustness of the periodic controller, as demonstrated in the following case study:

A simulation is performed with a time-periodic model, including not only 56 states for rotor dynamics, but an additional 34 states for 17 elastic fuselage modes. The consideration of the flexible fuselage changes the dynamic properties of the rotor system and, therefore, can be considered to be a “robustness test” for the controller. Note that the controller design considered here does not yet include any error models or considerations for neglected fuselage modes. The “robustness test” with fuselage modes, therefore, is somewhat unspecific but can still give an indication of the controller’s robustness.

Figure 6.10 shows the results of the simulation with the time-periodic controller and time-periodic model, including fuselage modes. The three controlled hub quantities and three accelerations at the pilot seat position are shown. The accelerations are unchanged in x direction, decreased in y direction, and increased in z direction. Such a “mixed” result was expected, since the controller was designed to reduce hub loads, which does not necessarily imply a reduction in accelerations in the fuselage [33]. The performance in the hub loads is degraded in comparison to simulations without fuselage, but the controller still reduces vibration in all three controlled quantities. In contrast, the time-constant controller destabilizes the time-periodic model with flexible structure modes included in this case study. This

seems to be due to the fact that the scheduled controller is adapted to the periodicity of the system and can compensate the flexible modes with robustness, whereas the time-constant controller must cope with both periodicity and flexibility, which obviously demands too much of robustness. Table 6.1 summarizes the results of the simulations for the time-constant and time-periodic controllers.

This result does not imply that it is impossible to design a time-constant controller based on the rotor dynamics only that is robust in the above-mentioned sense, since there is always a trade-off between robustness and performance in the controller design. The case study only shows that for this particular trade-off between robustness and performance, the time-periodic controller is superior, but at the expense of an increased degree of complexity in the controller due to the required scheduling.

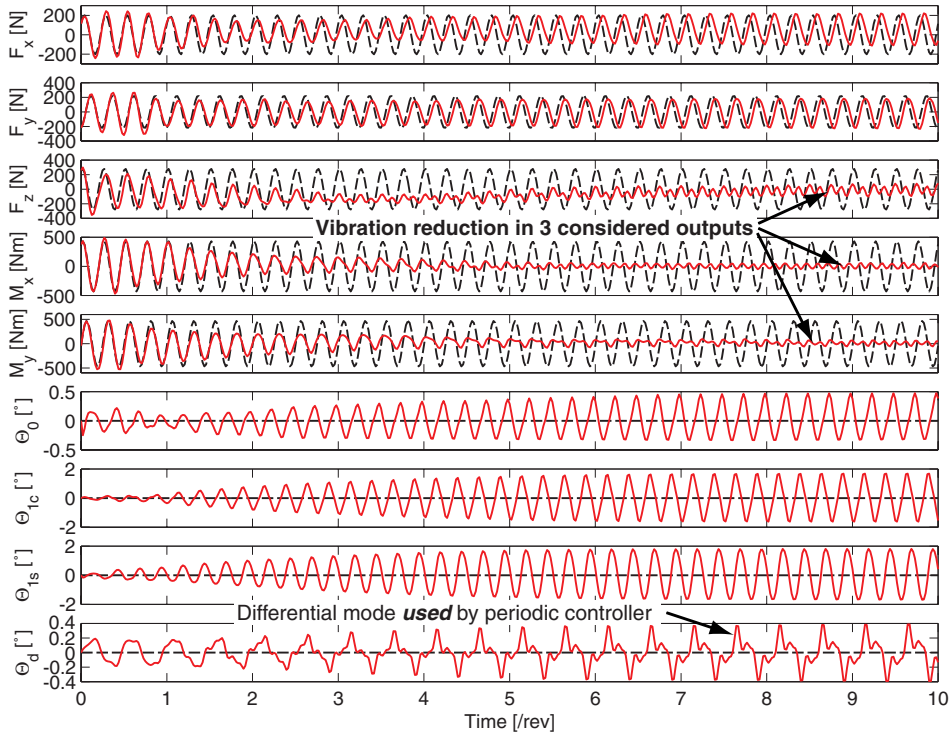

Figure 6.9 Vibration reduction with time-periodic controller and 56 state time-periodic model, high flight speed, baseline vibration (dashed) vs. controlled vibration (solid)

6.2.3 Disturbance Rejection

An important issue in the control design is the sensitivity of the closed-loop system to disturbances, e.g. gusts affecting one or several rotor blades. To simulate a gust maneuver, one rotor blade is pitched up one degree for a duration it takes the blade to advance ten degrees, i.e. a pulse input to one blade is simulated. The results are compared for the uncontrolled and the controlled cases. Here, the forces in x and y direction are most interesting, since the

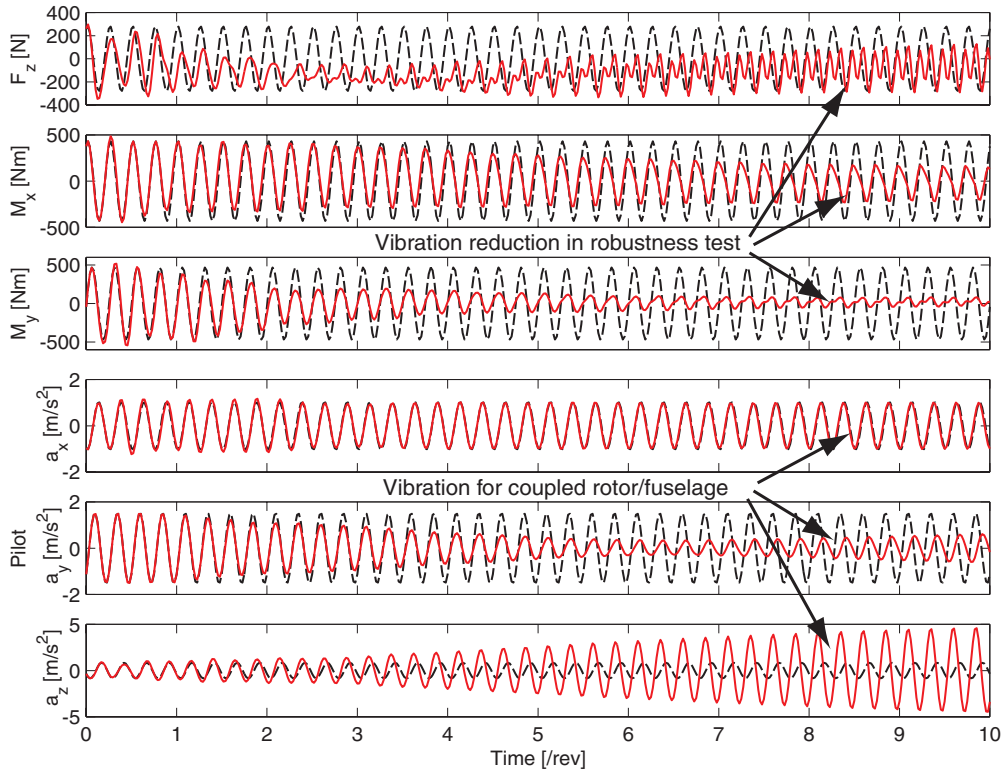

Figure 6.10 Robustness test: Vibration reduction time-periodic controller designed for rigid fuselage simulated with flexible fuselage, baseline (dashed) vs. controlled (solid)

Table 6.1 Case study: Performance of the controllers simulated with various models

Design Goals:	**Time-Constant Model**	**Time-Periodic Model**	**Time-Periodic Model incl. Flexible Fuselage**
Time-Constant Controller	FULFILLED (designed for)	FULFILLED (due to robustness)	***NOT*** FULFILLED (not enough robustness)
Time-Periodic Controller	- (not applicable)	FULFILLED (designed for)	FULFILLED (due to robustness; but performance degraded)

weakly damped lag modes mostly affect F_x and F_y. Figure 6.11 shows the improvements achieved by the controller with respect to decay times.

Section 6.4 gives a detailed analysis of the disturbance rejection properties of the closed-loop system in the frequency domain and the possibilities and limitations of damping enhancement for the lag modes.

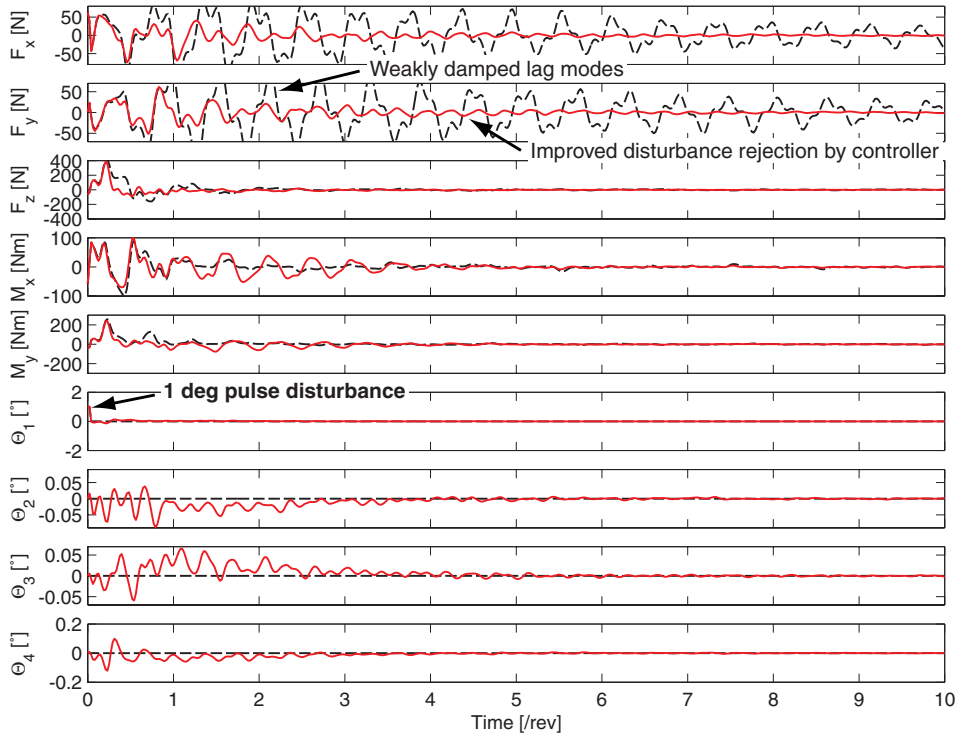

Figure 6.11 Disturbance rejection with time-periodic controller and 56 state time-periodic model, high flight speed, uncontrolled response (dashed) vs. controlled response (solid)

6.3 Fuselage Vibration Controller

The final goal of helicopter vibration reduction is to reduce vibration, not necessarily at the rotor hub[2], but at specific points in the fuselage, e.g. at the pilot seat or in the load compartment [33]. The model, on which the controller design is based, is then required to include both rotor dynamics and fuselage dynamics. Using the results from Section 2.3.5, the controller presented in this section is based on a model including 17 flexible fuselage modes.

A reduction in vibration at one specific location in the fuselage can lead to reduced or increased vibration at other locations, depending on the dynamic properties of the system. Depending on the mission definition of the helicopter, different design objectives are conceivable: For surveillance and transport helicopters, vibration reduction at the pilot/copilot position may be of prior importance, whereas for a rescue helicopter, the load compartment, which is the location of the injured person, becomes more important.

2. A complete cancellation of all six forces and moments at the rotor hub would be ideal, since no vibration would then be transmitted to the fuselage. However, it is not possible to completely cancel out six outputs due to the limited number of degrees of freedom.

Three different cases are examined in the following: First, vibration reduction at the pilot position only[3]; second, vibration reduction in the load compartment only; and finally, simultaneous vibration reduction at both the pilot and load compartment positions is considered. In all three cases, during the controller design, both off-design locations in the fuselage and at the rotor hub have to be monitored closely in order to avoid violations of structural load limits.

The results of the simulation given in Figure 6.12 show that it is possible to reduce vibration considerably at the pilot position in all three directions (accelerations in x, y, and z direction). Taking into account the only available measurement at the copilot seat position in y direction, a simultaneous vibration reduction of -89% at the pilot and copilot position is achieved. Simultaneously, vibration at the load compartment is increased by $+32\%$. Closed-loop simulations with 17 fuselage modes used for design and with all 32 fuselage modes are shown in Figure 6.12. Since no significant difference is observed, the design based on a reduced model with only 17 fuselage modes is justified.

The results of the simulation for a controller design targeting vibration at the load compartment only are shown in Figure 6.13. Vibration can be reduced by -80% in the load compartment. However, this is accomplished by an increased level of vibration of $+81\%$ at the pilot and copilot seat.

Figure 6.14 shows the results of the simulation for simultaneous vibration reduction at the pilot seat and in the load compartment. Vibration is reduced in all six outputs, as well as at the copilot position. As expected due to the fact that now more outputs are considered than degrees of freedom are available, performance is degraded in comparison to the results for single locations. The average vibration reduction achieved simultaneously at the pilot and copilot seat, as well as in the load compartment is -47%. Although some fine tuning and adjustment of the weighting functions for the individual outputs might help to distribute the vibration reduction more equally among the outputs, the key finding remains the same: If more independent outputs are considered for vibration reduction than degrees of freedom are available (here: three), vibration cannot be cancelled, but only reduced moderately.

Figure 6.15 shows the corresponding hub loads and actuator strokes for simultaneous vibration reduction at the pilot seat and in the load compartment. An interesting aspect that emerges here is the increased hub load. The average increase in hub vibration is $+293\%$. Similar findings have been obtained by [33], where vertical hub shears increased by a factor of three to six when HHC inputs aimed at minimizing fuselage accelerations were introduced. This indicates that vibration reduction in the helicopter fuselage does not necessarily lead to reduced vibration at the rotor hub and vice versa: A vibration reduction at the rotor hub does not necessarily lead to reduced vibration in the fuselage.

3. For the copilot position, measurements of the vibration level were only available in y direction for instrumentation reasons.

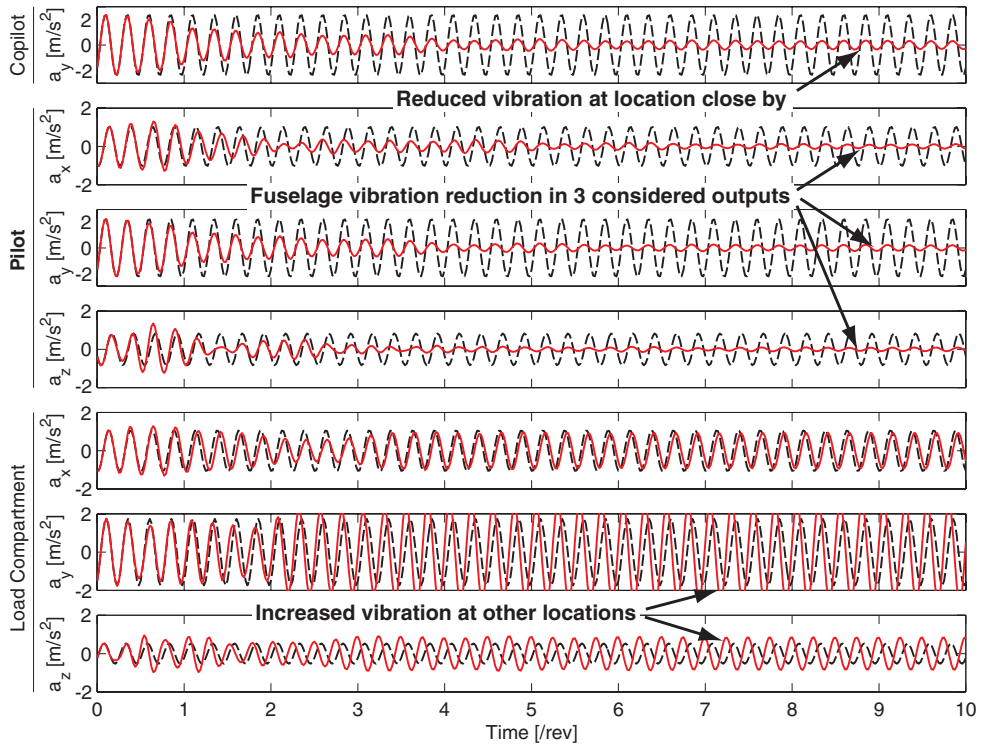

Figure 6.12 Fuselage vibration reduction at pilot position, both time-constant controller and plant with 17 fuselage modes, baseline (dashed) vs. controlled (solid)

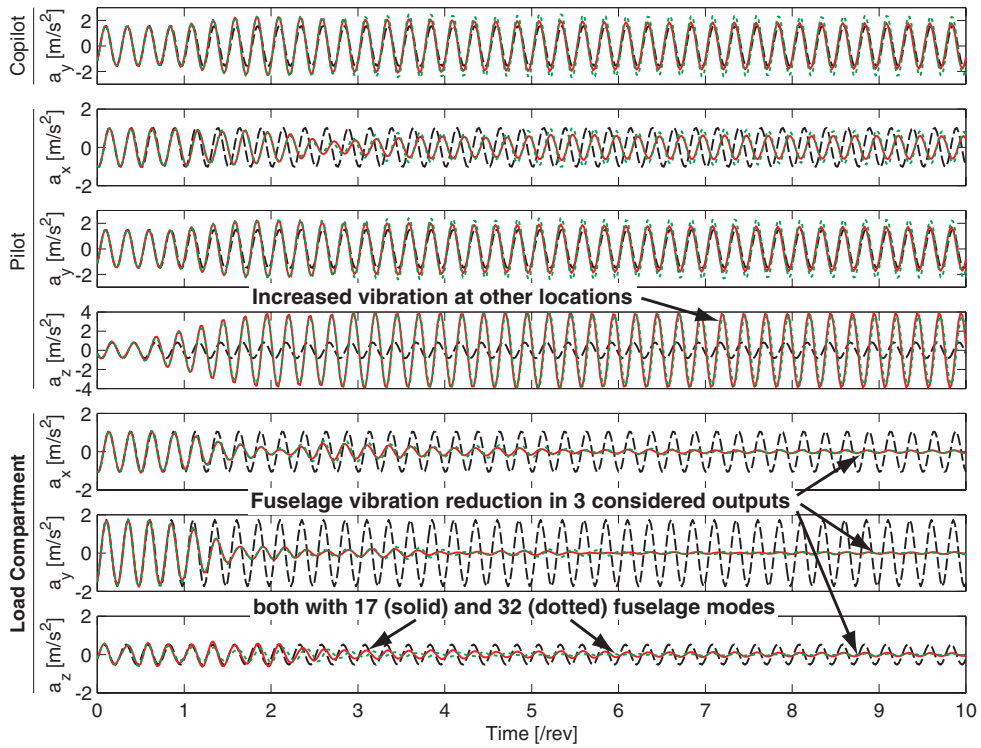

Figure 6.13 Fuselage vibration reduction in the load compartment, time-constant, baseline (dashed) vs. simulation with 17 (solid) and 32 (dotted) fuselage modes

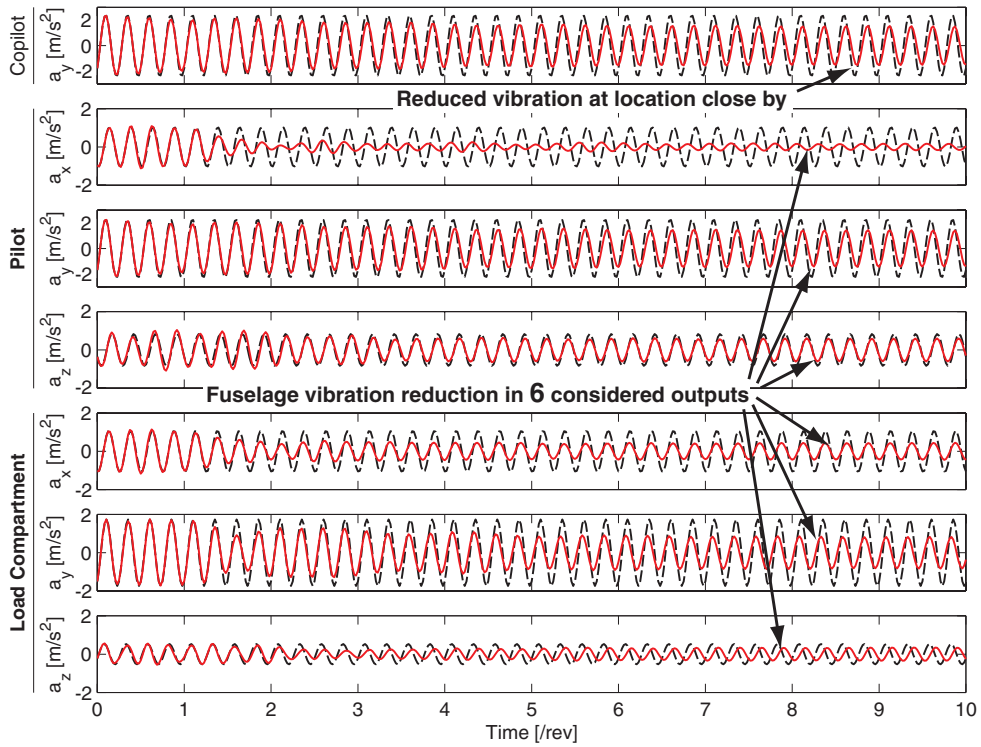

Figure 6.14 Simultaneous vibration reduction pilot and load compartment, both time-constant controller and plant with 17 fuselage modes, baseline (dashed) vs. controlled (solid)

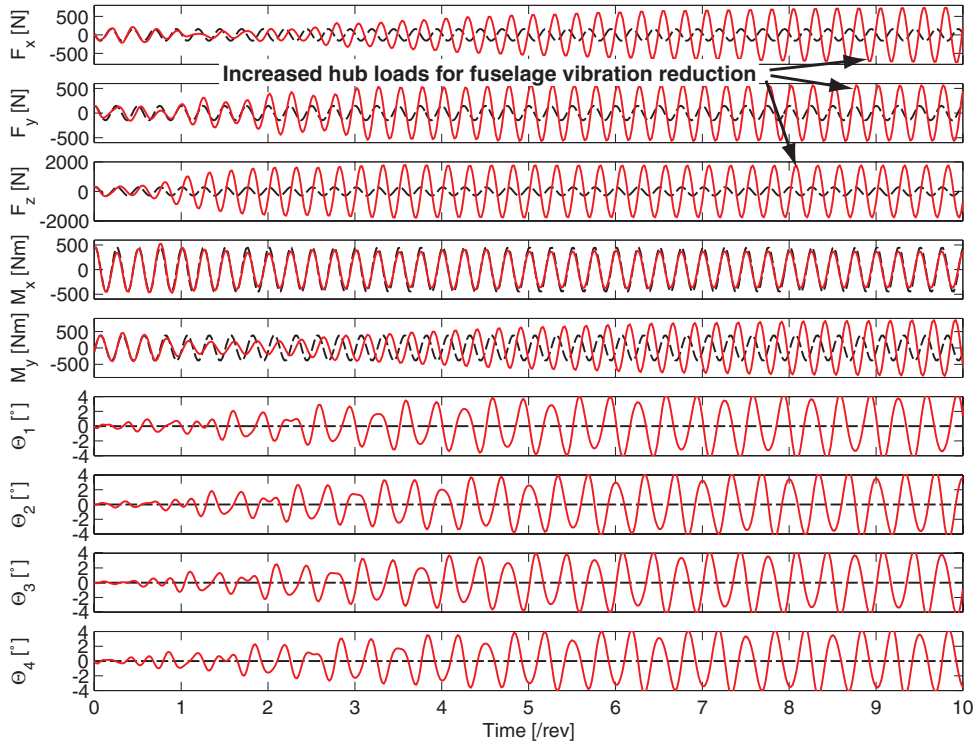

Figure 6.15 Hub loads and actuator stroke for simultaneous vibration reduction pilot and load compartment, time-constant, 17 fuselage modes, baseline (dashed), controlled (solid)

6.4 Lag Damping Enhancement

In addition to reducing vibration at the blade passage frequency N/rev , a main objective of the control law design is to increase damping, especially in the weakly damped lag modes. This section examines the possibilities of lag damping from the nonrotating frame in more detail.

As described in the previous chapter, the control strategy for increasing damping is to use an observer-based controller and to feed back the (observed) rates of the modes to be controlled. The physical mechanism of lag damping augmentation is as follows: The observed lag rate is fed back to the individual blade pitch control. A blade flapping rate is thus generated, which results in an in-plane moment due to the Coriolis force opposing the lag motion, as shown in Section 2.1.1, Figure 2.1. Since the opposing Coriolis force is proportional to the lag rate, blade damping is augmented [38].

By definition, the observer requires that the modes to be controlled are observable in the measured outputs. The frequency domain analysis of the plant in Section 2.2.1 revealed that the cyclic forms of the lag modes are not expected to cause any problems, whereas the collective lag form is only observable in M_z. Moreover, the differential lag mode cannot be controlled by a time-constant controller based on a time-constant approximation of the time-periodic plant, since the differential mode is not observable (“reactionless” mode) in the time-constant system.

In order to analyze the influence of the availability of M_z as a measurement, two time-constant controllers[4] are designed for the plant. Both controllers use all three forces and the moments about the pitch and yaw axes, whereas the second controller is also able to utilize a measurement of the moment about the torque axis M_z. The section of the pole map containing the most relevant second lag mode is given in Figure 6.16 (a). Both controllers increase damping in the cyclic forms. With both controllers, the critical damping of the cyclic modes is increased from the minimum open-loop damping of 0.5% to 2% in the closed-loop. However, collective lag mode damping can only be increased to >2% when a measurement of M_z is available, whereas the collective pole remains almost unchanged when M_z cannot be fed back. In both designs, the differential mode remains unchanged.

Figure 6.16 (b) shows the results for a time-periodic controller. The controller is based on the same design parameters as above, with the exception of time-periodicity. The open-loop pole locations of the plant are compared with the Poincaré exponents (closed-loop pole locations of the Floquet-transformed time-periodic closed-loop system). While the results of the cyclic and collective modes are only slightly improved, the key result is that the time-periodic controller allows one to control the differential mode. Differential second lag mode

4. Note: These results should not be compared directly to the results of the controllers presented in the previous sections. In the previous sections, the controllers were optimized for maximum damping enhancement, whereas in this case-study, optimization was stopped at 2% critical damping and all controllers were calculated using identical design parameters in order to allow meaningful comparisons.

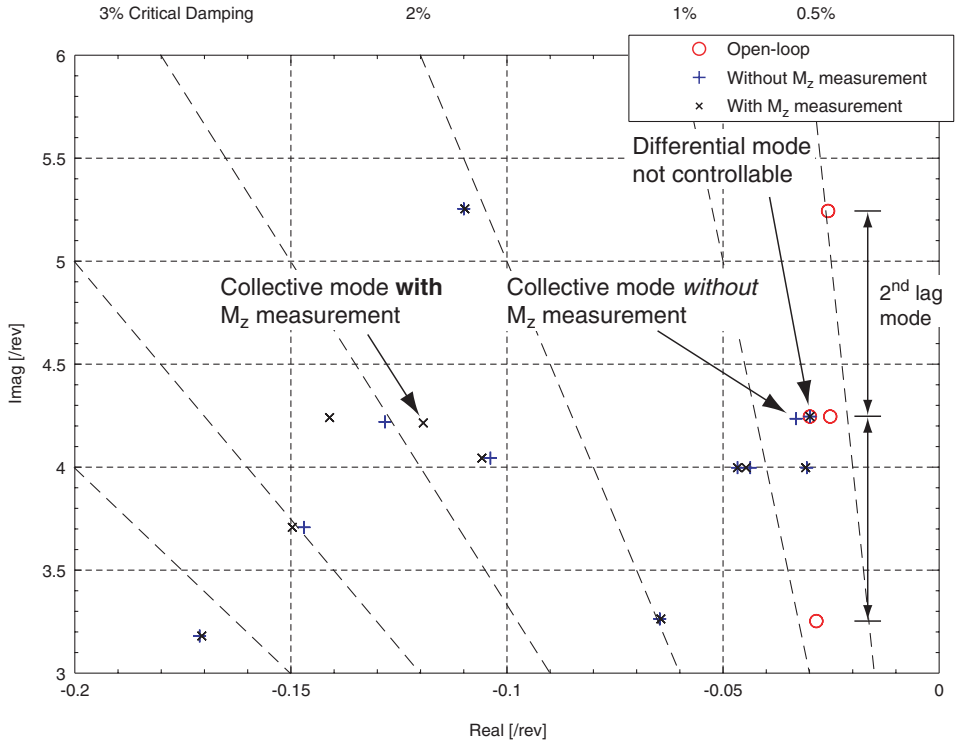

Figure 6.16 **(a)** Open-loop pole locations vs. closed-loop pole locations, comparison of controller with and without measurement of M_z available for feedback

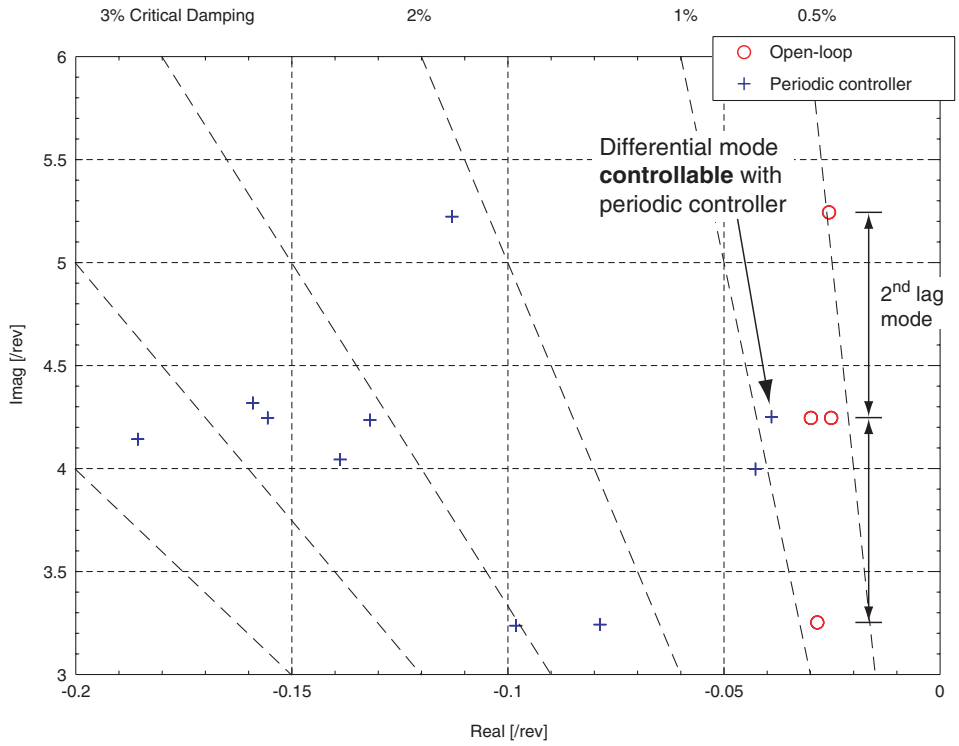

Figure 6.16 **(b)** Open-loop pole locations vs. closed-loop Poincaré exponents (closed-loop pole locations of the Floquet-transformed periodic system with time-periodic controller)

damping is increased to approximately 1% critical damping. The possible differential damping enhancement is not as large as for the cyclic or collective form. This is due to the dynamic properties of the plant and not to periodicity or the gain-scheduled time-periodic implementation of the controller, since time-constant controller designs for fictitious time-constant rotors "fixed" at specific azimuthal positions (see Figure 2.6) yield similar results. Although the differential damping enhancement is smaller than that for the cyclic and collective forms, the time-periodic controller allows one to increase second lag mode damping from minimal 0.5% critical damping to 1% in the differential form and to 2%-3% in the collective and cyclic form, whereas with a controller design based on the constant coefficient approximation, it is not possible to control the differential form from the nonrotating system.

6.5 Required Actuator Stroke

A key component of an individual blade control system is the actuator. As previously noted, a variable length pitch link is used for individual blade root control. The blade root actuator has limited authority in terms of piston stroke, which corresponds to degrees pitch angle.

Table 6.2 shows a summary of the maximum actuator commands observed in closed-loop simulations for various control objectives described in the previous sections.

Blade root actuators of the IBC system in the BO 105 helicopter were flight tested with an amplitude of $\pm 1.1°$ [91]. Amplitudes of $\pm 2.0°$ were evaluated in wind tunnel tests with a 1:1 BO 105 rotor equipped with an IBC system [85]. The maximum amplitude of the actuator for the BO 105 rotor IBC system is $\pm 3.0°$ [50]. Blade root actuators for a CH-53G helicopter individual blade control system offer a maximum amplitude of up to $\pm 6.0°$ [86].

Table 6.2 Maximum IBC pitch angles for various simulation/control objectives

Simulation/Control Objective	**Max. IBC Pitch Angle**
Hub vibration reduction in $[F_x, F_y, F_z]$	$\pm 1.0°$
Hub vibration reduction in $[F_z, M_x, M_y]$	$\pm 1.7°$
Fuselage vibration reduction pilot + load compartment	$\pm 4.0°$
$1°$ impulse disturbance rejection	$\pm 0.1°$

Chapter 7
Conclusion

7.1 Summary

A control law to reduce vibration and increase lag damping in helicopters using individual blade control has been developed. H_∞ control synthesis was used to design one robust controller based on a reduced-order model that can be used to alleviate vibration in different operating conditions at different helicopter flight speeds. The damping enhancement achieved leads to a significantly reduced gust sensitivity.

A simple analytical model for an N-blade rotor, including the basic features of rotor behavior and flap and lag dynamics, was developed and used to analyze the potential of individual blade control and examine the dependence on the number of rotor blades.

The control law design and simulations are based on a complex aeromechanical analysis model, including advanced rotor aerodynamics in addition to detailed kinematics and detailed dynamics derived with the commercial helicopter analysis software Camrad II.

As concerns hub loads, vibration can be cancelled (-99%) in three outputs simultaneously, e.g. all three hub forces or the vertical hub force and the roll and pitch moments. Using the same controller as designed for high speed flight at a different operating point with low speed descent flight where BVI vibration occurs, oscillatory loads were also reduced by -96%, demonstrating the robustness of the controller. A number of more than three outputs exceeds the number of three degrees of freedom available for vibration reduction of the four-blade rotor. Vibration can then only be reduced moderately, e.g. by -49% for all three hub forces and the two moments about the roll and pitch axis. However, a reduction in hub vibration does not necessarily lead to reduced vibration in the cabin. Fuselage accelerations increased by a factor of up to three when IBC inputs aimed at minimizing hub loads were introduced.

Therefore, a finite-element model of the flexible fuselage was coupled with the aeromechanical rotor model via pitch/mast bending. The resulting coupled rotor-fuselage model was used to calculate and control vibration at locations in the cabin, such as at the pilot and copilot seats and in the load compartment. By targeting cabin accelerations, simultaneous

vibration reduction at the pilot and copilot seats of -89% was achieved, at the expense of an increased level of vibration of $+32\%$ in the load compartment. Considering both the pilot and copilot seats and the load compartment simultaneously, an average vibration reduction of -47% was obtained. When fuselage vibration was reduced, oscillatory hub loads were increased by a factor of up to four.

The use of a model-based control strategy enabled lag damping to be enhanced from 0.5% to >3% critical damping without using dedicated lag rate sensors in the blades. Only the hub loads must be measured. However, because the lag rate of the blades in the rotating frame has to be reconstructed from measurements in the nonrotating system, some restrictions apply. Increased damping in the cyclic modes is straightforward, whereas damping enhancement in the collective mode requires measurement of the torque moment. Finally, differential lag mode damping can only be increased using periodic control.

In order to consider the plant's periodicity in the controller design, a time-periodic gain-scheduled controller was developed. The results of the simulation confirmed the common viewpoint that incorporating more knowledge about the plant into the controller, instead of designing a more robust and thus conservative controller, improves performance or robustness against other influences.

Both the time-constant and time-periodic controllers were designed using reduced-order models. Existing model reduction techniques for linear time-constant systems were extended to linear time-periodic systems. The reduced-order time-periodic models produced proved suitable for controller design purposes.

An optimization-based weight selection procedure was developed. This allowed one to systematize the process of adjusting weighting functions and to consider multi-model aspects.

Floquet-Lyapunov theory was used in the analysis of the time-periodic open-loop and closed-loop systems. In the control synthesis, however, the Floquet-Lyapunov transformed system did not necessarily represent a good choice as a basis for the control law design. It emerged that the transformed system, although by definition having a constant system matrix A, had a significantly increased level of periodicity in the matrices B and C, i.e. the total periodicity of the state-space representation (and thus the error when neglecting higher harmonic terms) was increased considerably. Therefore, the control law design was based on a constant coefficient approximation of a Fourier transformed system. Its single harmonic $4/\mathrm{rev}$ transfer function from IBC inputs in nonrotating coordinates to (nonrotating) hub loads "internally contains" the physical $3/\mathrm{rev}$, $4/\mathrm{rev}$, and $5/\mathrm{rev}$ transmission paths of the rotating system, making it an ideal basis for control law design.

7.2 Contributions

The following is a list of the contributions this dissertation makes to the area of helicopter rotor control.

- Design of several BO 105 controllers for different vibration reduction objectives (hub loads, or pilot/copilot seats, and/or load compartment) that are robust against changes in flight speed.
- Development of a coupled rotor-fuselage model that allows vibration to be reduced in the fuselage, which is generally not achieved by decreasing hub loads.
- Active lag damping enhancement without dedicated sensors in the rotor blades.
- Development of a periodic controller that is able to control the “reactionless” differential mode from the nonrotating system.
- Extension of model reduction techniques for continuous linear time-constant systems to continuous linear time-periodic systems.
- Systematic analysis of the extent to which the number of degrees of freedom available for vibration reduction depends on the number of blades.

7.3 Directions for Future Research

Flight tests of the proposed control law are planned with the BO 105 helicopter that is equipped with the individual blade root control system. At first, controllers that focus on one aspect, either vibration reduction or damping enhancement, shall be flown. In contrast to classical SISO controllers, where individual gains can be increased manually during a flight test series, a family of controllers designed for an increasing level of control authority are planned to be tested successively.

An interesting direction of research would be to apply the proposed control strategy to a different individual blade control system in the rotating frame, e.g. to a rotor with actuated flaps. It is assumed that it is possible to repeat the controller design making only minor changes, since only the matrices B and D of the state-space representation of the plant are changed for a different type of actuation.

Another useful direction for future research would be to design an equivalent controller for a helicopter with more than four rotor blades in order to make use of the higher number of degrees of freedom.

Appendix A

A.1 Fourier Coordinate Transformation

The inverse of the Fourier coordinate transformation [43], [39], [80] introduced in Section 2.1.4 is given by:

$$\beta^{(m)} = \beta_0 + \sum_n (\beta_{nc} \cos n\psi_m + \beta_{ns} \sin n\psi_m) + \beta_d (-1)^m \tag{A.1}$$

The summation index n goes from 1 to $(N-1)/2$ for N odd and from 1 to $(N-2)/2$ for N even. The azimuth of the m^{th} blade ($m = 1$ to N) is $\psi_m = \psi + m \cdot \Delta\psi$, with the dimensionless time variable $\psi = \Omega t$ for constant rotational speed Ω and the equal azimuthal spacing between the blades $\Delta\psi = 2\pi/N$.

The rotor speed is constant $\dot{\Omega} = 0$. The transformation of the first and second time derivatives is given by:

$$\begin{aligned}
\dot{\beta}^{(m)} &= \dot{\beta}_0 + \sum_n [(\dot{\beta}_{nc} + n\Omega\beta_{ns}) \cos n\psi_m + (\dot{\beta}_{ns} - n\Omega\beta_{nc}) \sin n\psi_m] + \dot{\beta}_d (-1)^m \\
\ddot{\beta}^{(m)} &= \ddot{\beta}_0 + \sum_n [(\ddot{\beta}_{nc} + 2n\Omega\dot{\beta}_{ns} - n^2\Omega^2\beta_{nc}) \cos n\psi_m \\
&\quad + (\ddot{\beta}_{ns} - 2n\Omega\dot{\beta}_{nc} - n^2\Omega^2\beta_{ns}) \sin n\psi_m] + \ddot{\beta}_d (-1)^m
\end{aligned} \tag{A.2}$$

The first derivatives of the multiblade coordinate transformation are given by:

$$\begin{aligned}
\frac{1}{N} \sum_{m=1}^{N} \dot{\beta}^{(m)} &= \dot{\beta}_0 \\
\frac{2}{N} \sum_{m=1}^{N} \dot{\beta}^{(m)} \cos n\psi_m &= \dot{\beta}_{nc} + n\Omega\beta_{ns}
\end{aligned} \tag{A.3}$$

$$\begin{aligned}
\frac{2}{N}\sum_{m=1}^{N}\dot{\beta}^{(m)}\sin n\psi_m &= \dot{\beta}_{ns} - n\Omega\beta_{nc} \\
\frac{1}{N}\sum_{m=1}^{N}\dot{\beta}^{(m)}(-1)^m &= \dot{\beta}_d(-1)^m
\end{aligned} \qquad \text{(A.3 continued)}$$

The second derivatives of the multiblade coordinate transformation are given by:

$$\begin{aligned}
\frac{1}{N}\sum_{m=1}^{N}\ddot{\beta}^{(m)} &= \ddot{\beta}_0 \\
\frac{2}{N}\sum_{m=1}^{N}\ddot{\beta}^{(m)}\cos n\psi_m &= \ddot{\beta}_{nc} + 2n\Omega\dot{\beta}_{ns} - n^2\Omega^2\beta_{nc} \\
\frac{2}{N}\sum_{m=1}^{N}\ddot{\beta}^{(m)}\sin n\psi_m &= \ddot{\beta}_{ns} - 2n\Omega\dot{\beta}_{nc} - n^2\Omega^2\beta_{ns} \\
\frac{1}{N}\sum_{m=1}^{N}\ddot{\beta}^{(m)}(-1)^m &= \ddot{\beta}_d(-1)^m
\end{aligned} \qquad \text{(A.4)}$$

A.2 Analytical Rotor Model

The analytical rotor model described in Chapter 2 is available in nonlinear and linear form as C-code or as state-space matrices, respectively. A family of models for rotors with $N = 3$ to 7 blades is available.

In the following, a short summary of the model equations, states, inputs, and outputs is given. The nonlinear second-order differential equations of the flap (β) and lag (ζ) motion as derived in Section 2.1.1 are given in Table A.1.

Table A.1 Second-order nonlinear differential equations of motion per blade

Flap Differential Equation	$I^*_\beta(\ddot{\beta} + \nu^2_\beta\beta) - 2I^*_{\beta\zeta}\beta\dot{\zeta} = \dfrac{K_\beta\beta_p}{I_b(1-e)\Omega^2} + \gamma M_F$
Lag Differential Equation	$I^*_\zeta(\ddot{\zeta} + \nu^2_\zeta\zeta) + 2I^*_{\beta\zeta}\beta\dot{\beta} + C^*_\zeta\dot{\zeta} = \gamma M_L$

The nonlinear system of first-order differential equations for one blade is derived based on the second-order differential equations of motion. The system is of the form given in Table A.2.

Table A.2 System of first-order nonlinear differential equations per blade

$\dot{x}(\psi) = f(x(\psi), u(\psi), \psi)$	
$y(\psi) = g(\dot{x}(\psi), x(\psi), u(\psi), \psi)$	
IBC Input	$u(\psi) = \theta(\psi)$
State Vector	$x(\psi) = [\dot{\beta}(\psi), \beta(\psi), \dot{\zeta}(\psi), \zeta(\psi)]^{\mathrm{T}}$
Rotating Blade Root Loads Output	$y(\psi) = [S_x(\psi), S_r(\psi), S_z(\psi), N_l(\psi), N_f(\psi)]^{\mathrm{T}}$

The entire rotor consists of N of the above systems for N blades. The outputs are the rotor hub loads in the nonrotating frame. Both inputs and states are transformed to MBC. The system can be linearized about a trim condition. The resulting linear time-periodic system is given in Table A.3.

Table A.3 System of linear time-constant differential equations for the rotor

$\dot{X}(\psi) = A(\psi)X(\psi) + B(\psi)U(\psi)$	
$Y(\psi) = C(\psi)X(\psi) + D(\psi)U(\psi)$	
IBC Input Vector	$U(\psi) = [\theta_0(\psi), \theta_{nc}(\psi), \theta_{ns}(\psi), \theta_d(\psi)]^{\mathrm{T}}$
State Vector	$X(\psi) = [\dot{\beta}_0, \dot{\beta}_{nc}, \dot{\beta}_{ns}, \dot{\beta}_d, \dot{\zeta}_0, \dot{\zeta}_{nc}, \dot{\zeta}_{ns}, \dot{\zeta}_d, \beta_0, \beta_{nc}, \beta_{ns}, \beta_d, \zeta_0, \zeta_{nc}, \zeta_{ns}, \zeta_d]^{\mathrm{T}}(\psi)$
Nonrotating Hub Loads Output	$Y(\psi) = [F_x, F_y, F_z, M_x, M_y, M_z]^{\mathrm{T}}(\psi)$

The harmonic index n goes from $n = 1$ to $(N-1)/2$ for N odd and from $n = 1$ to $(N-2)/2$ for N even. The differential degree of freedom (index d) only exists if N is even.

The dimensions of the plant are given in Table A.4.

Table A.4 Dimensions of the system for the rotor

Plant Dimensions	
Inputs	N
States	$4 \cdot N$
Outputs	6

A.3 Floquet-Lyapunov Transformation

The Floquet-Lyapunov theory for solving linear time-periodic systems is summarized in the following [14], [79].

The linear equations of motion of a system with periodically varying parameters may be written as

$$\dot{x}(t) = A(t)x(t) \tag{A.5}$$

with the period T:

$$A(t) = A(T+t) \tag{A.6}$$

The solution to (A.5) is given by the transition matrix $\Phi(t, 0)$ as

$$x(t) = \Phi(t, 0)x(0) \tag{A.7}$$

$\Phi(t, 0)$ satisfies the differential equation

$$\dot{\Phi}(t, 0) = A(t)\Phi(t, 0) \tag{A.8}$$

with the initial condition $\Phi(0, 0) = I$. Floquet's theorem states that

$$\Phi(t, 0) = F(t)e^{Jt}F^{-1}(0) \tag{A.9}$$

where J is a constant matrix that can be written in Jordan normal form

$$J = \mathrm{diag}\left(\begin{bmatrix}\omega_1 & \omega_2 & \dots & \omega_n\end{bmatrix}\right) \tag{A.10}$$

where ω_i are the Poincaré exponents, the analog of the eigenvalues of the system matrix of a linear time-constant system. The matrix $F(t)$ would be the constant eigenvector matrix for a time-constant system. Here, $F(t)$ is time-periodic with the period T. The solution to the time-periodic problem is given for any t if J and $F(t)$ are known over one period.

From (A.9) it follows that

$$\Phi(T, 0) = F(T)e^{JT}F^{-1}(0) \tag{A.11}$$

and using $F(0) = F(T)$, (A.11) can be written as:

$$\Phi(T, 0) = F(0)e^{JT}F^{-1}(0) \tag{A.12}$$

Consequently, $F(0)$ is the eigenvector matrix of $\Phi(T, 0)$; the diagonal matrix of eigenvalues is given by:

$$e^{JT} = \operatorname{diag}\left(\left[\lambda_1 \ \lambda_2 \ \dots \ \lambda_n\right]\right) \tag{A.13}$$

The following equation holds for the i^{th} element:

$$e^{\omega_i T} = \lambda_i \tag{A.14}$$

To solve the Floquet problem, $F(t)$ is required over one period. Substituting (A.9) in (A.8) yields:

$$\dot{F}(t) = A(t)F(t) - F(t)J \tag{A.15}$$

This differential equation can be solved with the initial condition $F(0)$, known from the solution to the eigenvalue problem (A.12).

From (A.14) it follows that

$$\omega_i = \frac{1}{T}\ln\lambda_i = \frac{1}{T}[\ln|\lambda_i| + i \cdot \arg(\lambda_i) + i \cdot 2\pi \cdot k] \tag{A.16}$$

where the integer k denotes the Poincaré multiplier that can be freely chosen.

If modal variables η are introduced by

$$x(t) = F(t)\eta(t) \tag{A.17}$$

then a time-periodic system of the form

$$\begin{aligned} \dot{x}(t) &= A(t)x(t) + B(t)u(t) \\ y(t) &= C(t)x(t) + D(t)u(t) \end{aligned} \tag{A.18}$$

becomes

$$\begin{aligned} \dot{\eta}(t) &= F(t)^{-1}[A(t)F(t) - \dot{F}(t)]\eta(t) + F(t)^{-1}B(t)u(t) \\ y(t) &= C(t)F(t)\eta(t) + D(t)u(t) \end{aligned} \tag{A.19}$$

Using (A.15), this can be written as:

$$\begin{aligned} \dot{\eta}(t) &= J\eta(t) + F(t)^{-1}B(t)u(t) \\ y(t) &= C(t)F(t)\eta(t) + D(t)u(t) \end{aligned} \tag{A.20}$$

Since $F(t)$ is periodic and, therefore, bounded, the stability of the system is governed by the constant matrix J alone. Thus, the Floquet transformation opens up the possibility of analyzing the stability of time-periodic systems in the same way as for time-constant systems.

Choosing the Poincaré multipliers such that ω_i is close to the natural frequency of the corresponding mode, reduces the degree periodicity of $F(t)$ and thus helps to improve the convergence of control design algorithms applied to the Floquet transformed system [15].

A.4 H_∞ Controller Algorithm

This section outlines the algorithm used to solve the sub-optimal H_∞ control problem; see [95] and the original papers [36], [31] for a detailed description.

A state-space realization of the generalized plant P is given by:

$$\begin{bmatrix} \dot{x} \\ z \\ v \end{bmatrix} = \begin{bmatrix} A & B_1 & B_2 \\ C_1 & D_{11} & D_{12} \\ C_2 & D_{21} & D_{22} \end{bmatrix} \cdot \begin{bmatrix} x \\ w \\ u \end{bmatrix} \tag{A.21}$$

The algorithm presented here is for the regular problem, with:

$$D_{11} = 0, D_{22} = 0, D_{12}^{\mathrm{T}} \cdot \begin{bmatrix} C_1 & D_{12} \end{bmatrix} = \begin{bmatrix} 0 & I \end{bmatrix}, \begin{bmatrix} B_1 \\ D_{21} \end{bmatrix} \cdot D_{21}^{\mathrm{T}} = \begin{bmatrix} 0 \\ I \end{bmatrix} \tag{A.22}$$

The algorithm for the general problem without assumption (A.22) is given in [36]. The following assumptions are required to hold for both the regular and general cases:

- (A, B_2, C_2) is stabilizable and detectable
- D_{12} and D_{21} have full rank
- $\begin{bmatrix} A - j\omega I & B_2 \\ C_1 & D_{12} \end{bmatrix}$ has full column rank for all ω
- $\begin{bmatrix} A - j\omega I & B_1 \\ C_2 & D_{21} \end{bmatrix}$ has full row rank for all ω.

A stabilizing controller $K(s)$ with $\left\| F_l(P, K) \right\|_\infty < \gamma$ then exists if and only if:

- $H_\infty = \begin{bmatrix} A & \gamma^{-2}B_1B_1^{\mathrm{T}} - B_2B_2^{\mathrm{T}} \\ -C_1^{\mathrm{T}}C_1 & -A^{\mathrm{T}} \end{bmatrix}$ has no imaginary axis eigenvalues and

  $X_\infty = \mathrm{Ric}(H_\infty) \geq 0$ exists, where $\mathrm{Ric}(H_\infty) \geq 0$ is the symmetric, positive semi-definite stabilizing solution of the algebraic Riccati equation with the corresponding Hamiltonian matrix H_∞

- $J_\infty = \begin{bmatrix} A^{\mathrm{T}} & \gamma^{-2}C_1^{\mathrm{T}}C_1 - C_2^{\mathrm{T}}C_2 \\ -B_1B_1^T & -A \end{bmatrix}$ has no imaginary axis eigenvalues and

  $Y_\infty = \mathrm{Ric}(J_\infty) \geq 0$ exists

- $\rho(X_\infty Y_\infty) < \gamma^2$.

A state-space realization of the central H_∞ controller K is then given by

$$\begin{bmatrix} \dot{x}_K \\ u \end{bmatrix} = \begin{bmatrix} \hat{A}_\infty & -Z_\infty L_\infty \\ F_\infty & 0 \end{bmatrix} \cdot \begin{bmatrix} x_K \\ v \end{bmatrix} \tag{A.23}$$

with

$$\begin{aligned} \hat{A}_\infty &= A + \gamma^{-2}B_1B_1^{\mathrm{T}}X_\infty + B_2F_\infty + Z_\infty L_\infty C_2 \\ F_\infty &= -B_2^{\mathrm{T}}X_\infty \\ L_\infty &= -Y_\infty C_2^{\mathrm{T}} \\ Z_\infty &= (I - \gamma^{-2}X_\infty Y_\infty)^{-1} \end{aligned} \tag{A.24}$$

The controller K is of the same order as the generalized plant P.

References

[1] Altmikus, A. R. M., Wagner, S., Hablowetz, T., Well, K. H., “On the Accuracy of Modular Aeroelastic Methods Applied to Fixed and Rotary Wings”, 18th AIAA Applied Aerodynamics Conference, Denver, 2000

[2] Arcara, P., Bittanti, S., Lovera, M., “Active Control of Vibrations in Helicopters by Periodic Optimal Control”, IEEE International Conference on Control Applications, Hartford, 1997

[3] Arcara, P., Bittanti, S., Lovera, M., “Periodic Control of Helicopter Rotors for Attenuation of Vibrations in Forward Flight”, IEEE Transactions on Control Systems Technology, 8(6), pp. 883-894, 2000

[4] Arnold, U. T. P., Müller, M., Richter, P., “Theoretical and Experimental Prediction of Individual Blade Control Benefits”, 23rd European Rotorcraft Forum, Dresden, 1997

[5] Barnard, R. H., Philpott, D. R., “Aircraft Flight”, Longman Scientific & Technical, ISBN 0-582-23656-8, 1995

[6] Bates, D. G., Postlethwaite, I., “Robust Multivariable Control of Aerospace Systems”, Delft University Press, ISBN 90-407-2317-6, 2002

[7] Bernhard, A. P. F., Chopra, I., “Development of a Smart Moving-Blade-Tip and an Active-Twist Rotor Blade Driven by a Piezo-Induced Bending-Torsion Coupled Beam”, 53rd AHS Annual Forum, Virginia Beach, 1997

[8] Bertogalli, V., Bittanti, S., Lovera, M., “Simulation and Identification of Helicopter Rotor Dynamics Using General-Purpose Multibody Code”, Journal of the Franklin Institute, 366(5), pp. 783-797, 1999

[9] Besser, R., “Technik und Geschichte der Hubschrauber”, Band 1, Bernard & Graefe Verlag, ISBN 3-7637-5408-3, 1982

[10] Bittanti, S., Colaneri, P., “Invariant Representations of Discrete-Time Periodic Systems”, Automatica, 36(12), pp. 1777-1793, 2000

[11] Bittanti, S., Lorito, F., Strada, S., “An LQ Approach to Active Control of Vibrations in Helicopters”, Journal of Dynamic Systems, Measurement and Control, 118, pp. 482-488, 1996

[12] Büter, A., Breitbach, E., “Adaptive Blade Twist - Calculations and Experimental Results”, 25th European Rotorcraft Forum, Rome, 1999

[13] Bramwell, A. R. S, “Helicopter Dynamics”, Butterworth-Heinemann, ISBN 0-7506-5075-3, 2001

[14] Calico, R. A., Wiesel, W. E., “Control of Time-Periodic Systems”, Journal of Guidance, Control and Dynamics, 7(6), pp. 671-676, 1984

[15] Calise, A. J, Wasikowski, M. E., Schrage, D. P, “Optimal Output Feedback for Linear Time-Periodic Systems”, Journal of Guidance, Control and Dynamics, 15(2), pp. 416-423, 1992

[16] Cantoni, M. W., “Linear Periodic Systems: Robustness Analysis and Sampled-Data Control”, Dissertation, St. John’s College, Cambridge, 1998

[17] Chan, W., Brocklehurst, A., “Performance Enhancement Evaluation of an Actuated Trailing Edge Flap”, 26th European Rotorcraft Forum, The Hague, 2000

[18] Chen, P. C., Chopra, I., “Hover Testing of Smart Rotor with Induced-Strain Actuation of Blade Twist”, AIAA Journal, 35(1), pp. 6-16, 1997

[19] Chen, P. C., Chopra, I., “Induced Strain Actuation of Composite Beams and Rotor Blades with Embedded Piezoceramic Elements”, Smart Materials and Structures, 5(1), pp. 35-48, 1996

[20] Chen, P. C., Chopra, I., “Wind Tunnel Test of a Smart Rotor Model with Individual Blade Twist Control”, Journal of Intelligent Material Systems and Structures, 8(5), pp. 414-425, 1997

[21] Chiu, T. K., Friedmann, P. P., “Vibration Suppression in Helicopter Rotor/Flexible Fuselage System Using the ACSR Approach with Disturbance Rejection, 52nd AHS Annual Forum, Washington, 1996

[22] Chopra, I., “Development of a Smart Rotor”, 19th European Rotorcraft Forum, Como, 1993

[23] Cole, D. G., “Harmonic and Narrowband Disturbance Rejection for Linear Time-Periodic Plants”, Dissertation, Virginia Polytechnic Institute and State University, Blacksburg, 1998

[24] Cribbs, R. C., Friedmann, P. P., “Vibration Suppression in Helicopters with the ACSR Approach Using an Improved Control Algorithm”, 25th European Rotorcraft Forum, Rome, 1999

[25] Cribbs, R. C., Friedmann, P. P., Chiu, T., “Coupled Helicopter Rotor/Flexible Fuselage Aeroelastic Model for Control of Structural Response”, AIAA Journal, 38(10), pp. 1777-1788, 2000

[26] Davison, E. J., Furguson, I. J., “The Design of Controllers for the Multivariable Robust Servomechanism Problem Using Parameter Optimization Methods”, IEEE Transactions on Automatic Control, AC-26(1), pp. 93-110, 1981

[27] Degener, M., Uerlings, P., “Standschwingungsversuch am DFVLR-Hubschrauber BO 105”, Aerodynamische Versuchsanstalt Goettingen, Technical Report IB 253-80 J 07, 1981

[28] Derham, R. C., Hagood, N. W., “Rotor Design Using Smart Materials to Actively Twist Blades”, 52nd AHS Annual Forum, Washington, 1996

[29] Dieterich, O., “Application of Modern Control Technology for Advanced IBC Systems”, 24th European Rotorcraft Forum, Marseilles, 1998

[30] Doyle, J. C., et al., “Xmath X_μ - Manual”, Integrated Systems Inc., Santa Clare CA, USA, 1994

[31] Doyle, J. C., Glover, K., Khargonekar, P. P., Francis, B. A., “State-Space Solutions to Standard H_2 and H_∞ Control Problems”, IEEE Transactions on Automatic Control, AC-34(8), pp. 831-847, 1989

[32] Flamm, D. S., “A New Shift-Invariant Representation for Periodic Linear Systems”, System and Control Letters 17, pp. 9-14, 1991

[33] Friedmann, P., Millott, T., “Vibration Reduction in Rotorcraft Using Active Control: A Comparison of Various Approaches”, Journal of Guidance, Control and Dynamics, 18(4), pp. 664 - 673, 1995

[34] Fulton, M. V., Ormiston, R. A., “Small-Scale Rotor Experiments with On-Blade Elevons to Reduce Blade Vibratory Loads in Forward Flight”, 54th AHS Annual Forum, Washington, 1998

[35] Goldberg, D. E., “Genetic Algorithms in Search, Optimization, and Machine Learning”, Addison-Wesley, ISBN 0-201-15767-5, 1989

[36] Glover, K., Doyle, J. C., “State-Space Formulae for all Stabilizing Controllers that Satisfy an H_∞ Norm Bound and Relations to Risk Sensitivity”, Systems & Control Letters 11, pp. 167-172, 1988

[37] Hablowetz, T., Mannchen, T., Well, K. H., “Advanced Helicopter Flight Simulation with Controller in the Loop”, 26th European Rotorcraft Forum, The Hague, 2000

[38] Ham, N. D., Behal, B. L., McKillip Jr., R. M., “Helicopter Rotor Lag Damping Augmentation Through Individual-Blade-Control”, Vertica, 7(4), pp. 361-371, 1983

[39] Hohenemser, K. H., Sheng-Kuang Yin, “Some Applications of the Method of Multiblade Coordinates”, Journal of the American Helicopter Society, 17(3), pp. 3-12,1972

[40] Hsu, T.-K., Peters, D. A., “Coupled Rotor/Airframe Vibration Analysis by a Combined Harmonic-Balance, Impedance-Matching Method”, 36th AHS Annual Forum, Washington, 1980

[41] Jacklin, S. A., Blaas, A., Teves, D., Kube, R., “Reduction of Helicopter BVI Noise, Vibration and Power Consumption Through Individual Blade Control”, 51st AHS Annual Forum, Fort Worth, 1995

[42] Johnson, W., “CAMRAD II Comprehensive Analytical Model of Rotorcraft Aerodynamics and Dynamics”, Johnson Aeronautics, Palo Alto, California, 1999

[43] Johnson, W., “Helicopter Theory”, Dover Publications, ISBN 0-486-68230-7, 1994

[44] Johnson, W., “Technology Drivers in the Development of CAMRAD II”, AHS Aeromechanics Specialists Conference, San Francisco, 1994

[45] Khargonekar, P. P., Poolla, K., Tannenbaum, A., “Robust Control of Linear Time-Invariant Plants Using Periodic Compensation”, IEEE Transactions on Automatic Control, AC-30(11), pp. 1088-1096, 1985

[46] Kretz, M., “Active Elimination of Stall Conditions”, Vertica, 6, pp 49-58, 1982

[47] Kretz, M., “Research in Multicyclic and Active Control of Rotary Wings”, Vertica, 1, pp. 95-105, 1976

[48] Kretz, M., Larché, M., “Future of Helicopter Rotor Control”, Vertica, 4, pp. 13-22, 1980

[49] Kube, R., van der Wall, B. G., Schultz, K.-J., Splettstoesser, W. R., “IBC Effects on BVI Noise and Vibrations A Combined Numerical and Experimental Investigation”, 55th AHS Annual Forum, Montreal, 1999

[50] Kunze, O., Arnold, U. T. P., Waaske, S., “Development and Design of an Individual Blade Control System for the Sikorsky CH-53G Helicopter”, 55th AHS Annual Forum, Montreal, 1999

[51] Lahey, R. S., Miller, M. P., Reymond, M., (Editors), “MSC/NASTRAN Reference Manual”, Version 68, The MacNeal-Schwendler Corporation, 1994

[52] Landmann, B., “Aufbau und Validierung eines Hubschrauberrotormodells”, Diploma Thesis, University of Stuttgart, Institute of Flight Mechanics and Control, IFR_SR_00_003, 2000

[53] Lee, Y. J., Balas, M. J., “Controller Design of Periodic Time-Varying Systems via Time-Invariant Methods”, Journal of Guidance, Control, and Dynamics, 22(3), pp. 486-488, 1999

[54] Leishman, J. G., “Principles of Helicopter Aerodynamics”, Cambridge University Press, ISBN 0-521-66060-2, 2000

[55] Leishman, J. G., Nguyen, K. Q., “State-Space Representation of Unsteady Airfoil Behavior”, AIAA Journal, 28(5), pp. 836-844, 1990

[56] Levine, W. S., Athans, M., “On the Determination of the Optimal Constant Output Feedback Gains for Linear Multivariable Systems”, IEEE Transactions on Automatic Control, AC-15(1), pp. 44-48, 1970

[57] Lin, Y.-J., Lee, T., Choi, B., Saravanos, D., “An Application of Smart-Structure Technology to Rotor Blade Tip Vibration Control”, Journal of Vibration and Control, 5, pp. 639-658, 1999

[58] Lovera, M., Verhaegen, M., Chou, C. T., “State Space Identification of MIMO Linear Parameter Varying Models”, Mathematical Theory of Networks and Systems Symposium, Padova, 1998

[59] Maciejowski, J. M., “Multivariable Feedback Control”, Addison-Wesley, ISBN 0-201-1824-2, 1989

[60] Mannchen, T., “Hubschrauber-Rotorblattregelung Entwurf mittels H_∞-Verfahren”, Diploma Thesis, University of Stuttgart, Institute of Flight Mechanics and Control, IFR_SR_98_001, 1998

[61] Mannchen, T., Well, K. H., “Helicopter Vibration Reduction Using Periodic Robust Control”, AIAA Guidance, Navigation and Control Conference, AIAA-2001-4034, Montreal, 2001

[62] Mannchen, T., Well, K. H., “Influence of Number of Rotor Blades on Helicopter Active Vibration Reduction Potential”, 28th European Rotorcraft Forum, Bristol, 2002

[63] McKillip Jr., R. M., “Periodic Control of the Individual-Blade-Control Helicopter Rotor”, Vertica, 9(2), pp. 199-225, 1985

[64] Mettler, B., Tischler, M. B., Kanade, T., “System Identification of Small-Size Unmanned Helicopter Dynamics”, 55th AHS Annual Forum, Montreal, 1999

[65] Meyer, R. A., Burrus, C. S., “A Unified Analysis of Multirate and Periodically Time-Varying Digital Filters”, IEEE Transactions on Circuits and Systems, CAS-22(3), 1975

[66] Miao, W.-L., Kottapalli, S. B. R., Frye, H. M., “Flight Demonstration of Higher Harmonic Control (HHC) on S-76”, 42nd AHS Annual Forum, Washington, 1986

[67] Miao, W.-L., Twomey, W. J., Wang, J. M., “Challenge of Predicting Helicopter Vibration”, AHS International Meeting on Advanced Rotorcraft Technology and Disaster Relief, Gifu, Japan, 1998

[68] Milgram, J., Chopra, I., “Helicopter Vibration Reduction with Trailing Edge Flaps”, AIAA/ASME/ASCE/AHS/ASC Structural Dynamics and Materials Conference, New Orleans, 1995

[69] Millott, T. A., Friedmann, P. P., “Vibration Reduction in Hingeless Rotors Using an Actively Controlled Trailing Edge Flap: Implementation and Time Domain Simulation”, AIAA Conference, AIAA-94-1304-CP, 1994

[70] Millott, T. A., Welsh, W. A., “Helicopter Active Noise and Vibration Reduction”, 25th European Rotorcraft Forum, Rome, 1999

[71] Moerder, D. D., Calise, A. J., “Convergence of a Numerical Algorithm for Calculating Optimal Output Feedback Gains”, IEEE Transactions on Automatic Control, AC-30(9), pp. 900-903, 1985

[72] Müller, M., Arnold, U.T.P., Morbitzer, D., “On the Importance and Effectiveness of 2/REV IBC for Noise, Vibration and Pitch Link Load Reduction”, 25th European Rotorcraft Forum, Rome, 1999

[73] Myrtle, T., Friedmann, P., “Vibration Reduction in Rotorcraft Using the Actively Controlled Trailing Edge Flap and Issues Related to Practical Implementation”, 54th AHS Annual Forum, Washington, 1998

[74] Narkiewicz, J. P., Done, G. T. S., “Overview of Smart Structure Concepts for Helicopter Rotor Control”, 2nd European Conference on Smart Structures and Materials, Glasgow, 1994

[75] Nitzsche, F., “Designing Efficient Helicopter Individual Blade Controllers Using Smart Structures”, AIAA Conference, AIAA-94-1766-CP, 1994

[76] Nitzsche, F., Breitbach, E., “Individual Blade Control of Hinged Blades Using Smart Structures”, Smart Materials and Structures, 3(2), pp. 171-180, 1994

[77] Nitzsche, F., Breitbach, E., “Vibration Control of Rotary Wings Using Smart Structures”, Smart Materials and Structures, 3(2), pp. 181-189, 1994

[78] Payne, P. R., “Higher Harmonic Rotor Control”, Aircraft Engineering, August, 1958

[79] Peters, D. A., Hohenemser, K. H., “Application of the Floquet Transition Matrix to Problems of Lifting Rotor Stability”, Journal of the American Helicopter Society, 16(2), pp. 25-33, 1971

[80] Peters, D. A., Ormiston, R. A., “Flapping Response Characteristics of Hingeless Rotor Blades by a Generalized Harmonic Balance Method”, NASA TN D-7856, 1975

[81] Polychroniadis, M., Achache, M., “Higher Harmonic Control: Flight Tests of an Experimental System on a SA 349 Research Gazelle”, 42nd AHS Annual Forum, Washington, 1986

[82] Postlethwaite, I., Smerlas, A., Walker, D. J., Gubbels, A. W., Baillie, S. W., Strange, M. E., Howitt, J., “H_∞ Control of the NRC Bell 205 Fly-by-Wire Helicopter”, Journal of the American Helicopter Society, 44(4), pp. 276-284, 1999

[83] Postlethwaite, I., Walker, D. J., “The Design of Helicopter Flight Control Systems Using Advanced H_∞ Control”, American Control Conference, Baltimore, 1994

[84] Quackenbush, T. R., “Testing of a Stall Flutter Suppression System for Helicopter Rotors Using Individual-Blade-Control”, 39th AHS Annual Forum, St. Louis, 1983

[85] Richter, P., Blaas, A., “Full Scale Wind Tunnel Investigation of an Individual Blade Control System for the BO 105 Hingeless Rotor”, 50th AHS Annual Forum, Washington, 1994

[86] Richter, P., König, W., “Einzelblattsteuerung (IBC) für den Transporthubschrauber CH-53G”, Deutscher Luft- und Raumfahrtkongress, Hamburg, 2001

[87] Rodgers, J. P., Hagood, N. W., “Preliminary Mach-Scale Hover Testing of an Integral Twist-Actuated Rotor Blade”, SPIE Conference on Smart Structures and Integrated Systems, San Diego, 1998

[88] Roth, D., Dieterich, O., Bebesel, M., Pongratz, R., Kube, R., Munser, H., “Individual Blade Root Control Demonstration Recent Activities”, 27th European Rotorcraft Forum, Moscow, 2001

[89] Safonov, M. G., Chiang, R. Y., “A Schur Method for Balanced Truncation Model Reduction”, IEEE Transactions on Automatic Control, AC-34(7), pp. 729-733, 1989

[90] Sahasrabudhe, V., Thompson, P. M., Aponso, B. L., Chen, C., “Smart Rotor Active Control”, 54th AHS Annual Forum, Washington, 1998

[91] Schimke, D., Arnold, U. T. P., Kube, R., “Individual Blade Root Control Demonstration Evaluation of Recent Flight Tests”, 54th AHS Annual Forum, Washington, 1998

[92] Schulz, G., “Active Multivariable Vibration Isolation for a Helicopter”, Automatica, 15, pp. 461-466, 1979

[93] Schwenger, M., “Hubschrauber-Vibrationsreduktion Reglerentwurf für eine unterschiedliche Anzahl der Rotorblätter”, Diploma Thesis, University of Stuttgart, Institute of Flight Mechanics and Control, IFR_SR_01_017, 2001

[94] Sinha, S. C., Joseph, P., “Control of General Dynamic Systems With Periodically Varying Parameters Via Liapunov-Floquet Transformation”, Transactions of the ASME, 116, pp. 650-658, 1994

[95] Skogestad, S., Postlethwaite, I., “Multivariable Feedback Control”, Wiley, ISBN 0-471-94227-4, 1996

[96] Smerlas, A. J., Walker, D. J., Postlethwaite, I., Strange, M. E., Howitt, J., Gubbels, A. W., “Evaluating H_∞ Controllers on the NRC Bell 205 Fly-By-Wire Helicopter”, Control Engineering Practice, 9, pp. 1-10, 2001

[97] Sorour, M., “Implementierung von Rotor-Zellenkopplungen für Regelkonzepte zur Vibrationsminderung bei Hubschraubern durch Einzelblattregler”, Diploma Thesis, University of Stuttgart, Institute of Flight Mechanics and Control, IFR_SR_00_016, 2000

[98] Splettstoesser, W. R., Kube, R., Wagner, W., Seelhorst, U., Boutier, A., Micheli, F., Mercker, E., Pengel, K., “Key Results From a Higher Harmonic Control Aeroacoustic Rotor Test (HART)”, 21st European Rotorcraft Forum, Saint-Petersburg, 1995

[99] Stilwell, D. J., “State-Space Interpolation for a Gain-Scheduled Autopilot”, Journal of Guidance, Control, and Dynamics, 24(3), pp. 460-465, 2001

[100] Stoppel, J., “Idealisierung des Hubschraubers PAH1 nach der Methode der Finiten Elemente, MBB Technical Report, 1987

[101] Straub, F. K., “A Feasibility Study of Using Smart Materials For Rotor Control”, Smart Materials and Structures, 5(1), pp. 1-10, 1996

[102] Strehlow, H., Mehlhose, R., Znika, P., “Passive and Active Vibration Control Activities in the German Helicopter Industry”, Aero Tech 92 Conference, Birmingham, 1992

[103] Strehlow, H., Rapp, H., “Smart Materials for Helicopter Rotor Active Control”, AGARD Conference Proceedings 531, pp. 5.1-5.16, 1992

[104] de Terlizzi, M., Friedmann, P. P., “Active Control of Vibration due to BVI and experimental correlation”, 25th European Rotorcraft Forum, Rome, 1999

[105] de Terlizzi, M, Friedmann, P. P., “Active Control of BVI Induced Vibration Using a Refined Aerodynamic Model and Experimental Correlation”, 55th AHS Annual Forum, Montreal, 1999

[106] Teves, D., Klöppel, V., Richter, P., “Development of Active Control Technology in the Rotating System, Flight Testing and Theoretical Investigations”, 18th European Rotorcraft Forum, Avignon, 1992

[107] Tischler, M. B., Cauffman, M. G., “Frequency-Response Method for Rotorcraft System Identification: Flight Application to BO 105 Coupled Rotor/Fuselage Dynamics”, Journal of the American Helicopter Society, 37(3), pp. 3-17, 1992

[108] Tomashofski, C. A., Tischler, M. B., “Flight Test Identification of SH-2G Dynamics in Support of Digital Flight Control System Development”, 55th AHS Annual Forum, Montreal, 1999

[109] Torok, M. S., “Aeroelastic Analysis of Active Rotor Control Concepts for Vibration Reduction”, 52nd AHS Annual Forum, Washington, 1996

[110] Tung, Chee, Kube, R., Brooks, T. F., Rahier, G., “Prediction and Measurement of Blade-Vortex Interaction”, Journal of Aircraft, 35(2), pp. 260-266, 1998

[111] Varga, A., “Periodic Lyapunov Equations: Some Applications and New Algorithms”, International Journal of Control, 67(1), pp. 69-87, 1997

[112] Voulgaris, P. G., Dahlem, M. A., Valavani, L. S., “H_∞ and H_2 Optimal Controllers for Periodic and Multirate Systems”, Automatica, 30(2), pp. 251-263, 1994

[113] Wu, D.-H., Sinha, S. C., “A New Approach in the Analysis of Linear Systems with Periodic Coefficients for Application in Rotorcraft Dynamics”, The Aeronautical Journal, pp. 9-16, January, 1994

[114] Yeo, H., Chopra, I., “Effects of Modelling Refinements on Coupled Rotor/Fuselage Vibration Analysis, 54th AHS Annual Forum, Washington, 1998

[115] Yeo, H., Chopra, I., “Fundamental Issues Related to the Prediction of Coupled Rotor/ Airframe Vibration”, 25th European Rotorcraft Forum, Rome, 1999